POLITECNICO
MILANO 1863

SCUOLA DI INGEGNERIA INDUSTRIALE
E DELL'INFORMAZIONE

Particle Finite Element Method applied to sediment transport and erodible surfaces

Tesi di Laurea Magistrale in
Mathematical Engineering - Ingegneria Matematica

Author: **Simone Martini**

Student ID: 953255
Advisor: Prof. Corigliano Alberto
Co-advisors: Prof. Cremonesi Massimiliano
Academic Year: 2022-23

Abstract

This master's thesis work in Mathematical Engineering in collaboration with the Civil Engineering Department was born with the main intention of studying the effects of floods on the territory. The urgency was created by the flood events in the Marche region on the 15th and 16th of September 2022, in which there were 12 victims, 50 injured and 150 people displaced. In total, the monetary damage amounted to approximately EUR 2 billion.
In this context, floods are a term that refers to the overflowing of a river that brings with it debris and sediment with the serious risk of damaging everything around it. Consequently, the intent of this thesis is to simulate erosion and sediment transport in order to help studying the risks and consequences of such an event.
In order to do this, the pre-existing particle finite element method for the fluid was used, integrating the sediment information into the code as a scalar concentration variable. This addition to the code was done in the form of a diffusion-transport equation, evaluating the effect of each term on the model. In this part of the work, knowledge of mathematical analysis was essential to assess the correct functioning of the equation within the code.
Under these objectives, an extensive analysis was made of the results of many tests performed using this model, and not only in the area of sediment transport. Indeed, the dynamics of diffusion-transport in a fluid can also describe a contaminant: some tests have been carried out in this light, evaluating the areas damaged by the spillage of a contaminant.
Finally, the focus also shifted to the research for an erosion model to study the main effect of river overflow or, in a particular case studied in this thesis, marine erosion of beaches. This area of study is also important in analysing the risk of beaches disappearing. Thus, such work can assess the criticality of certain places to the erosion by sea waves that slowly carry away the beach sediment.

Keywords: Particle Finite Element Method, Computational Fluid Dynamics, Flooding, Erosion

Abstract in lingua italiana

Questo lavoro di tesi magistrale in ingegneria Matematica in collaborazione con il dipartimento di ingegneria Civile è nato con il principale intento di studiare gli effetti delle alluvioni sul territorio. L'urgenza è stata creata dagli eventi alluvionali avvenuti nelle Marche del 15 e 16 settembre 2022, in cui ci sono state 12 vittime, 50 feriti e 150 persone sfollate. In totale, il danno monetario è stato di circa 2 miliardi di Euro. In questo contesto, le alluvioni sono termine che fa riferimento all'esondazione del fiume che porta con sè detriti e sedimento con il grave rischio di danneggiare tutto ciò che c'è intorno. Di conseguenza l'intento di questa tesi è di simulare l'erosione e il trasporto del sedimento per poter aiutare lo studio di rischi e conseguenze di un avvenimento del genere.
Per poter fare ciò, ci si è avvalsi del metodo già preesistente degli elementi finiti particellari per il fluido, integrando il sedimento nel codice come una variabile scalare di concentrazione. Questa aggiunta al codice è stata fatta sotto forma di un'equazione di diffusione-trasporto, valutando l'effetto di ogni singolo termine sul modello. In questa parte dell'elaborato, è stata fondamentale la conoscenza dell'analisi matematica per valutare il corretto funzionamento dell'equazione all'interno del codice.
Sotto questi obiettivi, è stata fatta una larga analisi dei risultati di molti test eseguiti utilizzando questo modello, non solamente nell'ambito di trasporto del sedimento. Difatti, la dinamica di diffusione-trasporto in un fluido può interessare anche un contaminante: alcuni test sono stati effettuati sotto questa luce, valutando le aree danneggiate dallo spillamento di un contaminante.
Infine, il focus è passato anche sulla ricerca di un modello di erosione per studiare l'effetto principale dello straripamento del fiume oppure, in un caso particolare studiato in questa tesi, dell'erosione marina delle spiagge. Anche questo ambito di studio è importante nell'analisi del rischio di scomparsa delle spiagge. Quindi un lavoro del genere può valutare le criticità di alcuni luoghi all'erosione dovuta alle onde del mare che piano piano portano via il sedimento della spiaggia.

Parole chiave: Metodo agli Elementi Finiti Particellari, Fluidodinamica Computazionale, Alluvioni, Erosione

Contents

Introduction

Studying the effects of flooding events in the territory is fundamental in order to evaluate a way of simulating natural disasters that include river overflow. The aim is to build a model that can be the starting point of many risk assessment simulations regarding river-bank and beach erosion, land damages or even destruction of buildings due to flooding events. The disaster happened in the Marche region on the 15th and 16th of September is the main example where this thesis sets its application. It may help predict the causes and consequences of potential climatic disasters. In order to achieve this objective, a model for the flow movement composed by fluid and sediment must be built. A large variety of models of this kind are available in the literature, with different types of approaches.
Messa et al. [25] study a two phase flow in order to get the best possible approximation of the problem. This leads to a very complex set of equations and a very high computational cost. Indeed, solving the equations for the fluid and for the trajectory of the solid may require a high effort in the modelling part. To make things worse, almost all two-phase approaches use an Eulerian-Eulerian mesh or an Eulerian-Lagrangian mesh [26]. So in the literature the fluid phase is mainly solved in an Eulerian mesh. This is not our case since the starting fluid framework relies on a Lagrangian mesh. So the two-phase modeling is avoided.
Many different works use an equation for the sediment transport considering the volumetric concentration as a variable. This equation is applied in the framework of river flow or sea movement. Rowan et al. [31] present a weakly coupled model with an advection-diffusion equation that describes the sediment behaviour in the fluid. This model has a drawback to address: it works only when the concentrations are low. To this matter, in this work high concentrations are considered when the target is to check the correct mathematical behaviour of the model. Towards the end of the work, following [18], a modification is taken into account to consider the low concentration hypothesis.
Regarding the erosion process, the research is initially driven by finding a simple way to describe the change of the morphology of the bed. Galano et al. [15] explore the idea of applying the Shields shear stress criterion in order to see if the particle on the flow-bed interface is dragged away or not. The violation condition is based on checking if the value

of the shear stress on the bottom surpasses a limit value. However, in the paper that describes this model, the particle that is snatched from the bottom and becomes part of the fluid is not considered as sediment. Here, the idea is to consider the eroded particles to become part of the mixture of fluid-sediment. In order to get the best possible approximation, a totally coupled model is considered: it addresses the loss of energy in the fluid due to its eroding action by changing its density and viscosity.
The starting mathematical model used is the Particle Finite Element Method (PFEM). This method is characterized by the usage of a Lagrangian mesh, which has the peculiarity of being able to follow the particles trajectory. This framework has also many benefits numerically, mostly because the solution system becomes linear. This creates a very easy way to find the solution, but it is an approach which is more complex to manage. This is due to the fact that the mesh moves along with the fluid and has to be frequently reconstructed. So, it seems that the computational cost lost from solving a linear system is gained by making a new mesh when needed. Actually, following [7], the cost gained is not so much since the remeshing is done only by reconstructing the connectivity of the mesh. The position of the nodes remain the same. This makes the code more easy to use and faster than other models that solve numerically the Navier-Stokes equations. This approach takes the ALE version of the solving system and simplifies it in order to get a more efficient solver.

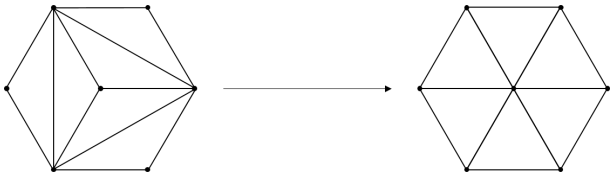

Figure 1: Before and after the remeshing procedure

In figure 1, it can be seen that the mesh before is more stretched leading, in worst cases, to have a bad solution of the problem in terms of stability. After remeshing, the connectivity is changed and the triangles have a more uniform shape.
One of the main focus in this project is to check the robustness of the model after each block is added. Indeed, the structure of the work has been conceived as a step by step built model. Each chapter considers a particular aspect of the total system, and checks its correct functionality through mathematical convergence analysis, stability issues, dominated advection problems and confrontation with other models through test cases. This computational saving is kept in mind throughout the whole work, especially when a way to describe the sediment motion is searched. The physical model that relies on considering a mixture of fluid-sediment is feasible with the PFEM framework: in this way, it can be used to describe the majority of concrete problems regarding sediment transport

and erosion. To this matter, future development can include fluid-structure interaction considering the simulation of buildings collapse due to flooding events.

Thesis structure

Chapter 1 - State of art
In this chapter an overview of the state of the art is provided for the sediment equation and the erosion model.

Chapter 2 - Sediment equation: Diffusion problem
The sediment equation is introduced and its diffusion part is studied in order to insert it in the code. Convergence analysis and comparison with the heat equation is made in order to check the correct functionality.

Chapter 3 - Sediment equation: Transport through gravity
The effect of gravity on the model is studied considering a transport term in the equation. The transport dominated problem and its stabilization are considered to have correct results also in these particular cases.

Chapter 4 - Sediment equation: Transport through fluid motion
Here the fluid motion is activated and so new problems are addressed, such as: imposing boundary conditions to Eulerian nodes, modifying the stabilization term for the transport dominated problem and treating the limits of using a weakly coupled model. All the changes are controlled considering some test cases.

Chapter 5 - Sediment equation: Complete model
In this chapter, 4 different studies are attacked in order to see what the model can achieve in different fields. The main focus is on mixing, contamination and turbulence problems.

Chapter 6 - Bed erosion model
A model for erosion based on the Shields scouring criterion is presented. This basic model checks the shear stress at the bed level in order to check if the sediment particles are eroded or not. Some tests are presented in order to evaluate the fields of application of this model.

Chapter 7 - Conclusions and future developments
The final chapter summarizes the results of all the simulations performed, giving a final overview of what this model can represent in concrete and useful cases. Possible developments for this thesis work are then explained.

1 | State of Art

There are many different problems in the engineering field that require a description of the transport of sediment in a fluid flow. The aim is to find a model that can represent the majority of river transport and erosion problems. The state of art is structured in such a way that the fluid framework and the sediment one are addressed in their completeness. The fluid framework is described using a Lagrangian model, while the sediment one is studied considering a model for transport and erosion.

1.1. Fluid modeling

1.1.1. Lagrangian framework

The particle finite element method is a numerical tool that relies on the Lagrangian framework. This point of view is focused on the small fluid particle moving, tracking its movement in space and in particular its trajectory. Regarding the Eulerian point of view, a fixed volume of moving particles is studied, not caring for the single particle movement. Numerically speaking, there are many differences between the Eulerian approach and Lagrangian one. First of all, using a Lagrangian approach, we can solve the fluid dynamic problem using a mesh that follows the moving particles. In this way the Navier-Stokes problem becomes linear since the non linear convective term is contained inside the total derivative. In other words, the integration points move with the fluid, making this method useful for fluids which have a history dependent behaviour.
Considering an Eulerian mesh, the nodes are fixed and do not move while the fluid moves inside the grid. In this formulation, the convective term has to be considered and the problem is more difficult to treat, opening for a very large number of methods that aim to make the system solvable numerically. In practice, a mixed formulation is used and is called Arbitrary Lagrangian Eulerian (ALE) formulation [10], which solves in some nodes the Eulerian system and in the other ones the Lagrangian one. This system for weakly compressible fluids is shown in 1.1.

$$\begin{cases} \rho\left[\dfrac{\partial \mathbf{u}}{\partial t} + (\mathbf{u_c}\cdot\nabla)\,\mathbf{u}\right] = \nabla\cdot\boldsymbol{\sigma} + \rho\mathbf{b} \quad \text{on } \Omega^t\times[0,T] \\ \dfrac{\partial p}{\partial t} + (\mathbf{u_c}\cdot\nabla)\,p + K\,(\nabla\cdot\mathbf{u}) = 0 \quad \text{on } \Omega^t\times[0,T] \end{cases} \tag{1.1}$$

Where $\mathbf{u_c}(\mathbf{x},t) = \mathbf{u}(\mathbf{x},t) - \mathbf{r}(\mathbf{x},t)$, with $\mathbf{r}(\mathbf{x},t)$ denoting the mesh velocity. To recover the Lagrangian formulation, just set $\mathbf{u_c} = 0$; while for the Eulerian one, set $\mathbf{u_c} = \mathbf{u}$ (the velocity of the mesh is null in this case). K is the fluid bulk modulus, $\boldsymbol{\sigma}(\mathbf{x},t)$ is the stress tensor and $\boldsymbol{b}(\mathbf{x},t)$ are the body forces.

1.1.2. Particle Finite Element Method

The mathematical method used to attack the fluid problem is the Particle Finite Element Method. This approach allows us to track easily boundaries and interfaces making the boundary condition imposition more immediate.
One of the biggest consequences of using a Lagrangian mesh is its deterioration. Since the nodes follow the movement of the fluid, if the deformations are very big the mesh could eventually be very distorted. In order to avoid this, Cremonesi et al. [7] consider a remeshing technique so that a new mesh is created. The related drawback of creating a new grid at each time is that the computational cost is very high. This cost is lowered by only building a new connectivity and keeping the nodes at the same position of the previous mesh. The new connectivity is built using the Delaunay tessellation.

This method has many different applications where it can be helpful, especially in fluid-structure interaction problems. Franci et al. [14] presents the simulation of the Vajont disaster of 1963 where the river overflowed beyond the limit of the dam, flooding the nearby country and causing the death of almost 2000 people. Bravo et al. [4] instead describes the simulation of the movement of an erodible bed of a river using the PFEM method. This paper describes the Exner equation, which will be a topic of discussion in [1.2].

As described in [7] the general solution scheme of the PFEM can be summarized in these steps:

1. Insert in the domain a set of points which are the starting particles considered in the system (1.1a);
2. Generate a mesh with these particles (1.1b);
3. Recover the internal and external boundaries of the domain (1.1c);

4. Solve the Lagrangian form of the equations using FEM (1.1d);
5. Compute the particle movement and update the position of the nodes (1.1e, 1.1f, 1.1g);
6. Pass to the next time step, if remeshing is needed go turn back to step 2, if not go to step 5.

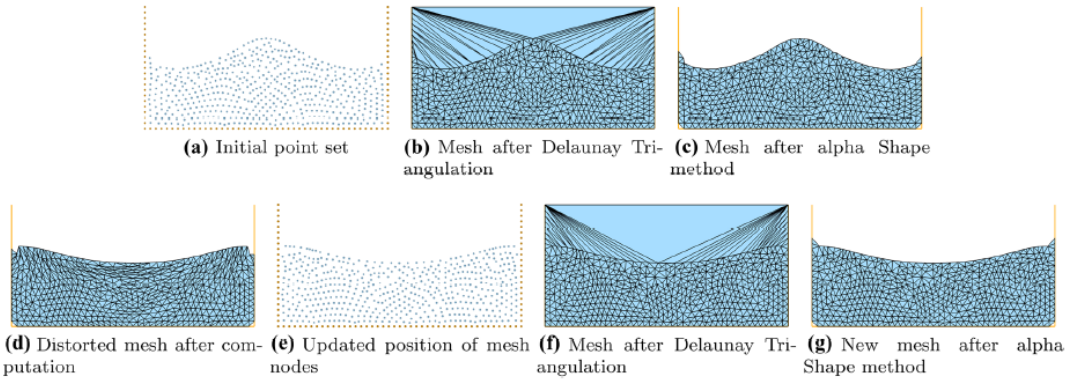

Figure 1.1: Steps of PFEM [7]

1.1.3. Delaunay triangulation

To generate the mesh from the particle nodes, the Delaunay triangulation is used. Starting from a set of N points, the Voronoï diagram is defined as the partition of the domain Ω in convex regions T_i where to each region is related a node of the set. In this way all the points of T_i are included in it following this definition:

$$T_i = \{\mathbf{x} \in \Omega : \quad d(\mathbf{x}, \mathbf{x_i}) \leq d(\mathbf{x}, \mathbf{x_j}) \quad \forall j \neq i\} \tag{1.2}$$

where $d(\mathbf{x}, \mathbf{x_i}) = ||x - x_i||$ is the Euclidean norm.

The Delaunay triangulation is built by connecting the center nodes of the T_i Voronoï cells which have a boundary in common. By making all the connections, the mesh is constructed.

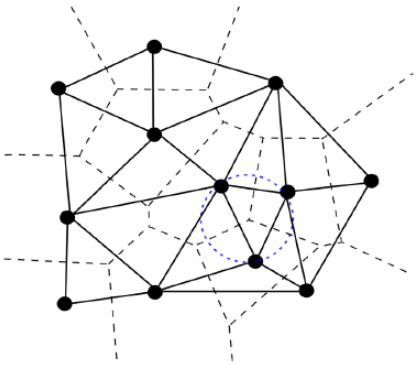

Figure 1.2: Voronoï diagram [7]

The problem of this method is that the resultant mesh can reproduce only a convex geometry, which is obviously a problem in many cases. To overcome this hitch when dealing with non-convex domains, the alpha-shape method is applied.

1.1.4. Alpha-shape method

A geometrical criterion based on the index of elemental distortion α_e is introduced to remove unnecessary elements from the mesh. As said in [23], the elements which do not fulfil the condition are the most distorted ones. This method is able to naturally deal with particles that detach from a surface or to define the contact interface between fluid and structure. The coefficient of elemental distortion is defined as:

$$\alpha_e = \frac{R_e}{h_{mean}} \tag{1.3}$$

where R_e is the radius of the circumsphere of the element and h_{mean} is the characteristic mesh size, which has to be chosen carefully. The criterion eliminates every element whose distortion coefficient is greater than a fixed threshold value $\overline{\alpha}$. In figure 1.3 is shown an example of domain which may require this method. The Delaunay tessellation applied to the R-form domain gives a not satisfactory result, since the final product does not represent correctly the desired one. To recover the correct form of the R letter, the alpha shape method is applied.

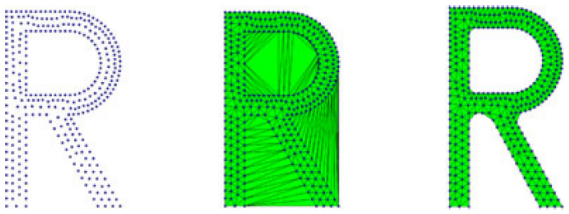

Figure 1.3: Application of the alpha-shape method to the R-figure [23]

Franci et al. [13] presents a very deep study on the alpha-shape method and makes some examples showing how the PFEM makes the phenomena more easier to understand since the free surface are tracked naturally.
This phase is very tricky, since eliminating elements can give life to some problems in the continuity equation. This is due to the fact that the presence of some new elements add fluid that was not there before, so there are inconsistencies in the mass conservation law. An example of this is shown in [13], where is presented a study of the collapse of a dam break against a rigid step. The setup of the test is presented in 1.4.

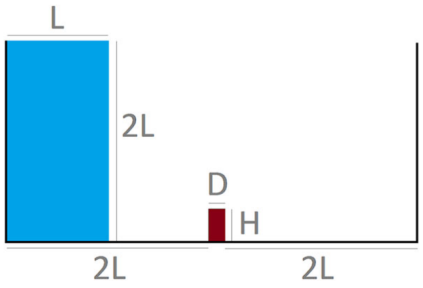

Figure 1.4: Initial geometry of the dam break test against a rigid step [13]

During the start of the simulation the elements move towards the right. During the movement of the water column we can see some mechanism of volume variation, in particular of two types related to creation and elimination of elements. To advance, the method must create some element ahead of the column, in order to solve the equations in those points where the fluid will be (figure 1.5a). On the other hand, during this process the height of the water column decrease in time and elements are deleted since the model does not care to find the solution where the fluid is no more present (figure 1.5b). If the sum of the volume of the erased elements is different than the new added, the overall volume is not conserved, possibly leading to mass oscillations.

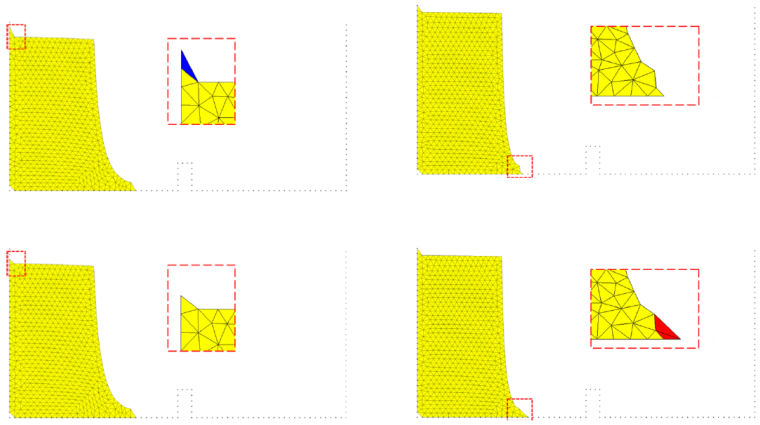

(a) Adding elements to the domain

(b) Removing elements to the domain

Figure 1.5: Two mechanism of volume variation [13]

In PFEM, contact surfaces are automatically tracked using the alpha-shape method, like contact with rigid walls, as shown in figure 1.6b. In this case when contact with surfaces is activated, elements are added and the overall volume is increased. Another feature present in the model is the ability to release a free particle from the flow, as we see in figure 1.6a. Considering this behaviour, the total volume is decreased: despite these possible fluctuations, choosing a proper value of α keeps a limited variation of the value of total volume.

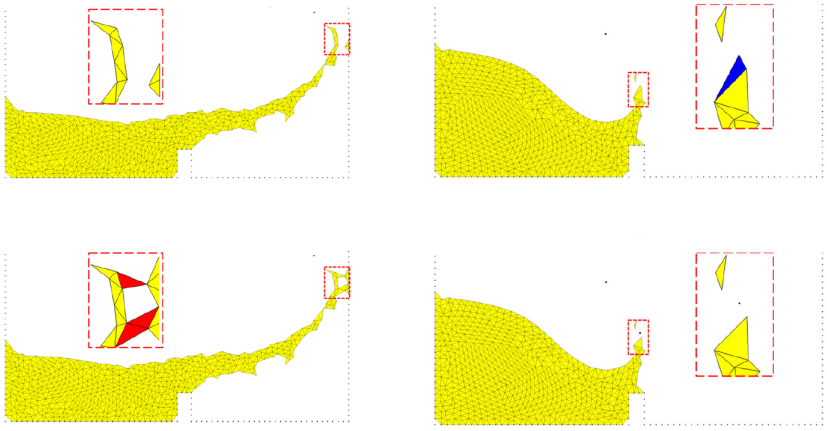

(a) Impact of a fluid with the boundary

(b) Formation of a free particle

Figure 1.6: Free particles and fluid-wall contact treatment [13]

1.1.5. Adding and removing nodes

To maintain a good quality of the mesh, a possible thing to do in this framework is to add and remove nodes. There are many different algorithms to treat situations where it can be useful to change the disposition of the computational points. These cases are two:

- if a node comes too close to another one or a boundary, it should be eliminated;
- if an element becomes too large then a node should be inserted inside it.

By doing this, the grid is no more considered a Delaunay mesh.

1.1.6. Space and time discretization

A consequence of remeshing done by changing only the connectivities and maintaining invariated the positions of the nodes is that only linear interpolation functions can be adopted. This is due to the fact that higher-order functions would require to remap the values of the solutions in the middle of the edges of the elements. Additionally, the curvature of the mesh is lost if high order elements are used, so only linear shape functions can be used in the PFEM framework. From a mathematical point of view this forced choice gives rise to another problem: choosing linear interpolating functions for velocity and pressure make the problem unstable because the inf-sup condition is not fulfilled. As a consequence, to study the problem using PFEM a proper stabilization method is needed.

For what concerns the time discretization, both implicit and explicit approaches can be adopted. Typically, implicit schemes are preferred with maybe considering fractional steps methods. As of late, explicit time integration formulations are more considered in the PFEM framework. They are very appealing for fast dynamical simulations and for non-linear problems that suffer from numerical issues with convergence. Explicit solvers are less computationally expensive since they give rise to a linear problem which is more easier to solve than the implicit one. The implicit treatment of the problem gives rise to a set of equations that must be resolved using particular methods like the Newton one or the fixed point one. The Courant-Friedrichs-Lewy stability condition must be fulfilled in order to have a stabilized solution without spurious oscillations. This property gives to the quality of the mesh a crucial role for the calculation efficiency of explicit methods, as the presence of excessively distorted elements can make the stable time step dimension vanish and compromise the calculation.

1.1.7. Boundary conditions

As said before, PFEM is very good at following modifications of the free surfaces, since they are automatically detected by the position of the external nodes of the domain. On the other hand, treating boundaries that require to have nodes with fixed velocity defined is tricky, giving less flexibility on the impositions of non zero Dirichlet boundary conditions. So complementary methods are searched in order to allow this kind of imposition. In free surface contours, the normal component of the stress tensor should vanish: in strong form this leads to the imposition of a null pressure at the boundary, leading to the violation of the mass conservation equation. In multi-fluid problems, a condition must be imposed on the interface between fluids. Even in fluid-structure interaction problems, an accurate imposition of boundary condition is very important.

If we want to impose slip boundary conditions to the problem, a case where the slip condition can be defined is when a correlation between the slip velocity and the tangential stress must be imposed. This relation is mediated through a material friction-like parameter. The slip condition is needed in several applications where a liquid flows on solid surfaces, and an example is the Navier boundary condition. As described in [9], the general slip condition can be illustrated with the Couette flow, where a flow is moving between two plates thanks to the movement of the upper plate, which is moving with a particular velocity. Figure 1.7 shows three different cases of slip. In (a), it can be seen that the velocity at the bottom is 0, which is the particular condition of no-slip condition; in (b), the velocity is greater than 0 so there is some slip; in the end in (c), the slip velocity is the same of the moving plate, so the condition applied is the free slip one. In this final case there is no dissipation of energy at the plate. A slip length h_{slip} can be defined as the distance from the lower plate to the point at zero velocity obtained extrapolating the linear velocity profile. This slip length is a property of the fluid-wall interface.

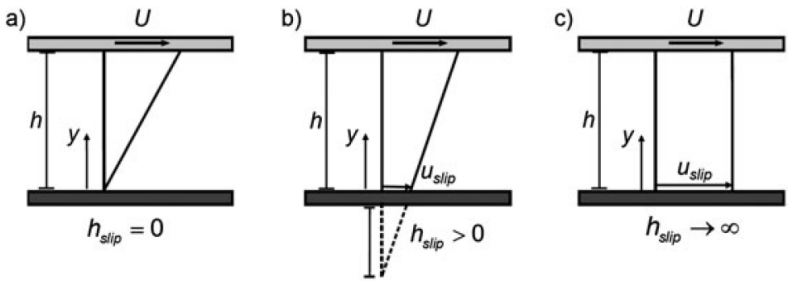

Figure 1.7: Different cases: (a) no slip ($h_{slip} = 0$), (b) slip ($h_{slip} > 0$), (c) free slip ($h_{slip} \to \infty$) [9]

In practice, the slip is present when a critical value of the tangential stress at the wall is reached, making this model an analogy with the Bingham one. This slip model is very useful for cases like the movement of a landslide over the side of a mountain. Examples of applications using the slip condition can be found in [9], [8] and [14].

Regarding inflow and outflow boundaries, the definition of the condition in the PFEM framework must be taken into account carefully. When a particular profile of velocity or pressure is imposed at the boundary, the nodes interested in this imposition move in the next time steps. In this way on the successive step they are no more forced to have the values imposed before, making the boundary condition definition lost. There are many way to deal with this problem, for example for inflows when the boundary nodes move away, a new set of points is introduced to occupy the empty space left. Cremonesi et al. [7, 10] instead defines fixed (Eulerian) nodes at the inlet so that they does not move in time and are always interested in the imposition of the condition values. For the outlet, the same comments regarding the inlet apply. No other big precautions should be adopted, if not that the nodes that go outside the computational domain must be relocated.

1.2. Models of transport

In this master thesis work, the interest is focused in considering a way to simulate the erosion and the transport of sediment in a river course. The aim shifts now in seeing what the literature has to offer in these regards.
Both the bed of a watercourse and its banks are composed of sediments that may be more or less cohesive. Depending on the current flowing through them, these may or may not move; the onset of motion depends on both the nature of the sediment and the speed of the current. The movement of the detached particles is called solid transport. Once the material has started moving, it can continue its motion in two substantially different ways:

1. Ground motion due to rolling, creeping or hopping: the material moves by rolling along the bottom or through alternating small jumps, detaching itself from the bottom for short periods and at a relatively small distance from the bottom (of the order of the particle size). The bottom transport causes important actions on hydraulic structures

2. Suspension motion: the particle is lifted to a height above the bottom of the order of the water level and then travels long distances without touching the bottom.

In figure 1.8, it is shown the two types of sediment movement, highlighting the different

ground motion of the sediment at the bed level.

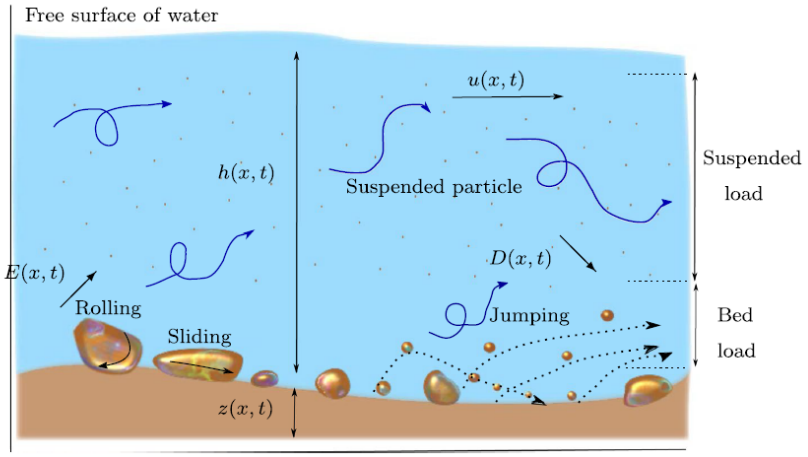

Figure 1.8: Sketch of bed load and suspended load sediment transport [16]

1.2.1. Suspension transport

For what concerns the suspended transport of sediment, an advection-diffusion equation is solved in order to find the volumetric concentration c:

$$\frac{\partial c}{\partial t} + \nabla \cdot \left(\mathbf{u} + w_s \frac{\mathbf{g}}{|\mathbf{g}|} \right) c = \nabla \cdot \left(\frac{\nu_t}{\sigma_c} \nabla \right) \tag{1.4}$$

w_s is the fall sediment velocity, defined as the velocity of the particle when dropped vertically in a quiescent fluid under the effect of gravity. ν_t is the sediment diffusivity and σ_c is the Schmidt number. Due to the interaction among settling grains, the settling velocity normally decreases as the concentration of the sediment increases. As shown in [29], the formula for w_s is:

$$w_s = (1 - c)^{\xi} \, w_{s0} \tag{1.5}$$

where w_{s0} is the settling velocity for natural sands in clear water, which is used in [32]:

$$w_{s0} = \frac{\nu}{d_{50}} \left[\left(10.36^2 + 1.049 D_*^3 \right)^{1/2} - 10.36 \right] \tag{1.6}$$

In [6], a different formulation of the falling sediment velocity is described, where it is shown that is independent on the concentration but dependent on the diameter d_{50}. [16] instead presents an equation constructed by considering the shallow water assumption,

which make the problem one-dimensional by integrating along the height of the water level. This equation inserts the effect of erosion and deposition, two terms that will be further studied in 1.3.1.

$$\frac{\partial (hc)}{\partial t}(x,t) + \frac{\partial (huc)}{\partial x}(x,t) = E(x,t) - D(x,t) \tag{1.7}$$

This model is very approximative given the hypothesis, but interesting since it considers the sediment deposition and erosion.

1.2.2. Bedload transport

The objective is now to understand whether in a certain watercourse, characterised by a certain flow rate (and velocity), the sediment on the bed is moving or standing still. Considering a model of a watercourse with sediment on the bottom, gradually increasing flows are introduced. As long as we do not consider a certain flow limit value, the sediment remains stationary on the river bed. Calling F the forces that originate motion and R the hydrodynamic resistance of the particles, we have:

- if $F < R$, the particles do not move;
- if $F > R$, the particles do move;

Consequently, there will be a flow Q such that the limit condition $F = R$ is reached. This situation is called limit equilibrium condition or incipient motion condition. However, it is more convenient to analyse the situation dynamically by considering the tangential actions at the boundary. The actions that the current exerts on the riverbed follow the direction of the current itself; due to the action-reaction principle, the forces that the bottom exert on the current are in the opposite direction. It is often convenient to refer to a mean tangential boundary action, called τ_0.
Considering a channel with a slope i_f, with a current in uniform motion, and isolating a section of riverbed of length L, we have that:

- The resistance acting on the bottom is $\tau_0 Lp$ where p is the wet perimeter;
- The acting force (water weight projected along the direction of the motion) is $\gamma \Omega L i_f$. γ is the specific weight and Ω is the area of the section.

Equalising the two terms gives the value of the tangential tension acting on the bottom in uniform motion:

$$\tau_0 = \gamma R i_f \tag{1.8}$$

Shields' investigation shows that particles on the bottom only stand still if

$$\tau_0 < \tau_{0,crit} \tag{1.9}$$

It is assumed that under critical conditions the resistance to motion of granules of diameter d and specific gravity γ_s equals the drag force at the bottom at the start of transport. Resistance depends linearly on the weight of the submerged granule (i.e. its own weight adjusted for Archimedes' thrust) and is therefore the final relation in the critical condition reads:

$$(\gamma_s - \gamma)d^3 = \frac{1}{\theta_{crit}}\tau_{0,crit}d^2 \tag{1.10}$$

So:

$$\theta_{crit} = \frac{\tau_{0,crit}}{(\gamma_s - \gamma)d} \tag{1.11}$$

θ_{crit} is the critical Shields number, which is basically the adimensionalisation of the shear stress. Generally to describe the current state of stress on the surface of the riverbed, the Shields parameter will be defined generally as in equation 1.12.

$$\theta = \frac{\tau}{(\gamma_s - \gamma)d} \tag{1.12}$$

If $\theta > \theta_{crit}$, the critical value is exceeded and on the bed level there will be a movement of the sediment. This will introduce a bedload transport per unit width. In [20], is presented a formulation of this new variable:

$$q_b = \begin{cases} 18.74\,(\theta - \theta_c)\,(\theta^{0.5} - \theta_c^{0.5})\,\sqrt{Rgd_{50}}d_{50} & \text{if } \theta > \theta_c \\ 0 & \text{if } \theta < \theta_c \end{cases} \tag{1.13}$$

$$\theta = \frac{\tau}{\rho g R d_{50}} \tag{1.14}$$

$$R = \frac{\rho_{sed} - \rho}{\rho} \tag{1.15}$$

which is a formula from the work of Engelund and Fredsøe [12]. Here, the critical value of the Shields parameter value is proposed by Allen [1]:

$$\frac{\theta_c}{\theta_{co}} = cos\beta + \frac{sin\beta}{tan\phi} \tag{1.16}$$

β is the slope angle between the sand bed and the horizontal plane and ϕ is the sediment angle of repose. θ_{co} is the threshold shields parameter that can be calculated following [32]:

$$\theta_{co} = \frac{0.3}{1 + 1.2D_*} + 0.055\left[1 - exp\left(-0.02\right)D_*\right] \tag{1.17}$$

where D_* is the dimensionless sand size.
Considering the morphological formation of the bed which may not be flat, the slope effect has to be considered. It modifies the value of the components of the bed load transport rate per unit width by considering also the elevation of the bed.

$$q_{bi} = q_b\frac{\tau_i}{|\tau|} - C|q_b|\frac{\partial\eta}{\partial x_i} \tag{1.18}$$

C is the constant which is used to reflect the slope effect on the sediment flux. Considering a particular direction, when the bed has a positive derivative, the value of q_b in that direction is decreased since gravity works against the movement of the sediment at the bed level. If the bed has a negative derivative, the opposite happens.

1.3. Models of erosion

To describe the morphological change of the bed elevation, different approaches are available in the literature. Some of them aim to describe it microscopically, considering the impact of the single particle with the bed. Others try to model the elevation change considering a new variable which is the bed height.

1.3.1. Exner equation

The Exner equation gives a way to describe the change in the height of the bed elevation. It is recovered by applying the mass continuity balance on the sediment:

$$\frac{\partial \eta}{\partial t} = \frac{1}{1-n}\left(-\nabla \cdot \mathbf{q_b} + D - E\right) \tag{1.19}$$

η is the bed height, n is the porosity of the bed. q_b is the bedload transport rate as we have seen it in equation 1.13. D and E are respectively the deposition rate and the entrainment rate of the sediment at the bed level, which are modeled in many different ways. In [30], Van Rijn defines them as:

$$D = c_s w_s \tag{1.20}$$

$$E = \frac{\nu + \nu_t}{\sigma_c}\frac{\partial c}{\partial z} \tag{1.21}$$

c_s is the sediment concentration very near to the bed. To compute this value, many empirical models can be adopted. It is interesting to notice that E depends on the vertical concentration gradient, which has to be evaluated near the bed. Claire et al. [6] evaluates D and E in the Exner equation at $z = \eta + \delta$, where δ is the interface that divides the bedload zone and the suspended sediment one. The structure of the Exner equation relates the erosion of the bed with the transport model that are described in 1.2. In this way erosion is a consequence of the actions of transport.

Another formulation for E and D can be found in [16]. The entrainment is due to turbulence, while the deposition is due to gravity:

$$E = \begin{cases} \varphi \frac{(\theta - \theta_c)u}{hd^{0.2}} & \text{if } \theta \geq \theta_c \\ 0 & \text{if } \theta < \theta_c \end{cases} \tag{1.22}$$

$$D = \gamma c \omega_0 \left(1 - \gamma c\right)^m \tag{1.23}$$

φ is a constant dimensionless number related to the sediment properties, while γ is the non-equilibrium adaption coefficient of the suspended load. For further information on these parameters check [5] and [34].

In many works the hypothesis of non cohesive sediment is made. For cohesive sediment, the critical shear stress for erosion is different from the critical shear stress for deposition, and at a particular bed shear stress, cohesive sediments undergo either erosion or deposition but not both simultaneously. Cohesionless sediments, on the other hand, have only one critical condition that is valid for both erosion and deposition and undergo simultaneous erosion and deposition processes under all bed shear stress conditions.

1.3.2. Particle erosion

A different way to approach the erosion problem can be seen by studying the particle contact with the bed of the river. The process of simulation of the wall wear is divided in three steps, as shown in figure 1.9 [28]. First, the simulation of the particle-laden flow is carried; then, the impact of the particle with the wall is analysed; in the end, a proper erosion model is applied and some particles are freed from the wall, becoming part of the flow. This procedure is iterated for each time step.

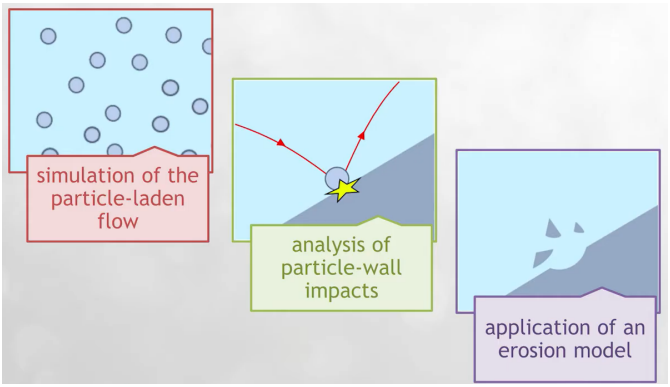

Figure 1.9: Steps of erosion [28]

The case of study will be the impact erosion on ductile targets, which is divided in two parts: cutting wear and deformation wear. The first phenomena consist in the formation of the crater by crawling. The removed bedload part is shifted to the side of the hole; the other phenomena consists in the nearly vertical impact of the particle with the wall. The hole is formed by compression. In [24], these two mechanisms are summed to form a new variable which is the total loss of material produced by an impact:

$$E_p = F_s \left(E_c + E_d\right) \tag{1.24}$$

F_s is a numerical coefficient related to particle shape, that take values of 1, 0.53, and 0.2 for sharp, nearly-rounded, and fully-rounded [22]. The formulation of the two components

is:

$$E_c = \begin{cases} C_1 m_p \frac{|v_p|^{2.41} sin\theta_p (2Kcos\theta_p - sin\theta_p)}{2K^2} & \text{if } \theta_p \leq K \\ C_1 m_p \frac{|v_p|^{2.41} cos^2\theta_p}{2} & \text{otherwise} \end{cases} \tag{1.25}$$

$$E_d = \begin{cases} C_2 m_p \left(|v_p|\, sin\theta_p - U_{tsh}\right) & \text{if } |v_p|\, sin\theta_p > U_{tsh} \\ 0 & \text{otherwise} \end{cases} \tag{1.26}$$

The parameters C_1, C_2, K and U_{tsh} are related to the material of the particle. v_p and θ_p are the particle velocity and angle of impact. It is worth to notice that the deformation wear occurs only if the component of the impact velocity normal to the wall exceeds the threshold value U_{tsh}.

The erosion potential caused by a particle depends on several types of parameters, which have direct or indirect effects on the detachment of material from the wall:

- Particle size
- Particle shape
- Particle material
- Impact velocity
- Impact angle

They all convey in this formulation that has to be found through experiments:

$$\dot{E}_p = \dot{m}_p f\left(v_p, \theta_p, \text{particle}, \text{target}\right) \tag{1.27}$$

Equations 1.25 and 1.26 are found starting from this functional relation. Described in a work of Messa et al. [27], the empirical relation is:

$$\dot{E}_i = \dot{m}_p F_s K v_p^n f\left(\theta_p\right) \tag{1.28}$$

$$f\left(\theta_p\right) = \left(sin\theta_p\right)^{b_1} \left(1.5 - sin\theta_p\right)^{b_2} \tag{1.29}$$

For each particle, one can calculate the mass flow of material removed from the soil $\dot{E}_i$ and then derive the amount of material removed per cell by summing the values of all

particles. From this value, one can then derive the penetration rate, i.e. the rate at which the erosion depth of the cell increases:

$$\dot{\eta}_{cell} = \frac{\sum_{i \in \text{cell}} \dot{E}_i}{A \rho_t} \tag{1.30}$$

From these information, the integral erosion ratio can be recovered. This value tells in what percentage the material is eroded with respect to total mass impacting the wall.

$$IER = \frac{\sum_{i \in \text{cell}} \dot{E}_i}{\dot{M}_s} \tag{1.31}$$

From this value, the number of particles that are released from the solid can be derived: simply multiply IER by the total number of particles. This can be useful in a Lagrangian view of the problem: the freed particles become part of the computation of the total system of equation.

2 | Sediment equation: Diffusion problem

In this chapter a first implementation of the sediment equation will be discussed. The action inspected here is the diffusion of the sediment in a fluid: this is helpful to see how the concentration changes due to the presence of a gradient in the domain. It may serve in concrete applications where the fluid is still and the sediment moves within it to find an equilibrium condition that satisfies all the boundary conditions. Generally, the aim of this thesis is to integrate correctly the sediment model within the PFEM framework. The fluid model is complete, the task is to couple it with the sediment. The equation that has to be implemented is a diffusion advection equation, and it can be found in many different papers present in the literature. It is described in section 1.2 and it reads:

$$\frac{\partial c}{\partial t} + \nabla \cdot \left[\left(\mathbf{u} + w_s \frac{\mathbf{g}}{|\mathbf{g}|} \right) c \right] = \nabla \cdot \left(\frac{\nu_t}{\sigma_c} \nabla c \right) \tag{2.1}$$

It is worth to underline that the transported particles do not have mass, so the sediment is treated like a concentration which is passively transported and diffused in the fluid, that in our case of study is water. For all the test studies, cohesionless sediment is considered. This work will be structured in the following way: as the first step, the base model with many hypothesis will be treated, then all the other pieces are inserted one by one. In this way, the full model will be built step by step giving a good overview of the meaning of each part.

2.1. Weak formulation

The first target is to study only the diffusion motion of the sediment. To do this the advection component should be eliminated: this can be achieved by considering null the effect of the gravity on the sediment. In this way the falling velocity term can be neglected by leaving us to:

$$\frac{\partial c}{\partial t} + \nabla \cdot (\mathbf{u}c) = \nabla \cdot \left(\frac{\nu_t}{\sigma_c} \nabla c \right) \tag{2.2}$$

In this chapter the focus remains still on the diffusive part of the equation: to this aim the fluid is still and does not move, so that in equation 2.2 $\mathbf{u} = 0 \ \frac{m}{s}$. Suppose also that the ratio between the sediment diffusivity and the Schmidt number is constant. The final form of the equation reads:

$$\frac{\mathrm{d}c}{\mathrm{d}t} = \frac{\nu_t}{\sigma_c} \Delta c \tag{2.3}$$

By rewriting the equation in this way, the Lagrangian framework can be exploited giving the described benefits in section 1.1. Due to the null velocity, the total derivative of the concentration appears: numerically speaking this term will be very easy to discretize since the sediment particles are followed.

The generic problem to solve is shown in 2.4: next step is to write its weak formulation.

$$\begin{cases} \dfrac{\mathrm{d}c}{\mathrm{d}t} - \dfrac{\nu_t}{\sigma_c} \Delta c = 0 \qquad \forall \mathbf{x} \in \Omega \subseteq \mathbb{R}^2, \quad \forall t \in (0, T] \\ c\left(\mathbf{x}, t = 0\right) = \overline{c}\left(\mathbf{x}\right) \qquad \forall \mathbf{x} \in \Omega \\ c\left(\mathbf{x}, t\right) = h\left(\mathbf{x}, t\right) \qquad \forall \mathbf{x} \in \partial\Omega = \Gamma \end{cases} \tag{2.4}$$

The choice of the space for the solution is $H^1(\Omega)$. Below are defined the solution and test spaces used for the derivation of the weak formulation.

$$V = \left\{ v \in H^1(\Omega) : v = h \ \ on \ \ \Gamma \right\} \tag{2.5}$$

$$V_0 = H^1_\Gamma(\Omega) \tag{2.6}$$

From the first space the solution is taken, while from the second one the test function is taken. V is defined in such a way that on the edge the function is equal to the boundary datum, while V_0 is defined like the last but considering a null value on the boundary. Since the problem is an elliptic one, the property of elliptic regularity applies so that it can be assured that the function is in $H^2(\Omega)$. This will be helpful when the error estimate are presented and discussed.

Multiply the equation with a function belonging to the test space and then integrate over

the domain, applying integration by parts to the term with the Laplacian. Then drop the boundary term since in V_0 the values at the boundaries are null:

$$\begin{aligned}\int_\Omega \frac{\mathrm{d}c}{\mathrm{d}t} v \,\mathrm{d}\Omega \; - \int_\Omega \frac{\nu_t}{\sigma_c} \Delta c \; v \,\mathrm{d}\Omega \; = \int_\Omega \frac{\mathrm{d}c}{\mathrm{d}t} v \,\mathrm{d}\Omega \; + \\ + \int_\Omega \frac{\nu_t}{\sigma_c} \nabla c \cdot \nabla v \,\mathrm{d}\Omega = 0 \qquad \forall v \in V_0\end{aligned} \tag{2.7}$$

The lift operator is introduced, which allows us to solve the problem by considering homogeneous Dirichlet boundary conditions:

$$c = \widehat{c} + \widetilde{h} \tag{2.8}$$

where $\widetilde{h}$ is defined such that $h = \widetilde{h}|_\Gamma$. In practice $\widetilde{h}$ is the extension of the boundary datum to the whole domain: is zero everywhere except on the boundary. After making this substitution in the equation, take to the second member all terms containing $\widetilde{h}$.

$$\begin{aligned}\int_\Omega \frac{\mathrm{d}\widehat{c}}{\mathrm{d}t} v \,\mathrm{d}\Omega \; + \int_\Omega \frac{\nu_t}{\sigma_c} \nabla \widehat{c} \cdot \nabla v \,\mathrm{d}\Omega = - \int_\Omega \frac{\mathrm{d}\widetilde{h}}{\mathrm{d}t} v \,\mathrm{d}\Omega \; + \\ - \int_\Omega \frac{\nu_t}{\sigma_c} \nabla \widetilde{h} \cdot \nabla v \,\mathrm{d}\Omega = 0 \qquad \forall v \in V_0\end{aligned} \tag{2.9}$$

From now on $\widehat{c}$ will be only c for simplicity. Define the bilinear form and the functional, which will be useful later:

$$a : V_0 \times V_0 \to \mathbb{R} \quad s.t. \quad a\,(k, r) = \int_\Omega \frac{\nu_t}{\sigma_c} \nabla k \cdot \nabla r \,\mathrm{d}\Omega \tag{2.10}$$

$$F : V_0 \to \mathbb{R} \quad s.t. \quad F\,(v) = - \int_\Omega \frac{\mathrm{d}\widetilde{h}}{\mathrm{d}t} v \,\mathrm{d}\Omega \; - \int_\Omega \frac{\nu_t}{\sigma_c} \nabla \widetilde{h} \cdot \nabla v \,\mathrm{d}\Omega \tag{2.11}$$

In the end, the weak formulation is: given $c\,(t = 0) = \overline{c}$, find $c \in V_0$ such that $\forall t \in (0, T]$ the equation 2.12 is satisfied.

$$\int_\Omega \frac{\mathrm{d}c}{\mathrm{d}t} \; v \,\mathrm{d}\Omega \; + a\,(c, v) = F\,(v) \qquad \forall v \in V_0 \tag{2.12}$$

2.1.1. Discretization in space and time

The discretization in space is now introduced: first of all define the space from which is taken the basis that will allow us to write the solution as a linear combination of its elements. The domain is discretized and the partition Υ_h is introduced, creating a number N of nodes all contained in the subset $\Phi = \{\mathbf{x}_1, \mathbf{x}_2, ..., \mathbf{x}_N\}$. Below are showed the definition of the piecewise linear finite element space and the new discretized solution and test spaces:

$$X_h^1 = \left\{ v \in C^0(\Omega) : v|_K \in P_1(\Omega) \quad \forall K \in \Upsilon_h \right\} \tag{2.13}$$

$$V_h = V \cap X_h^1 \quad , \quad V_{h,0} = V_0 \cap X_h^1 \tag{2.14}$$

Define the basis composed by the element-wise linear functions $\{\varphi_j\}_{j=1}^N \subseteq V_{h,0}$. Each function is defined as:

$$\varphi_j(\mathbf{x}) = \begin{cases} 1 & \text{if } \mathbf{x} = \mathbf{x}_j \\ 0 & \text{otherwise} \end{cases} \tag{2.15}$$

Now given the finite element approximated problem, the formulation becomes: find $c_h \in V_{h,0}$ such that for $c_h(t=0) = \overline{c}$ and $\forall t \in (0, T]$:

$$\int_\Omega \frac{\mathrm{d}c_h}{\mathrm{d}t} v_h \, \mathrm{d}\Omega + a_h(c_h, v_h) = F_h(v_h) \qquad \forall v_h \in V_{h,0} \tag{2.16}$$

Given the definition of the functional in 2.11, the force term on the right in this case will be zero since the datum will be always piecewise constant in space and in time. Since the solution c_h belongs to the discretized solution space, it can be written as the linear combination of the elements of the basis defined in 2.15:

$$c_h(\mathbf{x}, t) = \sum_{j=1}^{N} c_j(t) \varphi_j(\mathbf{x}) \tag{2.17}$$

Substitute this expression in the equation and take $v_h = \varphi_i(\mathbf{x})$ with $i = 1, 2, ...N$:

$$\int_{\Omega} \frac{\mathrm{d}}{\mathrm{d}t} \left(\sum_{j=1}^{N} c_j(t)\, \varphi_j(\mathbf{x}) \right) \varphi_i(\mathbf{x})\ \mathrm{d}\Omega + a_h \left(\sum_{j=1}^{N} c_j(t)\, \varphi_j(\mathbf{x}), \varphi_i(\mathbf{x}) \right) = 0 \tag{2.18}$$

The time derivative can be brought outside the integral because the domain is independent from time. Since the integral of the sum is equal to the sum of the integrals, the summation can be taken outside. This can be done with the nodal variables $c_j(t)$. In the end, the system ends up to be written like this:

$$\sum_{j=1}^{N} \left(\int_{\Omega} \varphi_j(\mathbf{x})\ \varphi_i(\mathbf{x})\ \mathrm{d}\Omega \right) \frac{\mathrm{d}c_j(t)}{\mathrm{d}t} + \sum_{j=1}^{N} a_h\left(\varphi_j(\mathbf{x}), \varphi_i(\mathbf{x})\right) c_j(t) = 0 \tag{2.19}$$

Now introduce the matrices that will allow the definition of the linear system. The two matrices are the mass one and the stiffness one.

$$M_{ij} = \int_{\Omega} \varphi_j(\mathbf{x})\, \varphi_i(\mathbf{x})\, \mathrm{d}\Omega \tag{2.20}$$

$$\begin{aligned} A_{ij} &= a\left(\varphi_j(\mathbf{x}), \varphi_i(\mathbf{x})\right) \\ &= \int_{\Omega} \frac{\nu_t}{\sigma_c} \nabla\varphi_j(\mathbf{x}) \cdot \nabla\varphi_i(\mathbf{x})\ \mathrm{d}\Omega \end{aligned} \tag{2.21}$$

After having defined the matrices, it is straightforward to notice in the summation the matrix product, that allows to reduce the equation to this linear system:

$$\underline{\underline{\mathbf{M}}}\dot{c}(t) + \underline{\underline{\mathbf{A}}}c(t) = 0 \tag{2.22}$$

Clearly, since the number of nodes are N, it should be that $\underline{\underline{\mathbf{M}}} \in \mathbb{R}^{N\times N}$ and $\underline{\underline{\mathbf{A}}} \in \mathbb{R}^{N\times N}$. Passing to the discretization in time, it is important to understand how to treat the time derivative of the concentration. The time domain is partitioned in steps with $\Delta t^n = t^{n+1} - t^n$, which are not necessarily equal.

Since a Lagrangian mesh is used, the remeshing phase has to be performed when the grid is too distorted. This implies a high computational cost even if in this model this phase is done by only making a new connectivity. So it is helpful to use the very simple explicit Euler approximation of the equation, that saves some computational cost gained by remeshing.

$$\dot{\underline{c}}\left(t^{n+1}\right) = \frac{\underline{c}\left(t^{n+1}\right) - \underline{c}\left(t^{n}\right)}{\Delta t^{n}} \tag{2.23}$$

All the other terms in the equation are considered as known at the time instant t^n. The final system that has to be solved is:

$$\underline{\underline{\mathbf{M}}}\underline{\mathbf{c}}^{n+1} = \left(\underline{\underline{\mathbf{M}}} - \underline{\underline{\mathbf{A}}}\Delta t^{n}\right)\underline{\mathbf{c}}^{n} = \underline{\mathbf{f}}^{n} \tag{2.24}$$

2.1.2. Matrix assembling

Consider now the construction of the diffusion matrix $\underline{\underline{\mathbf{A}}}$. Consider a triangular element: the local concentration can be written in this way:

$$\begin{aligned} c &= \begin{bmatrix} \varphi_1(x,y) & \varphi_2(x,y) & \varphi_3(x,y) \end{bmatrix} \begin{bmatrix} c_1 \\ c_2 \\ c_3 \end{bmatrix} \\ &= \underline{\mathbf{l}}^T \underline{\mathbf{c}}^L \end{aligned} \tag{2.25}$$

So that the gradient is

$$\begin{aligned} \nabla c = \nabla\left[\varphi_1 c_1 + \varphi_2 c_2 + \varphi_3 c_3\right] &= \begin{bmatrix} \varphi_{1,x} c_1 + \varphi_{2,x} c_2 + \varphi_{3,x} c_3 \\ \varphi_{1,y} c_1 + \varphi_{2,y} c_2 + \varphi_{3,y} c_3 \end{bmatrix} \\ = \begin{bmatrix} \varphi_{1,x} & \varphi_{2,x} & \varphi_{3,x} \\ \varphi_{1,y} & \varphi_{2,y} & \varphi_{3,y} \end{bmatrix} \begin{bmatrix} c_1 \\ c_2 \\ c_3 \end{bmatrix} &= \underline{\underline{\mathbf{B}}}\underline{\mathbf{c}}^L \end{aligned} \tag{2.26}$$

Considering the definition 2.21, the effect of the diffusion term on the concentration of the i-th node is:

$$\begin{aligned} a(c, \varphi_i) &= \int_\Omega \frac{\nu_t}{\sigma_c} \nabla c \cdot \nabla \varphi_i \, \mathrm{d}\Omega = \int_\Omega \frac{\nu_t}{\sigma_c} \underline{\underline{\mathbf{B}}}\underline{\mathbf{c}}^L \cdot \nabla \varphi_i \, \mathrm{d}\Omega \\ &= \int_\Omega \frac{\nu_t}{\sigma_c} \underline{\underline{\mathbf{B}}}^T \nabla \varphi_i \cdot \underline{\mathbf{c}}^L \, \mathrm{d}\Omega \\ &= \underline{\mathbf{A}}_i \cdot \underline{\mathbf{c}}^L \end{aligned} \tag{2.27}$$

So the local diffusion matrix can be finally written as:

$$\underline{\underline{\mathbf{A}}}^L = \begin{bmatrix} \underline{\mathbf{A}}_1^T \\ \underline{\mathbf{A}}_2^T \\ \underline{\mathbf{A}}_3^T \end{bmatrix} = \begin{bmatrix} \int_\Omega \frac{\nu_t}{\sigma_c} \left(\nabla\varphi_1\right)^T \underline{\underline{\mathbf{B}}} \mathrm{d}\Omega \\ \int_\Omega \frac{\nu_t}{\sigma_c} \left(\nabla\varphi_2\right)^T \underline{\underline{\mathbf{B}}} \mathrm{d}\Omega \\ \int_\Omega \frac{\nu_t}{\sigma_c} \left(\nabla\varphi_3\right)^T \underline{\underline{\mathbf{B}}} \mathrm{d}\Omega \end{bmatrix} = \int_\Omega \frac{\nu_t}{\sigma_c} \underline{\underline{\mathbf{B}}}^T \underline{\underline{\mathbf{B}}} \mathrm{d}\Omega \tag{2.28}$$

Each integral is computed using the mid point rule: all the values inside the integral are evaluated at the mid point and then this value is multiplied by the area of integration. Passing to the mass matrix, the transformation onto the elementary triangle is performed. This can be done through a linear transformation of the coordinate system, which includes the computation of the Jacobian. The linear transformation map is shown in figure 2.1:

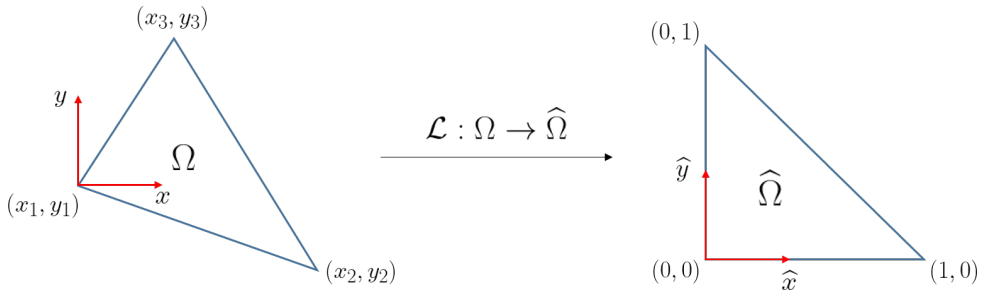

Figure 2.1: Transformation map from a distorted element to the elementary triangle

$$M_{ij} = \int_\Omega \varphi_j\left(\mathbf{x}\right) \varphi_i\left(\mathbf{x}\right) \mathrm{d}\Omega = \int_{\widehat{\Omega}} \varphi_j\left(\widehat{\mathbf{x}}\right) \varphi_i\left(\widehat{\mathbf{x}}\right) J \mathrm{d}\widehat{\Omega} \tag{2.29}$$

In this case the Jacobian is simply two times the area of the element. Keeping in mind that the integrals are calculated via the mid-point rule, the final matrix is:

$$\underline{\underline{\mathbf{M}}}^L = \frac{area}{12} \begin{bmatrix} 2 & 1 & 1 \\ 1 & 2 & 1 \\ 1 & 1 & 2 \end{bmatrix} \tag{2.30}$$

Finally the global matrices are composed by the local ones, passing through the connectivity of the grid.

2.1.3. Code implementation and system resolution

The overall assembling is done with a parallel computation, involving different cores in order to speed up the code. Each core takes on a fraction of the total number of elements and of each element computes its local matrix. Then this is immediately applied to the local concentration, giving as result a vector shown in 2.31.

$$d_i^L = \sum_{j=1}^{3} \left(-A_{ij}^L c_j^L\right) \qquad \text{for} \quad i = 1, 2, 3 \tag{2.31}$$

This diffusion vector called $\underline{\mathbf{d}}^L$ is added to the global vector through the connectivity. In this way each core has a part of the global diffusion vector $\underline{\mathbf{d}}$.
As it may be seen from 2.30, recovering the mass matrix is not a big deal computationally speaking. After each core computes the mass matrices for the elements available to them, a lumping is done so that each core has a vector containing the sum of the values on the columns.

$$m_i^L = \sum_{j=1}^{3} M_{ij}^L \qquad \text{for} \quad i = 1, 2, 3 \tag{2.32}$$

In the end, each core computes its global mass lumped vector m_i passing through the connectivity of the mesh. The resolution part of the system in the code is treated with a for loop on the nodes. Until now, every core has computed their part of the global vectors $\underline{\mathbf{m}}$ and $\underline{\mathbf{d}}$. Now a summation of these is done over all the cores, giving as result two complete vectors.
During the assembling of the global vectors $\underline{\mathbf{m}}$ and $\underline{\mathbf{d}}$, only the internal nodes are considered and not then boundary ones. This is done because the boundary conditions are applied directly to the solution vector and are not enforced automatically by solving the linear system. This means that in the code the dimensions of the global vectors are $(N - N_\Gamma)$, where N_Γ is the number of boundary nodes.
Then an analysis on the type of node considered is done. Each node is considered in a way such that it has a label in relation of where it is. If it is on the boundary, there is a Boolean variable called "bound" that will have assigned the value "True". Vice versa, the label will be "False" if the node is internal. To each node $\mathbf{x}_i$ in the for loop, its type is checked: if the considered point is on the boundary the value c_i is imposed; otherwise, the solution system is solved by performing the computation shown in 2.33. This procedure is repeated at each iteration until the end of the simulation.

$$c_i^{n+1} = c_i^n + \frac{d_i \Delta t^n}{m_i} \tag{2.33}$$

2.2. Bucket diffusion problem

To test the functionality of the mathematical setting built for the diffusion part of the equation, a simple test case is considered. The domain is shown in figure 2.2: a bucket $\Omega = [0,4] \times [0,4]$ m is filled with water and at the interface with the atmosphere the concentration of the sediment is set to be 1. The system to solve is the one shown in 2.4, the boundary condition is 2.34 and the inital solution is 2.35.

$$h(\mathbf{x},t) = 1\ ,\ \ \mathbf{x} \in \partial\Omega = \Gamma \tag{2.34}$$

$$\overline{c}(\mathbf{x}) = \begin{cases} 1 & \text{if } y = 4 \\ 0 & \text{otherwise} \end{cases} \tag{2.35}$$

σ_c will be always taken equal to 1. Instead the values of ν_t will change to make the code stronger and its effect will be inspected later.

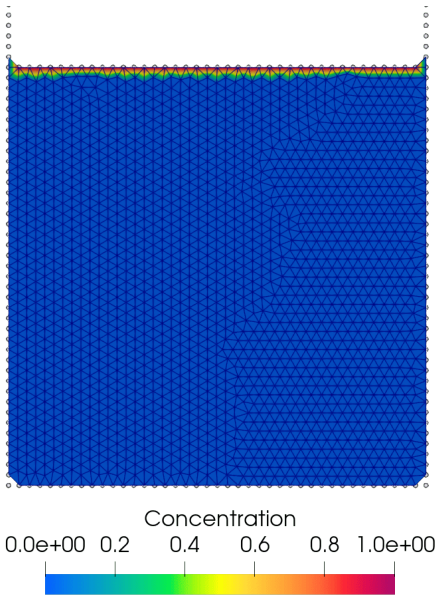

Figure 2.2: Initial solution, $h_m = 0.1\ m$

2.2.1. Stability in time issues

Performing several tests with different diffusivities values revealed many problems. For values of diffusivity in the order of $10^1\ \frac{m^2}{s}$ or bigger, the solution explodes. Bigger problems were created if the adopted mesh was finer. The mesh dimension h_m is an average value of

the external radius of the element. An example of critical instabilities is shown in figure 2.3, where the values of concentration are out of scale.

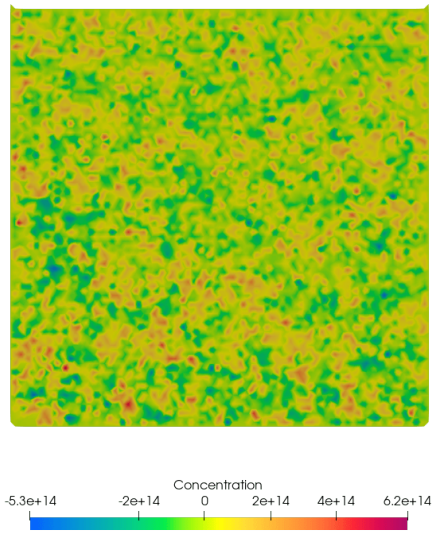

Figure 2.3: $\nu_t = 10\ \frac{m^2}{s}$, $\sigma_c = 1$, $h_m = 0.1\ m$

This problem is related to the CFL condition: in order to not have stability issues, Δt^n must be recalibrated to consider the insertion of the new equation. Without the sediment equation the CFL condition reads [10]:

$$\Delta t^n = C_N \min_e \frac{h_e^n}{v_e} \tag{2.36}$$

where h_e is a current characteristic size of the deformed element e, v_e is the speed of dilational waves in the fluid depending on the element density and C_N is a safety parameter. The speed of dilational waves depends on the coefficient of comprimibility: it should be infinite in principle, but in our case it can be taken big and not infinity. This is due to the fact that the deviatoric stress is much bigger than the volumetric one, where inside is found the coefficient of comprimibility:

$$\sigma = \mathbf{D}\varepsilon = \sigma_{dev} + \sigma_{vol} \simeq \sigma_{dev} \tag{2.37}$$

$$\sigma_{vol} = \frac{k}{3}\varepsilon_{vol} \tag{2.38}$$

Since the volumetric component of the stress is neglected, the value of k and so of v_e can

be chosen to be big but not infinity. In this latter case, the approximation made in 2.37 would not be true. In the code its value is $v_e = 250\ \frac{m}{s}$.
For what concerns the modification of the CFL condition for the added sediment equation, a new velocity of propagation due to the diffusion of the particles is introduced. This velocity has been obtained by dividing the sediment diffusivity with the current characteristic size of the deformed element:

$$v_d = \frac{\nu_t}{h_e^n} \tag{2.39}$$

The modified CFL condition now writes:

$$\begin{aligned} \Delta t^n &= C_N \min_e \left(\frac{h_e^n}{v_e}, \frac{h_e^n}{v_d} \right) \\ &= C_N \min_e \left(\frac{h_e^n}{v_e}, \frac{(h_e^n)^2}{\nu_t} \right) \end{aligned} \tag{2.40}$$

This modification, along also with a change in the value of the constant C_N, heals the problem encountered. The results of the corrected simulation are shown in figure 2.4.

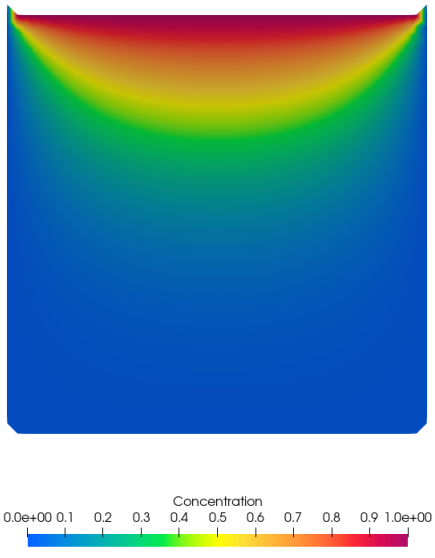

Figure 2.4: $\nu_t = 10\ \frac{m^2}{s}$, $\sigma_c = 1$, $h_m = 0.1\ m$

2.2.2. Convergence analysis

After having made different simulations varying the sediment diffusivity and the mesh size, a convergence analysis has been carried on. Since to do this task the analytical solution is required and this could be very long to find, a fictional solution is introduced. Its formula and shape are shown in equation 2.41 and in figure 2.5.

$$\widetilde{c}\left(x,y,t\right) = tsin\left(\pi x\right) cos\left(\pi y - \frac{\pi}{2}\right) \tag{2.41}$$

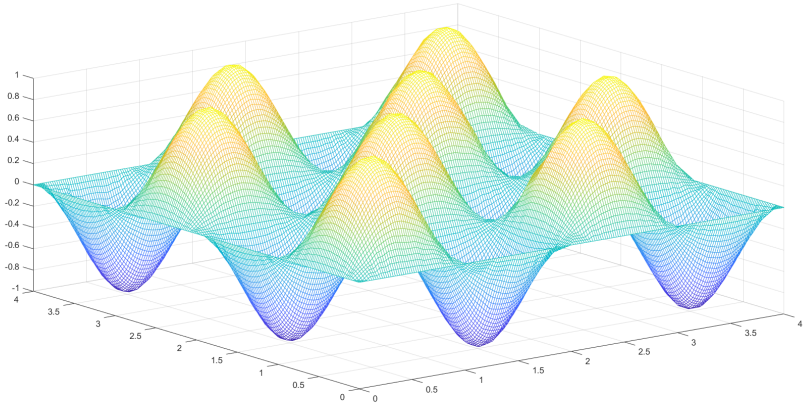

Figure 2.5: Fictional solution

It's a sinusoidal function which goes to zero at the boundaries, meaning that the boundary conditions imposed must be slightly changed. In order to make the solution fit the equation, also a fictional force term must be inserted, which is computed in 2.42.

$$\begin{aligned}\frac{\mathrm{d}\widetilde{c}}{\mathrm{d}t} - \frac{\nu_d}{\sigma_c}\Delta\widetilde{c} &= sin\left(\pi x\right) cos\left(\pi y - \frac{\pi}{2}\right) + 2\pi^2\frac{\nu_d}{\sigma_c} tsin\left(\pi x\right) cos\left(\pi y - \frac{\pi}{2}\right) \\ &= \left(1 + 2\pi^2\frac{\nu_d}{\sigma_c}t\right) sin\left(\pi x\right) cos\left(\pi y - \frac{\pi}{2}\right) = \widetilde{f}\end{aligned} \tag{2.42}$$

This new forcing has been inserted in the assembling phase inside the vector $\underline{\mathbf{d}}$. The diffusion equation gives to the solution the property of elliptic regularity so that it is assured to be inside the Hilbert space $H^2\left(\Omega\right)$. The error considered is in $L^2\left(\Omega\right)$, which has this convergence estimate:

$$\left\|c - c_h\right\|_{L^2(\Omega)} \leq \overline{C} h^{r+1} \left|c\right|_{H^{r+1}(\Omega)} \tag{2.43}$$

c is the real solution of the continuous problem, c_h is the approximated one, $\overline{C}$ is a constant, r is the grade of the polynomials used to represent the solution and $|\cdot|$ is the semi-norm. Four different meshes have been used, with an average dimension of the elements of: 0.2 m, 0.1 m, 0.08 m and 0.05 m. In figure 2.6 is shown the convergence result and in table 2.1 are displayed the values computed.
In our case $r = 1$ so that the rate of convergence should be 2. Lower grid dimensions should have been used in order to capture the perfect quadratic behaviour of the error. With the available tools, this could not be done: the restriction on the number of mesh nodes in GID© (the meshing program) limits the minimum size to 0.05 m. Nevertheless, the convergence result is in line with the theory.

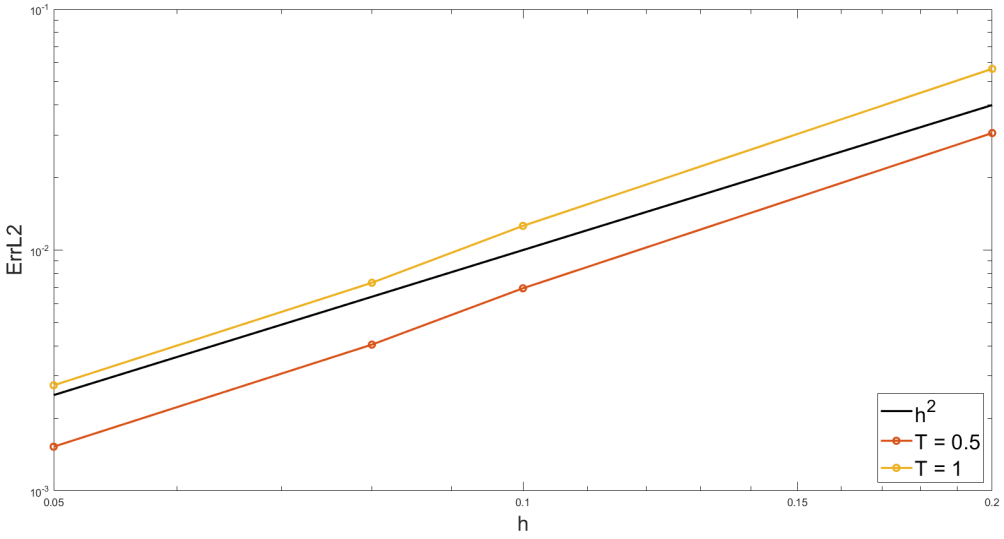

Figure 2.6: Plot of the L^2 error (log-log scale)

$\|c - c_h\|_{L^2(\Omega)}$				
h[m]	0.2	0.1	0.08	0.05
$T = 0.5s$	0.03607	0.00694	0.00405	0.00152
$T = 1s$	0.05656	0.01260	0.00731	0.00274

Table 2.1: Values of the L^2 errors

2.2.3. Comparison with ABAQUS © simulation

To assess the final accuracy of the model, a comparison with a simulation on the commercial software ABAQUS© has been done. The studied equation is analogous to the heat equation, which is implemented in the program and available for analysis. The set up is the same of the problem depicted in this chapter, with the only difference that the values

shown by the result interface are related to temperature. $T = 1°C$ has been imposed on the upper part of the domain, while $T = 0°C$ is the value on the other part of the boundary. The time of the simulation has been set to $1s$, the thermal diffusivity to 100 $\frac{m^2}{s}$ and the results at the final time are shown in figure 2.7a and 2.7b:

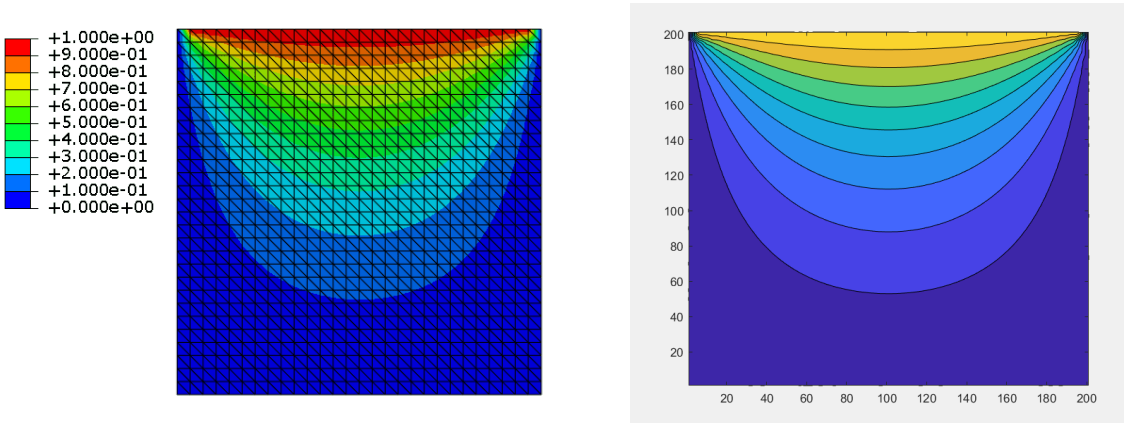

(a) ABAQUS: $\mu = 100\ \frac{m^2}{s}$, $h_m = 0.1\ m$ (b) PFEM: $\nu_t = 100\ \frac{m^2}{s}$, $\sigma_c = 1$, $h_m = 0.1\ m$

Figure 2.7: Isolines comparison between PFEM and ABAQUS simulations

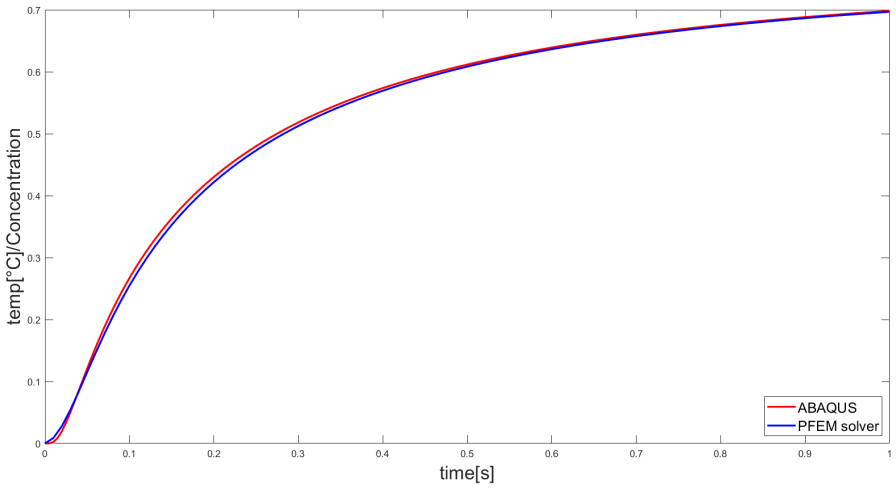

Figure 2.8: Comparison between the two solution in time in point $(2, 3.5)$

These images are showing the isolines with intervals of 0.1 unit between the different color schemes. The two solutions are in line with each other and so do the change of solution in time in a specific point, as shown in figure 2.8.

3 | Sediment equation: Transport through gravity

Now consider the effect of gravity on the sediment, an extra step compared to previous cases. This part of the phenomena can represent the deposit of sediment on the basis of the domain. Taking equation 2.1, the gravity term is somehow summed up with the velocity transport term. Normally the gravity is inserted in PDEs as a force term: however, in this case, the gravity can not act as a force because the sediment has no mass and can not be dropped down by a force. Still, to simulate the effect of gravity, a transport term is introduced: it is a velocity like parameter w_s called falling velocity, which has the same direction of the gravity. The falling velocity term may depend on the concentration, but for now is considered constant. From the equation 2.1, the new formulation dealt with in this chapter is recovered by dissolving the transport term:

$$\frac{\partial c}{\partial t} + \nabla \cdot (\mathbf{u}c) + \nabla \cdot \left(w_s \frac{\mathbf{g}}{|\mathbf{g}|} c \right) = \nabla \cdot \left(\frac{\nu_d}{\sigma_c} \nabla c \right) \tag{3.1}$$

As seen in 2.2, part of the advection term is considered null since $\mathbf{u} = 0 \ \frac{m}{s}$ and so the total derivative appears. In addition, consider constant ν_t and σ_c so that the Laplacian can appear.

$$\frac{\mathrm{d}c}{\mathrm{d}t} + \nabla \cdot \left(w_s \frac{\mathbf{g}}{|\mathbf{g}|} c \right) = \frac{\nu_t}{\sigma_c} \Delta c \tag{3.2}$$

3.1. Weak formulation

The new system to solve is the following:

$$\begin{cases} \dfrac{\mathrm{d}c}{\mathrm{d}t} + \nabla \cdot (w_s \dfrac{\mathbf{g}}{|\mathbf{g}|} c) - \dfrac{\nu_t}{\sigma_c} \Delta c = 0 \qquad \forall \mathbf{x} \in \Omega \subseteq \mathbb{R}^2, \quad \forall t \in (0, T] \\ c\left(\mathbf{x}, t = 0\right) = \bar{c}\left(\mathbf{x}\right) \qquad \forall \mathbf{x} \in \Omega \\ c\left(\mathbf{x}, t\right) = h\left(\mathbf{x}, t\right) \qquad \forall \mathbf{x} \in \partial\Omega = \Gamma \end{cases} \tag{3.3}$$

The final form of the new problem will not be derived step by step since it is practically the same of the diffusion problem shown in the previous chapter. It must be remembered that the fluid velocity is still zero because it has not yet been activated in the equation. To better approach the equation of the problem, apply the divergence term to the product so that:

$$\frac{\mathrm{d}c}{\mathrm{d}t} + \left(\nabla \cdot w_s \frac{\mathbf{g}}{|\mathbf{g}|}\right) c + \left(w_s \frac{\mathbf{g}}{|\mathbf{g}|}\right) \cdot \nabla c - \frac{\nu_t}{\sigma_c} \Delta c = 0 \tag{3.4}$$

The hyphotesis of constant falling velocity comes into play: considering this, the term with the divergence of the falling velocity goes away since all the terms derived are constant. In this way the final equation to study is:

$$\frac{\mathrm{d}c}{\mathrm{d}t} + \left(w_s \frac{\mathbf{g}}{|\mathbf{g}|}\right) \cdot \nabla c - \frac{\nu_t}{\sigma_c} \Delta c = 0 \tag{3.5}$$

Considering the 2D problem, the gravity acts downwards in the y direction and so the scalar product with the gradient of the concentration contains only the contribution of the derivative in y.

$$\frac{\mathrm{d}c}{\mathrm{d}t} - w_s \frac{\partial c}{\partial y} - \frac{\nu_t}{\sigma_c} \Delta c = 0 \tag{3.6}$$

The space of the solution and of the test function are the same as the problem of chapter 2. Integrate the equation over the domain and make the same simplifications of 2.7. In this way:

$$\int_\Omega \frac{\mathrm{d}c}{\mathrm{d}t} v \, \mathrm{d}\Omega + \int_\Omega \frac{\nu_t}{\sigma_c} \nabla c \cdot \nabla v \, \mathrm{d}\Omega - w_s \int_\Omega \frac{\partial c}{\partial y} v \, \mathrm{d}\Omega = 0 \qquad \forall v \in V_0 \tag{3.7}$$

The new inserted element in the equation is connected to a new bilinear form, which is define as:

$$p : V_0 \times V_0 \to \mathbb{R} \quad s.t. \quad p\left(k, r\right) = w_s \int_\Omega \frac{\partial k}{\partial y} v \, \mathrm{d}\Omega \tag{3.8}$$

Here a limit of the model can be pointed out: gravity acts only when there is a concentration gradient in the y direction. This is not an ideal situation since gravity should act in every case, but this is the main simplification of the suspended sediment model. The sediment does not have mass, it is carried by the fluid and does not interact with it. It is something which is passively transported around. In the next chapter, an upgrade that simulates this behaviour will be introduced. It is also noted that the lifting operator has been applied also in this case and the forcing functional introduced is set to zero due to the piecewise constant nature of the datum in space and in time.
The weak formulation for the gravity problem reads: given $c\left(t = 0\right) = \overline{c}$, find $c \in V_0$ such that $\forall t \in (0, T]$ the equation 3.9 is satisfied.

$$\int_\Omega \frac{\mathrm{d}c}{\mathrm{d}t} \, v \, \mathrm{d}\Omega \; - p\left(c, v\right) + a\left(c, v\right) = 0 \qquad \forall v \in V_0 \tag{3.9}$$

3.1.1. Discretization in space and time

As seen in section 2.1.1, a partition of the domain in a triangular mesh Υ_h is introduced and the finite element spaces X_h^1, V_h and $V_{h,0}$ are defined as in 2.13 and 2.14. Redefining the variables, functionals and bilinear forms in these spaces, the new weak formulation of the problem discretized in space is: find $c_h \in V_{h,0}$ such that for $c_h\left(t = 0\right) = \overline{c}$ and $\forall t \in (0, T]$ the equation 3.10 is satisfied.

$$\int_\Omega \frac{\mathrm{d}c_h}{\mathrm{d}t} \, v_h \, \mathrm{d}\Omega \; - p_h\left(c_h, v_h\right) + a_h\left(c_h, v_h\right) = 0 \qquad \forall v_h \in V_{h,0} \tag{3.10}$$

Exploiting the basis of the finite element test space of 2.15, the solution can be written as in 2.17, giving as result:

$$\begin{aligned} \sum_{j=1}^{N} \left(\int_\Omega \varphi_j\left(\mathbf{x}\right) \; \varphi_i\left(\mathbf{x}\right) \; \mathrm{d}\Omega \right) \; \frac{\mathrm{d}c_j\left(t\right)}{\mathrm{d}t} \; - \sum_{j=1}^{N} p_h\left(\varphi_j\left(\mathbf{x}\right), \varphi_i\left(\mathbf{x}\right)\right) c_j\left(t\right) + \\ + \sum_{j=1}^{N} a_h\left(\varphi_j\left(\mathbf{x}\right), \varphi_i\left(\mathbf{x}\right)\right) c_j\left(t\right) = 0 \end{aligned} \tag{3.11}$$

Then the new matrix related to the action of gravity is introduced in 3.12.

$$\begin{aligned} P_{ij} &= p_h\left(\varphi_j\left(\mathbf{x}\right), \varphi_i\left(\mathbf{x}\right)\right) \\ &= w_s \int_\Omega \frac{\partial \varphi_j}{\partial y} \varphi_i \, \mathrm{d}\Omega \end{aligned} \tag{3.12}$$

Considering this matrix along with the mass and stiffness matrices described in the previous chapter, the ordinary differential equation to solve in time is:

$$\underline{\underline{\mathbf{M}}}\dot{\underline{c}}\left(t\right) - \underline{\underline{\mathbf{P}}}\underline{c}\left(t\right) + \underline{\underline{\mathbf{A}}}\underline{c}\left(t\right) = 0 \tag{3.13}$$

As the other matrices, the gravity matrix belongs to the space $\mathbb{R}^{N\times N}$, where N is the number of nodes of the mesh domain. Regarding the discretization in time, the newly added term is considered as something known at each time instant since the time scheme used is the explicit Eulerian one. So the approximation of the time derivative is the same of 2.23. This gives rise to the following linear ststem to solve:

$$\underline{\underline{\mathbf{M}}}\underline{\mathbf{c}}^{n+1} = \left(\underline{\underline{\mathbf{M}}} + \underline{\underline{\mathbf{P}}}\Delta t^n - \underline{\underline{\mathbf{A}}}\Delta t^n\right)\underline{\mathbf{c}}^n = \underline{\mathbf{f}}^n \tag{3.14}$$

3.1.2. Assembling the gravity matrix

The gravity matrix is found following the computations done in section 2.1.2. To this aim, using the formulation of the concentration as 2.25, the y-derivative of the solution at the local mesh scale is recovered as:

$$\begin{aligned} \frac{\partial c}{\partial y} &= \frac{\partial}{\partial y}\left(\varphi_1 c_1 + \varphi_2 c_2 + \varphi_3 c_3\right) = \varphi_{1,y} c_1 + \varphi_{2,y} c_2 + \varphi_{3,y} c_3 \\ &= \begin{bmatrix} \varphi_{1,y} & \varphi_{2,y} & \varphi_{3,y} \end{bmatrix} \begin{bmatrix} c_1 \\ c_2 \\ c_3 \end{bmatrix} = \left(\underline{\underline{\mathbf{B}}}^T \hat{\underline{\mathbf{j}}}\right) \cdot \underline{\mathbf{c}}^L \\ &= \underline{\mathbf{b}}_y \cdot \underline{\mathbf{c}}^L \end{aligned} \tag{3.15}$$

with $\hat{\underline{\mathbf{j}}} = \begin{bmatrix} 0 \\ 1 \end{bmatrix}$ being the y-axis versor used to recover the second row of the $\underline{\underline{\mathbf{B}}}$ matrix, then denoted as the vector $\underline{\mathbf{b}}_y$.
Considering this notation, it is possible to write in a concise manner the local gravity matrix:

$$\begin{aligned} p\left(c,\varphi_i\right) &= w_s \int_{\Omega_k} \frac{\partial c}{\partial y}\varphi_i \, \mathrm{d}\Omega = w_s \int_{\Omega_k} \left(\underline{\mathbf{b}}_y \cdot \underline{\mathbf{c}}^L\right) \varphi_i \, \mathrm{d}\Omega \\ &= \left(w_s \int_{\Omega_k} \underline{\mathbf{b}}_y \varphi_i \, \mathrm{d}\Omega\right) \cdot \underline{\mathbf{c}}^L \\ &= \underline{\mathbf{P}}_i \cdot \underline{\mathbf{c}}^L \end{aligned} \tag{3.16}$$

The subscript k is related to the element on which the integral is made, since the computation of the matrix is local.

$$\underline{\underline{\mathbf{P}}}^L = \begin{bmatrix} \underline{\mathbf{P}}_1^T \\ \underline{\mathbf{P}}_2^T \\ \underline{\mathbf{P}}_3^T \end{bmatrix} = \begin{bmatrix} w_s \int_{\Omega_k} \underline{\mathbf{b}}_y^T \varphi_1 \, \mathrm{d}\Omega \\ w_s \int_{\Omega_k} \underline{\mathbf{b}}_y^T \varphi_2 \, \mathrm{d}\Omega \\ w_s \int_{\Omega_k} \underline{\mathbf{b}}_y^T \varphi_3 \, \mathrm{d}\Omega \end{bmatrix} = w_s \int_{\Omega_k} \underline{\mathbf{l}} \otimes \underline{\mathbf{b}}_y \, \mathrm{d}\Omega \tag{3.17}$$

The sign $\otimes$ refers to the outer product. As seen in the computation of the other matrices, each integral is computed using the mid point formula. The product between this matrix and the local concentration is added to the vector $\underline{\mathbf{d}}^L$ along with the diffusion action of the sediment.

$$d_i^L = \sum_{j=1}^{3} \left(-A_{ij}^L c_j^L + P_{ij}^L c_j^L\right) \qquad \text{for} \quad i = 1,2,3 \tag{3.18}$$

So it can be said that this vector is constructed like a force given by the actions of the diffusion and of the gravity. As before, through the connectivity the new global vector $\underline{\mathbf{d}}$ is recovered. In the end the solution at time instant t^{n+1} is found applying the equation 2.33.

3.2. Bucket with gravity transport

The domain in which the new problem is studied is the same as the previous chapter, namely the bucket filled with water. No movement of the fluid is imposed so that the study results can be analyzed considering the effect of gravity and comparing them with the ones due to only diffusion. The problem to study is 3.3 with the same conditions of the diffusion problem, namely 2.34 and 2.35.

3.2.1. Simulation results

In figures 3.1a and 3.1b is shown a comparison at time $T = 1s$ between considering the effect of gravity on the sediment and not considering it. It is clearly visible that the action of gravity enhances the movement of the sediment towards the bottom of the bucket. All the solutions are smooth and fulfill all the boundary conditions imposed by the problem. It can be seen that, considering that the height of the tank is $4m$, the sediment difference in positioning between the two cases is approximately of $1m$, reflecting that the values of the falling velocity is $w_s = 1\frac{m}{s}$. This is reasonable considering that the simulation time is 1 second.

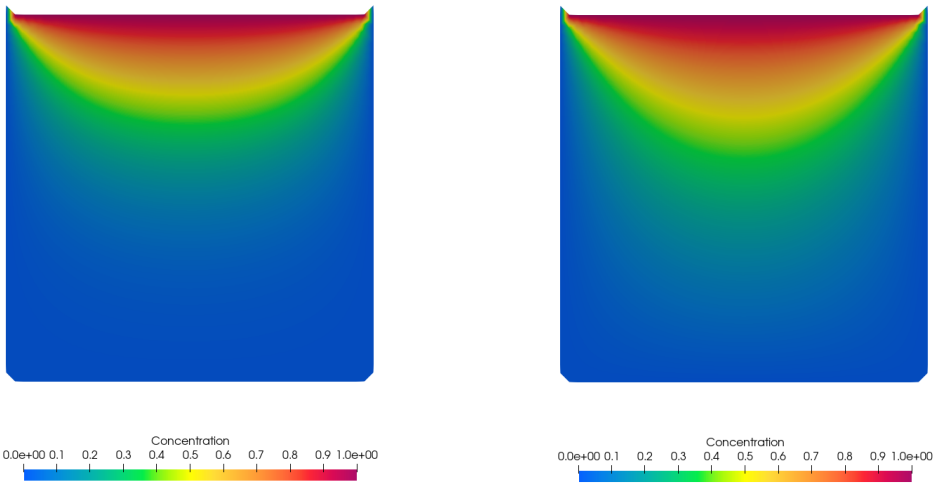

(a) $w_s = 0\ \frac{m}{s}$, $\nu_t = 1\ \frac{m^2}{s}$, $h_m = 0.1\ m$ (b) $w_s = 1\ \frac{m}{s}$, $\nu_t = 1\ \frac{m^2}{s}$, $h_m = 0.1\ m$

Figure 3.1: Comparison between considering gravity and not

3.2.2. Dependent formulation of the falling velocity on the concentration

Until now, the falling velocity parameter has been considered as something constant which does not depend on the solution. In this section, the effects of the concentration on w_s will be considered. Its formulation is like the one seen in equation 1.5:

$$w_s = (1 - c)^{\xi}\, w_{s0} \tag{3.19}$$

Given all the information in the literature, the hindered settling exponent is set equal to $\xi = 5$, while the settling velocity can be modified in function of the dimension of the

sediment particles. The weak formulation in this case changes since the second term in equation 3.4 is not eliminated. Considering the full equation in system 3.3, the transport term is bisected in this way:

$$\begin{aligned}\nabla \cdot (w_s \frac{\mathbf{g}}{|\mathbf{g}|} c) = \nabla \cdot \left(-w_s \bar{j} c\right) &= -w_{s0} \frac{\partial}{\partial y} \left(c \left(1-c\right)^{\xi}\right) \\ &= -w_{s0} \left[\frac{\partial c}{\partial y} \left(1-c\right)^{\xi} - \frac{\partial c}{\partial y} c\xi \left(1-c\right)^{\xi-1}\right] \\ &= -w_{s0} \frac{\partial c}{\partial y} \left(1-c\right)^{\xi} \left[1 - \frac{c\xi}{1-c}\right]\end{aligned} \tag{3.20}$$

This new term is non linear, but considering the explicit Euler time discretization scheme it gives no problems since it will be considered at the previous time instant. Rewriting the resulting equation and integrating, it becomes:

$$\begin{aligned}\int_{\Omega} \frac{\mathrm{d}c}{\mathrm{d}t} v \, \mathrm{d}\Omega \; + \int_{\Omega} \frac{\nu_t}{\sigma_c} \nabla c \cdot \nabla v \, \mathrm{d}\Omega \; + \\ - \int_{\Omega} w_{s0} \frac{\partial c}{\partial y} \left(1-c\right)^{\xi} \left[1 - \frac{c\xi}{1-c}\right] v \, \mathrm{d}\Omega = 0 \qquad \forall v \in V_0\end{aligned} \tag{3.21}$$

All the spaces and comments are the same of section 3.1. Also the bilinear formulation related to the gravity component is different, namely:

$$p : V_0 \times V_0 \to \mathbb{R} \quad s.t. \quad p\left(k, r\right) = \int_{\Omega} w_{s0} \frac{\partial k}{\partial y} \left(1-k\right)^{\xi} \left[1 - \frac{k\xi}{1-k}\right] r \, \mathrm{d}\Omega \tag{3.22}$$

With this modified bilinear form the weak formulation is the same as in the equation 3.9 for the continuous problem and as in 3.10 for the discretized problem in space. Regarding the assembling phase, here there are some differences with respect to the section 3.1.2. Since the formulation of the falling velocity is very intricate, the matrix $\underline{\underline{\mathbf{P}}}$ will not be recovered and used. Instead the value of the concentration at the previous time instant is substituted directly into the integral passing through the basis of the linear finite element space. In this way the term can be seen as a force vector:

$$\underline{F}_i^n = \int_{\Omega} w_{s0} \frac{\partial c^n}{\partial y} \left(1-c^n\right)^{\xi} \left[1 - \frac{c^n \xi}{1-c^n}\right] \varphi_i \, \mathrm{d}\Omega \tag{3.23}$$

where $c^n = \sum_{j=1}^{N} c_j^n \left(t\right) \varphi_j \left(\mathbf{x}\right)$. The final system is showed in equation 3.24.

$$\underline{\underline{\mathbf{M}}}\mathbf{c}^{n+1} = \left(\underline{\underline{\mathbf{M}}} - \underline{\underline{\mathbf{A}}}\Delta t^n\right)\underline{\mathbf{c}}^n - \underline{\mathbf{F}}^n\Delta t^n \tag{3.24}$$

The results show a more sensibility of the sediment to gravity in the points where the concentration is smaller, and less sensibility in points with high concentration. This is due to the nature of the formula of the falling velocity shown in 3.19:

$$\begin{aligned} c \to 0^+ \quad &\Rightarrow \quad w_s \to w_{s0} \\ c \to 1^- \quad &\Rightarrow \quad w_s \to 0^+ \end{aligned} \tag{3.25}$$

If the concentration goes to zero the falling velocity tends to be the one in clear water. This behaviour is confirmed by the results. Indeed the figures 3.2a and 3.2b show the difference between the case of constant falling velocity and the case of w_s dependent on the concentration.

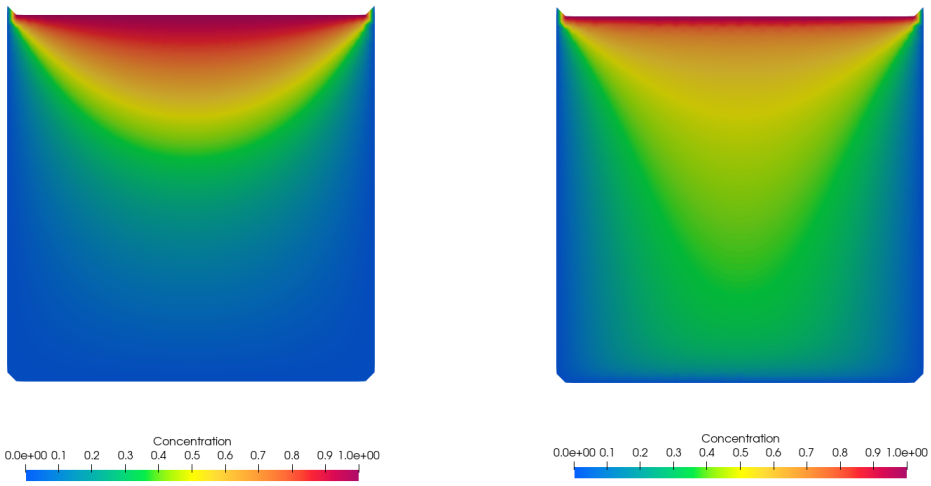

(a) $w_s = 1\ \frac{m}{s}$, $\nu_t = 1\ \frac{m^2}{s}$, $h_m = 0.1\ m$ (b) $w_{s0} = 10\ \frac{m}{s}$, $\nu_t = 1\ \frac{m^2}{s}$, $h_m = 0.1\ m$

Figure 3.2: Comparison between constant gravity and variable gravity

The results show that the sediment is less dragged down where is highly present and vice versa where there is less sediment.

3.3. Transport dominated problem

Now the focus is shifted to transported dominated problem. This is useful in order to make the approach stronger which can be good for some particular situations in concrete cases. The effect of gravity is increased while the diffusion action is limited by decreasing

the sediment diffusivity parameter ν_t. In this way the problem is stressed from a stability point of view of the solution: the task is to be able to reach the convergence of the solution also in this particular case.

3.3.1. Peclet number definition

In order to make an assessment of the correct functionality of the model in transport dominated problem, convergence must be reached. This is a focal point in the study since in these particular cases it is not trivial to have such property. Passing through the Ceà lemma and the interpolation error estimate, the Galerkin error inequality on this problem gives as result

$$\|c - c_h\|_V \leq \frac{M}{\alpha} \inf_{v_h \in V_h} \|c - v_h\|_{V_h} \leq \frac{M}{\alpha} h_k^r \, |c|_{H^{r+1}} \tag{3.26}$$

where M is the continuity constant, α is the coercivity constant and r is the grade of the polynomial chosen to represent the solution. When the upper-bounding constant $\frac{M}{\alpha}$ grows, which happens when the convective term dominates over the diffusive one, the Galerkin method can give inaccurate solutions. In such cases a suitable numerical stabilization must be introduced to avoid spurious solutions. In the problem processed in this chapter, the error inequality 3.26 must be fulfilled at each time instant in order to have an accurate solution. The task is now to find the continuity and coercivity constants.

- Continuity constant: find $M > 0$ such that $|a(c,v) - p(c,v)| \leq M \|c\|_V \|v\|_V$ $\forall v \in V$:

$$\begin{aligned}
|a(c,v) - p(c,v)| &\leq |p(c,v)| + |a(c,v)| \\
&\leq \left| w_s \int_\Omega \frac{\partial c}{\partial y} v \, \mathrm{d}\Omega \right| + \left| \int_\Omega \frac{\nu_t}{\sigma_c} \nabla c \cdot \nabla v \, \mathrm{d}\Omega \right| \\
&\leq \|w_s\|_{L^\infty} \int_\Omega \left| \frac{\partial c}{\partial y} v \right| \, \mathrm{d}\Omega + \left\| \frac{\nu_t}{\sigma_c} \right\|_{L^\infty} \int_\Omega |\nabla c \cdot \nabla v \,| \, \mathrm{d}\Omega \\
&\leq w_s \left\| \frac{\partial c}{\partial y} \right\|_{L^2} \|v\|_{L^2} + \frac{\nu_t}{\sigma_c} \|\nabla c\|_{L^2} \|\nabla v\|_{L^2} \\
&\leq w_s \|c\|_{H^1} \|v\|_{H^1} + \frac{\nu_t}{\sigma_c} \|c\|_{H^1} \|v\|_{H^1} \\
&\leq \left(w_s + \frac{\nu_t}{\sigma_c} \right) \|c\|_V \|v\|_V = M \|c\|_V \|v\|_V
\end{aligned}$$

- Coercivity constant: find $\alpha > 0$ such that $a(v,v) - p(v,v) \geq \alpha \|v\|_V^2 \quad \forall v \in V$:

$$\begin{aligned}
a(v,v) - p(v,v) &= -w_s \int_\Omega \frac{\partial v}{\partial y} v \, \mathrm{d}\Omega + \int_\Omega \frac{\nu_t}{\sigma_c} \nabla v \cdot \nabla v \, \mathrm{d}\Omega \\
&= -\frac{1}{2} w_s \int_\Omega \frac{\partial v^2}{\partial y} \, \mathrm{d}\Omega + \int_\Omega \frac{\nu_t}{\sigma_c} (\nabla v)^2 \, \mathrm{d}\Omega \\
&= -\frac{1}{2} \int_\Omega (w_s \mathbf{j}) \cdot \nabla v^2 \, \mathrm{d}\Omega + \int_\Omega \frac{\nu_t}{\sigma_c} (\nabla v)^2 \, \mathrm{d}\Omega \\
&= \cancel{\frac{1}{2} \int_\Omega \nabla \cdot (w_s \mathbf{j}) \, v^2 \, \mathrm{d}\Omega} - \cancel{\frac{1}{2} \int_\Gamma (\mathbf{j} \cdot \mathbf{n}) \, w_s v^2 \, \mathrm{d}\Omega} + \int_\Omega \frac{\nu_t}{\sigma_c} (\nabla v)^2 \, \mathrm{d}\Omega \\
&= \int_\Omega \frac{\nu_t}{\sigma_c} (\nabla v)^2 \, \mathrm{d}\Omega \\
&= \frac{\nu_t}{\sigma_c} \|\nabla v\|_{L^2}^2 \\
&\geq \frac{\frac{\nu_t}{\sigma_c}}{1 + C_\Omega^2} \|\nabla v\|_{H^1}^2 = \alpha \|\nabla v\|_V^2
\end{aligned}$$

  Where the Poincarè inequality has been used setting $C_\Omega = 0.5$. The two simplifications made are due to the fact that w_s is constant in space and v on the boundary is 0 due its belonging to the space V_0.

So in the end:

$$M = w_s + \frac{\nu_t}{\sigma_c} \tag{3.27}$$

$$\alpha = 0.8 \frac{\nu_t}{\sigma_c} \tag{3.28}$$

So the need of the discussed case is to have the ratio $\frac{M}{\alpha}$ to be small as possible. Unfortunately, considering different values of realistic parameters of w_s and $\frac{\nu_t}{\sigma_c}$ there is a good chance to not fulfill this condition. In the literature [3, 17, 33, 35], sediment diffusivity values range from 10^{-4} $\frac{m^2}{s}$ to 0.1 $\frac{m^2}{s}$, considering different types of materials that can be transported. While for the sediment falling velocity values can range from 10^{-5} $\frac{m}{s}$ to 0.01 $\frac{m^2}{s}$.
From 3.26, the Peclet number for the sediment equation is defined (considering linear polynomials, $r = 1$).

$$\mathbb{P}e_k = h_k \frac{M}{\alpha} = 1.25 h_k \left(\frac{w_s + \frac{\nu_t}{\sigma_c}}{\frac{\nu_t}{\sigma_c}} \right) = 1.25 h_k \left(1 + \frac{w_s \sigma_c}{\nu_t} \right) \tag{3.29}$$

Its value is computed for each element, so the condition should be fulfilled for each computational cell. If not, the stabilization term in that cell is inserted in the solution system. Now consider the real case where $\nu_t = 10^{-4}\ \frac{m^2}{s}$, $w_s = 0.01\ \frac{m}{s}$ and $\sigma_c = 1$ as usual. Following equation 3.29 the value of the Peclet number in this case for a mesh with $h_m = 0.1\ m$ is $\mathbb{P}e = \max_{k,t} \mathbb{P}e_k = 12.625$. The resulting concentration field at $T = 100\ s$ is shown in figure 3.3.

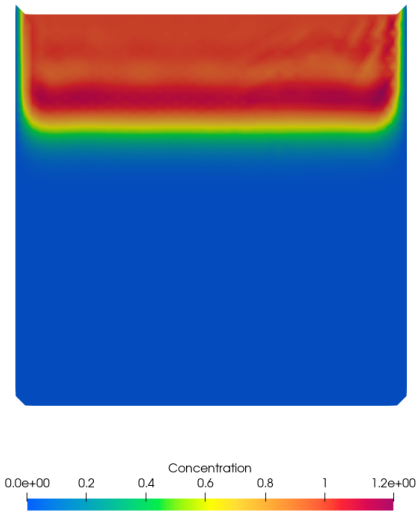

Figure 3.3: $\mathbb{P}e = 12.625$, $T = 100\ s$

It is clearly visible that the solution shows some bad behaviours, first of all the upper value reaches a number bigger than 1, which is not realistic. So the aim is to now stabilize the solution.

3.3.2. Streamline diffusion stabilization

The process of stabilization consists in adding new terms to the discretized equation. In general two terms are added, one bilinear form and one functional. The aim is now to find $c_h \in V_h$ such that:

$$\int_\Omega \frac{\mathrm{d}c_h}{\mathrm{d}t}\, v_h \,\mathrm{d}\Omega \; - p_h\left(c_h, v_h\right) + a_h\left(c_h, v_h\right) + s_h\left(c_h, v_h\right) = G_h\left(v_h\right) \qquad \forall v_h \in V_{h,0} \tag{3.30}$$

In the case of streamline diffusion, a new diffusive term is added in order to balance the highly advective nature of the problem. Indeed, if the falling velocity w_s is very high the Peclet number is also very high and could pass the threshold to have a stable solution.

$$
\begin{aligned}
s_h(c_h, v_h) &= \frac{h_k}{\|w_s\|_{L^\infty}} \int_{\Omega_k} \left(w_s \frac{\mathbf{g}}{|\mathbf{g}|} \cdot \nabla c_h \right) \left(w_s \frac{\mathbf{g}}{|\mathbf{g}|} \cdot \nabla v_h \right) \, \mathrm{d}\Omega \\
&= h_k w_s \int_{\Omega_k} \frac{\partial c_h}{\partial y} \frac{\partial v_h}{\partial y} \, \mathrm{d}\Omega
\end{aligned}
\tag{3.31}
$$

While $G_h(v_h) = 0 \;\; \forall v_h \in V_{h,0}$.
In the assembling phase, the stabilization matrix $\underline{\underline{\mathbf{S}}}$ is calculated as before passing through the local computation.

$$
\begin{aligned}
s_h(c_h, \varphi_i) &= h_k w_s \int_\Omega \frac{\partial c_h}{\partial y} \frac{\partial \varphi_i}{\partial y} \, \mathrm{d}\Omega = h_k w_s \int_\Omega \left(\underline{\mathbf{b}}_y \cdot \underline{\mathbf{c}}^L \right) \frac{\partial \varphi_i}{\partial y} \, \mathrm{d}\Omega \\
&= \left(h_k w_s \int_\Omega \underline{\mathbf{b}}_y \frac{\partial \varphi_i}{\partial y} \, \mathrm{d}\Omega \right) \cdot \underline{\mathbf{c}}^L \\
&= \underline{\mathbf{S}}_i \cdot \underline{\mathbf{c}}^L
\end{aligned}
\tag{3.32}
$$

$$
\underline{\underline{\mathbf{S}}}^L = \begin{bmatrix} \underline{\mathbf{S}}_1^T \\ \underline{\mathbf{S}}_2^T \\ \underline{\mathbf{S}}_3^T \end{bmatrix} = \begin{bmatrix} h_k w_s \int_{\Omega_k} \underline{\mathbf{b}}_y \frac{\partial \varphi_1}{\partial y} \, \mathrm{d}\Omega \\ h_k w_s \int_{\Omega_k} \underline{\mathbf{b}}_y \frac{\partial \varphi_2}{\partial y} \, \mathrm{d}\Omega \\ h_k w_s \int_{\Omega_k} \underline{\mathbf{b}}_y \frac{\partial \varphi_3}{\partial y} \, \mathrm{d}\Omega \end{bmatrix} = h_k w_s \int_{\Omega_k} \underline{\mathbf{b}}_y \otimes \underline{\mathbf{b}}_y \, \mathrm{d}\Omega \tag{3.33}
$$

From the definition, is visible that the magnitude of this component is regulated by the dimension of the element considered. So in the end, the components related to the term of 3.31 are inserted in the $\underline{\mathbf{d}}$ vector. The solution gains benefits after having added the streamline diffusion stabilization, as shown in figure 3.4.

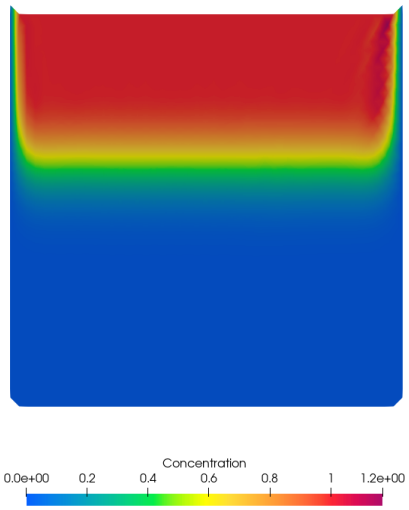

Figure 3.4: y-Stabilized solution: $\mathbb{P}e = 12.625$, $T = 100\ s$

However this does not cure all the spurious oscillations: on the right side of the bucket, the sudden change of the solution to 0 imposed by the boundary condition still gives a concentration higher than 1. Indeed the stabilization term heals only the variations along y and not along x. In order to get an even better solution, another term like 3.31 is introduced with the difference of acting on the x-direction. This means that the new bilinear form and matrix related to stabilization write:

$$s_h(c_h, v_h) = h_k w_s \int_{\Omega_k} \frac{\partial c_h}{\partial y}\frac{\partial v_h}{\partial y}\,\mathrm{d}\Omega + \delta h_k w_s \int_{\Omega_k} \frac{\partial c_h}{\partial x}\frac{\partial v_h}{\partial x}\,\mathrm{d}\Omega \tag{3.34}$$

$$\underline{\underline{\mathbf{S}}}^L = h_k w_s \int_{\Omega_k} \underline{\mathbf{b}}_y \otimes \underline{\mathbf{b}}_y\,\mathrm{d}\Omega + \delta h_k w_s \int_{\Omega_k} \underline{\mathbf{b}}_x \otimes \underline{\mathbf{b}}_x\,\mathrm{d}\Omega \tag{3.35}$$

δ is a parameter which takes values inside the interval $[0, 1]$. The effect is governed by a constant because the transport is in the y direction, so in x the stabilization acts with a smaller effect. The result is definitely positive since the values turns to be inside the correct range of $[0, 1]$. The resulting simulation is shown in figure 3.5, considering $\delta = 1$.

Figure 3.5: xy-Stabilized solution: $\mathbb{P}e = 12.625$, $T = 100\ s$

3.3.3. Convergence analysis

In order to check if the solution is still somehow accurate, the convergence analysis of the stabilized problem is proposed confronting its result to the one of problem 3.10. Consider the fictional solution 2.5 and plug it in 3.2. Then the forcing term is computed in order to satisfy the identity of the equation.

$$\frac{\mathrm{d}\widetilde{c}}{\mathrm{d}t} + \nabla \cdot \left(w_s \frac{\mathbf{g}}{|\mathbf{g}|} \widetilde{c} \right) - \frac{\nu_t}{\sigma_c} \Delta \widetilde{c} = \left(1 + 2\pi^2 \frac{\nu_t}{\sigma_c} t \right) sin\left(\pi x\right) cos\left(\pi y - \frac{\pi}{2}\right) + \\ + sin\left(\pi x\right) sin\left(\pi y - \frac{\pi}{2}\right) w_s \pi t = \widetilde{f} \tag{3.36}$$

The convergence rate in this case is between the linear and the quadratic one, as shown in figure 3.6. The interpolation error values instead are displayed in table 3.1. In particular Avijit et al. [2] derive a convergence estimate that shows a rate of convergence of $\frac{3}{2}$.

$$\|v\|_{L^2} \leq \frac{1}{\sqrt{\gamma}} |||v|||_{SD} \leq \frac{C}{\sqrt{\gamma}} h^{3/2} \tag{3.37}$$

Where the SD norm is derived from [21], with γ being a suitable constant.

$$|||v|||_{SD} := \left(\frac{\nu_t}{\sigma_c} \|\nabla v\|_{L^2}^2 + \gamma \|v\|_{L^2}^2 + \sum_{k=1}^{N} \left\| \sqrt{h_k w_s} \frac{\partial v}{\partial y} \right\|_{L(\Omega_k)^2}^2 \right)^2 \tag{3.38}$$

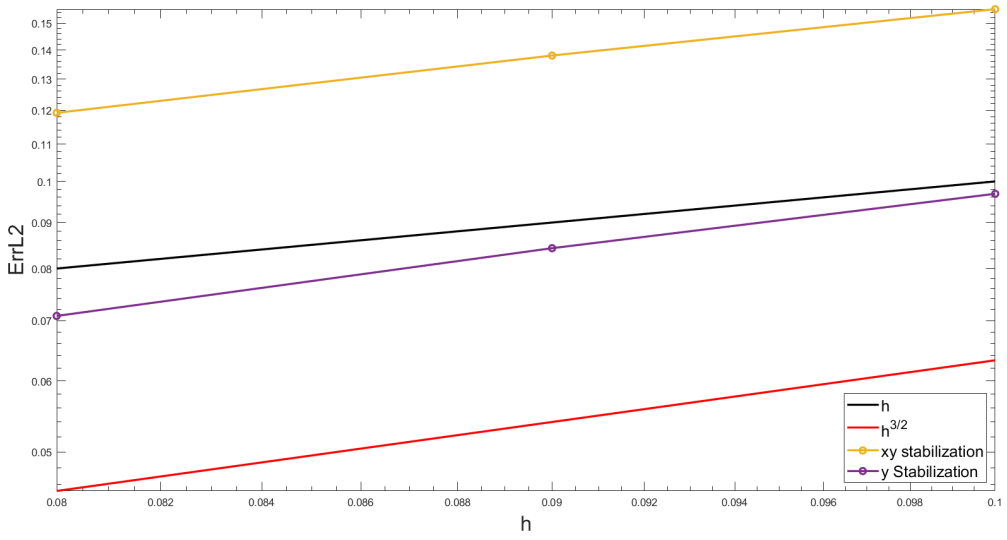

Figure 3.6: Convergence of the stabilized problem (log-log scale): $\mathbb{P}e = 12.625$, $T = 1\ s$

$\|c - c_h\|_{L^2(\Omega)}$, $T = 1s$			
h[m]	0.1	0.09	0.08
xy-stab	0.15544	0.13804	0.11919
y-stab	0.09687	0.08427	0.07085

Table 3.1: Values of the L^2 errors for the stabilized problem

The error is bigger with respect to the previous cases: this is due to the fact that some terms are added in the solving equation and modify the final solution, making it slightly different from the real one. Indeed for the double direction stabilization, the error is bigger than the y-stabilization since two terms are added instead of only one. Generally, it would be desirable to have strong consistency, which means that if the real solution c of the continuous problem is plugged, then:

$$s_h\left(c, v_h\right) = 0 \tag{3.39}$$

So the solution of the continuous problem is recovered. In the case of streamline diffusion, the property of consistency is verified but not in a strongly way. This means that:

$$s_h\left(c_h, v_h\right) \to 0 \quad as \quad h_k \to 0 \tag{3.40}$$

but not the condition 3.39. A more accurate stabilized solution should be reached by applying SUPG method (or GLS, in fact they are the same considering linear finite elements). Indeed, with respect to Streamline Diffusion, SUPG does fulfill the strong consistency property. On the other hand, computationally speaking is more onerous since there are too many terms to address and integrals to compute.

4 | Sediment equation: Transport through fluid motion

So far, the fluid was always still and not a big factor in the simulation. Now the focus shifts in considering a case where the fluid is moving, seeing the effects of its motion on the value of concentration. Adding this type of transport is important since it allows the water to have an impact on the sediment. Indeed, in the equation so far the velocity **u** was not present.

4.1. Solution in the Eulerian nodes

Considering a Lagrangian point of view of the problem, the attention must be paid to the imposition of conditions at the left and right hand sides, as said in section 1.1.5. If the domain is composed by inlet or outlet boundaries, there will be a passage of particles in and out of the domain. The mesh nodes are following the fluid movement, so when a node reaches the exit of the domain it will be compressed with other or in the worst case can exit the domain and be lost outside it. To avoid this problem, the nodes at the entrance and the exit are treated as Eulerian: in this way they are still and do not move with the fluid. This solution, together with the remeshing and alpha phase, gives as result a very good evolution of the position of the nodes.
Considering the Eulerian nodes, a different equation has to be solved in these points: the total derivative has to be split in the two components and so the Eulerian formulation of the equation is recovered.

$$\frac{\partial c}{\partial t} + \mathbf{u} \cdot \nabla c + \nabla \cdot (w_s \frac{\mathbf{g}}{|\mathbf{g}|} c) - \frac{\nu_t}{\sigma_c} \Delta c = 0 \tag{4.1}$$

Numerically speaking the challenge now shifts in finding a way to solve the Lagrangian formulation in some nodes and the Eulerian one on the outlet and inlet.

4.1.1. Solving system and matrix assembly

The structure of the model is more or less the same, but for the Eulerian nodes the computation includes a new term which has a convective matrix correlated. To recover the discretized form of the new term in equation 4.1, only Eulerian nodes are considered in the domain for now. Then through a restriction operator, the newly acquired matrix will have an effect only on the fixed nodes. Multiply the equation by the test function taken from the test space so that:

$$\int_\Omega \frac{\partial c}{\partial t} v \, \mathrm{d}\Omega + \int_\Omega \mathbf{u} \cdot (\nabla c)\, v \, \mathrm{d}\Omega + \int_\Omega \frac{\nu_t}{\sigma_c} \nabla c \cdot \nabla v \, \mathrm{d}\Omega - w_s \int_\Omega \frac{\partial c}{\partial y} v \, \mathrm{d}\Omega = 0 \qquad \forall v \in V_0 \tag{4.2}$$

Addressing the new term, a bilinear form has to be introduced:

$$e : V_0 \times V_0 \to \mathbb{R} \quad s.t. \quad e\,(k, r) = \int_\Omega \mathbf{u} \cdot (\nabla k)\, r \, \mathrm{d}\Omega \tag{4.3}$$

Like for all the other bilinear forms, the analogue in the discretized problem is shown in 4.4. The functional spaces are always the same as in the cases seen before.

$$e_h\,(\varphi_j, \varphi_i) = \int_{\Omega_k} \left(u_x \frac{\partial \varphi_j}{\partial x} + u_y \frac{\partial \varphi_j}{\partial y} \right) \varphi_i \, \mathrm{d}\Omega = E_{ij} \tag{4.4}$$

This matrix will always be effective in a portion of the nodes, since it is present only on Eulerian nodes. All the nodes which are fixed are saved in the set Ω_{eul} and so the restriction matrix $\overline{\overline{\mathbf{R}}} \in \mathbb{R}^{N \times N}$ is defined:

$$R_{i,j} = \begin{cases} 1 & \text{if } \mathbf{x_i}, \mathbf{x_j} \in \Omega_{eul} \\ 0 & \text{otherwise} \end{cases} \tag{4.5}$$

Considering the explicit time integration, the final linear system to solve is:

$$\underline{\underline{\mathbf{M}}}\mathbf{c}^{n+1} = \left(\underline{\underline{\mathbf{M}}} - \underline{\underline{\mathbf{E}}}^{n+1}\underline{\underline{\mathbf{R}}}\Delta t^n + \underline{\underline{\mathbf{P}}}\Delta t^n - \underline{\underline{\mathbf{A}}}\Delta t^n\right) \underline{\mathbf{c}}^n = \underline{\mathbf{f}}^n \tag{4.6}$$

The Eulerian matrix is time dependent, since inside the integral there are the two velocity components. This creates no problems since the value of the velocity is known at the

time instant t^{n+1}. This is due to the fact that the sediment equation is solved after the momentum equation.
The assembly of the convective matrix is treated in a different way with respect to the other components that were added before. So, the local convective matrix computation for a particular element is:

$$\begin{aligned} e\left(c,\varphi_i\right) &= \int_{\Omega_k}\left(u_x\frac{\partial c}{\partial x}+u_y\frac{\partial c}{\partial y}\right)\varphi_i \,\mathrm{d}\Omega \\ &= \int_{\Omega_k}\left(u_x\left(\underline{\mathbf{b}}_x\cdot\underline{\mathbf{c}}^L\right)+u_y\left(\underline{\mathbf{b}}_y\cdot\underline{\mathbf{c}}^L\right)\right)\varphi_i \,\mathrm{d}\Omega \\ &= \left(\int_{\Omega_k}\left(\underline{\mathbf{b}}_x u_x+\underline{\mathbf{b}}_y u_y\right)\varphi_i \,\mathrm{d}\Omega\right)\cdot\underline{\mathbf{c}}^L \\ &= \underline{\mathbf{E}}_i\cdot\underline{\mathbf{c}}^L \end{aligned} \tag{4.7}$$

$$\underline{\underline{\mathbf{E}}}^L=\begin{bmatrix}\underline{\mathbf{E}}_1^T\\ \underline{\mathbf{E}}_2^T\\ \underline{\mathbf{E}}_3^T\end{bmatrix}=\begin{bmatrix}\int_{\Omega_k}\left(\underline{\mathbf{b}}_x u_x+\underline{\mathbf{b}}_y u_y\right)\varphi_1 \,\mathrm{d}\Omega\\ \int_{\Omega_k}\left(\underline{\mathbf{b}}_x u_x+\underline{\mathbf{b}}_y u_y\right)\varphi_2 \,\mathrm{d}\Omega\\ \int_{\Omega_k}\left(\underline{\mathbf{b}}_x u_x+\underline{\mathbf{b}}_y u_y\right)\varphi_3 \,\mathrm{d}\Omega\end{bmatrix}=\int_{\Omega_k}\underline{\mathbf{l}}\otimes\left(\underline{\mathbf{b}}_x u_x+\underline{\mathbf{b}}_y u_y\right)\,\mathrm{d}\Omega \tag{4.8}$$

The velocity components are evaluated at the center of the considered element. After having computed the local matrix, a vector $\underline{\mathbf{e}}^L$ related to the convection term is recovered:

$$e_i^L=\sum_{j=1}^{3}\left(-E_{ij}^L c_j^L\right)\qquad\text{for}\quad i=1,2,3 \tag{4.9}$$

Then, through the connectivity, the global convection vector $\underline{\mathbf{e}}$ is found and summed up to the global force vector $\underline{\mathbf{d}}$. Finally, at instant t^{n+1} the concentration is:

$$c_i^{n+1}=c_i^n+\frac{\left(d_i+e_i\right)\Delta t^n}{m_i} \tag{4.10}$$

4.2. Transport in a channel flow

The effects of these new modifications are studied with a very simple problem: the channel flow. The water is moving from left to right and on the top and bottom boundaries the velocity is null. A horizontal velocity profile is imposed at the entrance and at the exit the natural condition is considered. Regarding concentration the system is the same of 3.3, but considering the diffusivity and falling velocity null.

$$\begin{cases} \dfrac{\partial c}{\partial t} + \mathbf{u} \cdot \nabla c = 0 & \forall \mathbf{x} \in \Omega \subseteq \mathbb{R}^2, \quad \forall t \in (0, T] \\ c\left(\mathbf{x}, t = 0\right) = \bar{c}\left(\mathbf{x}\right) & \forall \mathbf{x} \in \Omega \\ c\left(\mathbf{x}, t\right) = h\left(\mathbf{x}, t\right) & \forall \mathbf{x} \in \partial\Omega = \Gamma \end{cases} \tag{4.11}$$

where $\Omega = [0, 10] \times [0, 4]\ m$ and

$$h\left(\mathbf{x}, t\right) = \begin{cases} 1 & \text{if } x = 0 \\ 0 & \text{otherwise} \end{cases} \tag{4.12}$$

$$\bar{c}\left(\mathbf{x}\right) = \begin{cases} 1 & \text{if } x = 0 \\ 0 & \text{otherwise} \end{cases} \tag{4.13}$$

In figure 4.1 the starting solution at the initial instant is shown, noting that the concentration is 1 on the left side.

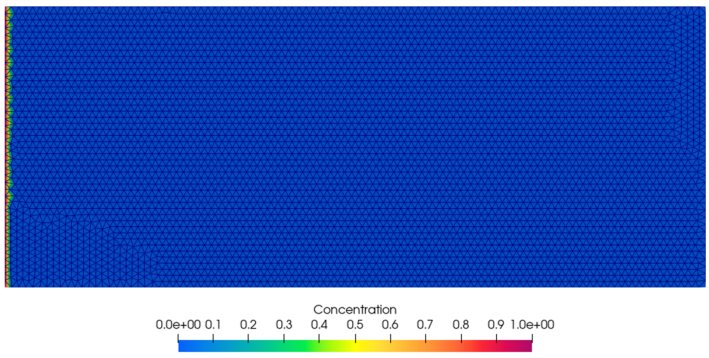

Figure 4.1: Initial solution

Considering the problem 4.11, the boundary conditions 4.12 and the initial solution 4.13, the time simulation is set to be 5 seconds. The resulting solution is shown in figure 4.2, using a mean mesh dimension $h_m = 0.1\ m$. From the result is clear that the concentration solution is transported only by the movement of the fluid, since the diffusion and the gravity transport do not have any influence. While the y-velocity is 0 in all the domain, the x-component varies in time in x and have constant values in y. This motivates the fact that the concentration far from the wall is constant along y, further remarked by the plot of the isolines for concentration.

In this test case, the global relocation of the nodes is a fundamental part of the correct functionality of the solver. Indeed, this type of relocation is essential in our problem since

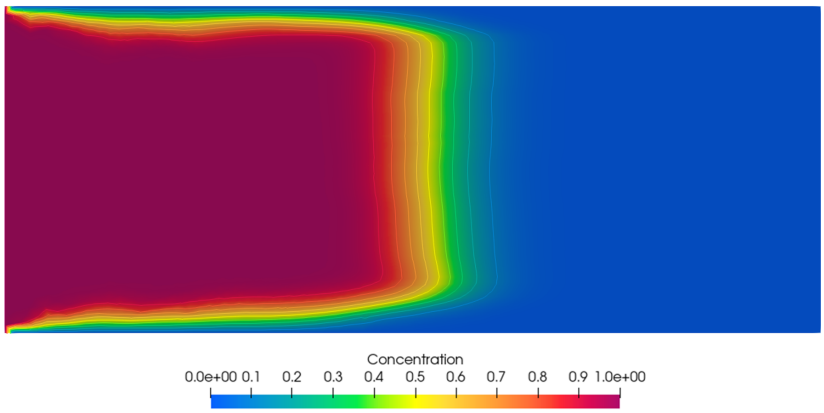

Figure 4.2: Concentration plot with isolines $T = 5\ s$, $\nu_t = 0\ \frac{m^2}{s}$, $w_s = 0\ \frac{m}{s}$, $h_m = 0.1\ m$

the nodes that thicken towards the exit of the channel are moved to the start. So these nodes are relocated to a different element from the previous one. In figure 4.3 is shown a part of the boundary at the end of the domain and at the start before the relocation. The elements at the end (4.3a) are compressed while the elements on the entrance are stretched (4.3b).

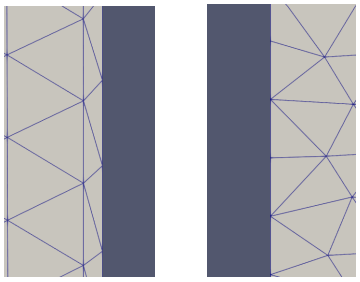

(a) Outlet (b) Inlet

Figure 4.3: Before relocation

The code creates a ranking of the elements that are most stretched. Then it takes the nodes of the most deformed elements and moves them into the elements that need them most according to the ranking made. So that the final result is a more homogeneous mesh as it can be seen in figure 4.4.

4.3. Circular source transport problem

Next test case is the transport of a circular source of concentration in the channel. The domain is the same as the case seen before and also the boundary condition for velocity and pressure. The concentration is fixed to be 0 but not in the outflow boundary. Here the

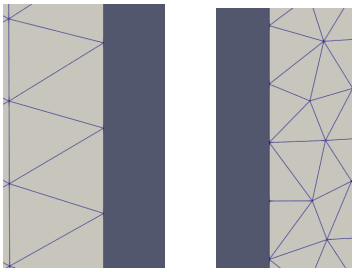

(a) Outlet (b) Inlet

Figure 4.4: After relocation

natural condition is imposed to let the concentration source exit the domain boundary. The initial solution for concentration is shown in 4.14 and in 4.5. Since the problem is due to only study the effect of transport, the diffusion is turned off.

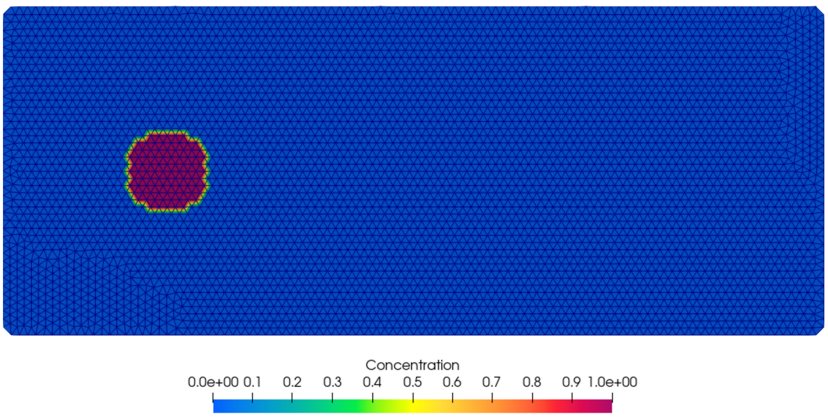

Figure 4.5: $t = 0\ s$, $\nu_t = 0\ \frac{m^2}{s}$, $w_s = 0.05\ \frac{m}{s}$, $h = 0.1\ m$

$$\overline{c}\,(\mathbf{x}) = \begin{cases} 1 & \text{if } (x-2)^2 + (y-2)^2 \leq 0.6^2 \\ 0 & \text{otherwise} \end{cases} \tag{4.14}$$

The time of the simulation is set to be 10 seconds, but after 8 seconds the source exits the domain. The four screenshots in figure 4.6 are taken at $t = 1\ s$, $t = 3\ s$, $t = 5\ s$ and $t = 8\ s$. The ball of concentration is transported to the right by the fluid flow, while in the meantime it is dragged down by gravity.

To obtain these result, a modification of the model has been made. In particular, the stabilization term has been updated since until now it would have considered only the transport due to gravity. Here, also the transport due to the fluid movement must be inserted in the integral, namely:

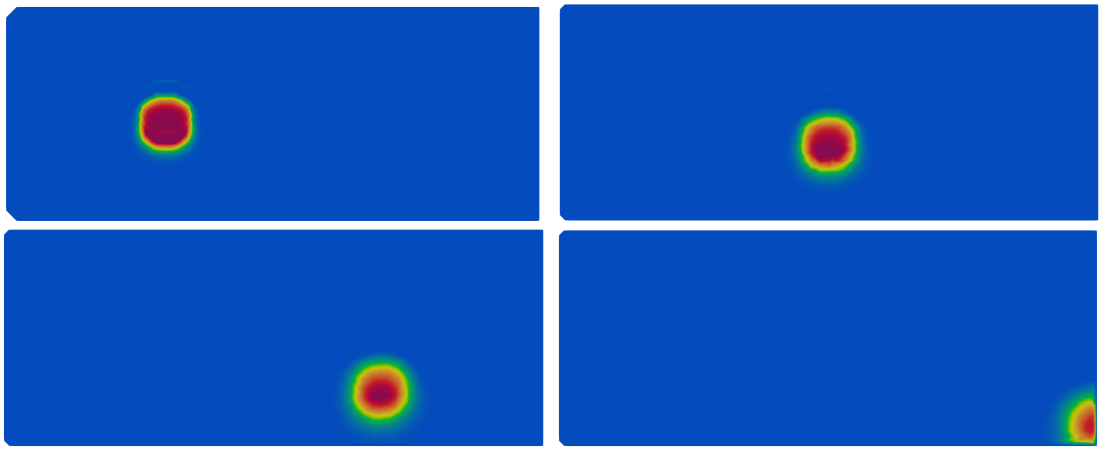

Figure 4.6: Concentration plot at: $t = 1s$, $t = 3s$, $t = 5s$ and $t = 8s$

$$s_h(c_h, v_h) = \frac{h_k}{\left\| w_s \frac{\mathbf{g}}{|\mathbf{g}|} + \mathbf{u} \right\|_{L^\infty}} \int_{\Omega_k} \left[\left(w_s \frac{\mathbf{g}}{|\mathbf{g}|} + \mathbf{u} \right) \cdot \nabla c_h \right] \left[\left(w_s \frac{\mathbf{g}}{|\mathbf{g}|} + \mathbf{u} \right) \cdot \nabla v_h \right] \, \mathrm{d}\Omega \quad (4.15)$$

The Peclet number has to be modified in order to consider also the transport of the fluid in the stabilization. So the computation of the solution is differentiated in base of the value of the Peclet number. If its value is bigger than 1, then the new bilinear form defined in 4.15 has to be inserted inside the weak formulation. After having calculated the new continuity and coercivity constants:

$$\mathbb{P}e_k = 1.25 h_k \frac{\left\| \mathbf{u} + w_s \frac{\mathbf{g}}{|\mathbf{g}|} \right\|_{L^\infty} + \frac{\nu_t}{\sigma_c}}{\frac{\nu_t}{\sigma_c}} \quad (4.16)$$

The local matrix is written in 4.17. The integrals are computed using the mean value formula, so the velocity is considered constant on the element, evaluated on its center.

$$\begin{aligned} \underline{\underline{\mathbf{S}}}^L = \frac{h_k}{\left\| w_s \frac{\mathbf{g}}{|\mathbf{g}|} + \mathbf{u} \right\|_{L^\infty}} & \int_{\Omega_k} (u_y - w_s)^2 \, \underline{\mathbf{b}}_y \otimes \underline{\mathbf{b}}_y \, \mathrm{d}\Omega + \int_{\Omega_k} (u_y - w_s) \, u_x \, \underline{\mathbf{b}}_y \otimes \underline{\mathbf{b}}_x \, \mathrm{d}\Omega + \\ & \int_{\Omega_k} (u_y - w_s) \, u_x \, \underline{\mathbf{b}}_x \otimes \underline{\mathbf{b}}_y \, \mathrm{d}\Omega + \int_{\Omega_k} u_x^2 \, \underline{\mathbf{b}}_x \otimes \underline{\mathbf{b}}_x \, \mathrm{d}\Omega \end{aligned} \quad (4.17)$$

The newly inserted integrals are 4, which increase the computational cost of the solution. Still, this computation is easier than any other stabilization method, like SUPG.

4.4. Channel transport solved with totally coupled model

Up to now, the modelling coupling between the sediment and the fluid has been only weak: the fluid has an influence on the sediment but not vice versa. Indeed in the advection-diffusion equation the velocity of the fluid is present but in the Navier-Stokes equations the concentration is not considered. This reinstates the hyphotesis that the sediment is passively transported by the fluid.
In order to have a totally coupled model, the Navier-Stokes has to be modified taking into account the concentration of sediment. The modified version considers the density and the viscosity of a mixture of the two substances.

$$\rho = \rho_f (1 - c) + \rho_s c \tag{4.18}$$

Here, ρ_f is the density of the fluid, ρ_s is the density of the sediment grain and c is the concentration. The density of the mixture is defined as a weighted balance between the sediment density and the water density. The weights are given by the amount of sediment present in the considered space: in our case this value is precisely the concentration. Regarding the viscosity of the mixture, the formula used is shown in 4.19, where μ_f is the viscosity of the fluid.

$$\mu = \mu_f (1 + 2.5c) \tag{4.19}$$

Due to the effect of the sediment, the viscosity is increased since the mixture gives rise to a bigger local shear stress. This equation is taken from a work that is dated at least to Einstein [11], where a very simple relation can be recovered considering a concentration less than 0.1. So this viscosity model can be used in flows where the sediment presence is not so big.

To test the effect of the total coupling, the problem considered is 3.3, considering the initial and boundary conditions 4.12 and 4.13. The imposed concentration on the left is set to 0.1, in order to fulfill the hypothesis of formula 4.19.
Regarding the values of the sediment density, gravel has been considered with density $\rho_s = 1680\ \frac{kg}{m^3}$. Looking at the results in figure 4.7a, it is visible that the higher density of the gravel drags the sediment downwards creating a drop of the concentration values in the higher part of the channel. Confronting the weakly coupled model with the total

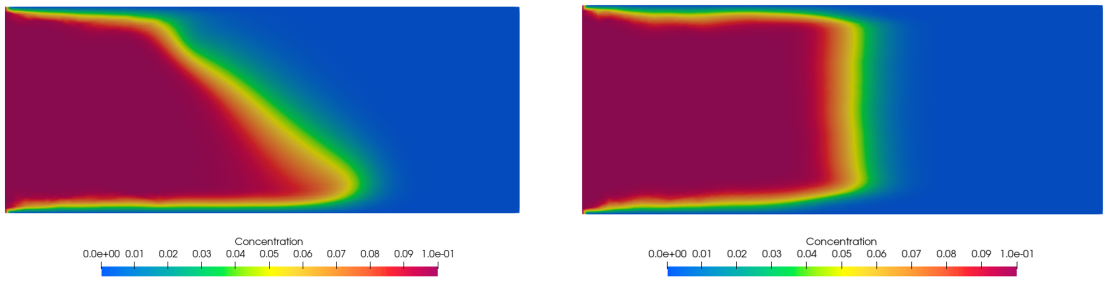

(a) $T = 5\ s$, $\nu_t = 0\ \frac{m^2}{s}$, $w_s = 0\ \frac{m}{s}$, $h = 0.1\ m$ (b) $T = 5\ s$, $\nu_t = 0\ \frac{m^2}{s}$, $w_s = 0\ \frac{m}{s}$, $h = 0.1\ m$

Figure 4.7: Comparison between totally coupled and weakly coupled model

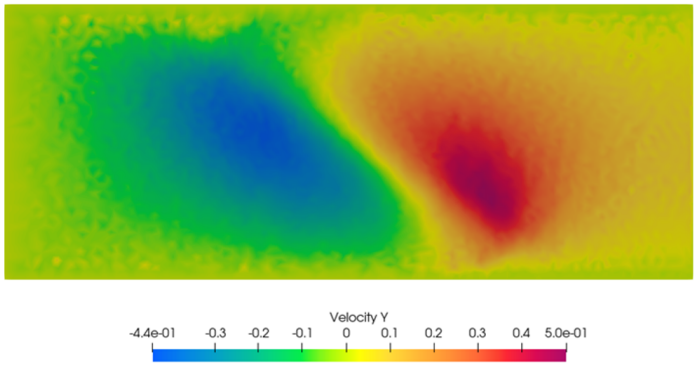

Figure 4.8: Plot of the y-velocity component at $T = 5\ s$

one, it can be noticed that the crest of the perturbation in figure 4.7a is dragged back and down by the bigger density of the sediment. This gives a more correct approximation of reality since in the case seen in 4.2 the sediment is not dragged down. The final time is $T = 5\ s$, and the parameters of the simulation are $\nu_t = 0\ \frac{m^2}{s}$, $w_s = 0\ \frac{m}{s}$, $h = 0.1\ m$. Also in the y-velocity plot 4.8, at the crest of the sediment perturbation there is a movement upwards of the fluid that moves aside since the sediment is settling on the bed.

5 | Sediment equation: Complete model

The interaction between a fluid and a sediment is a complex phenomenon of great relevance in many industrial and environmental applications. The ability to accurately simulate this type of interaction is of fundamental importance in understanding the processes that govern sediment transport, deposit formation and the behaviour of sediments under dynamic conditions.

In this chapter, a detailed study of simulations of the interaction between a fluid and a sediment will be presented. The main difficulties associated with this type of simulation will be discussed, including the description of the geometry and properties of the sediment. In particular, examples of applications of fluid-sediment interaction simulations in different contexts will be presented, such as passage through a hydraulic channel, modelling of mixing phenomena and analysis of pollution processes. The ultimate goal of this chapter is to provide the reader with a comprehensive overview of the methodologies available to simulate fluid-sediment interaction, along with the main challenges and opportunities that arise in this field of research.

5.1. Water contaminant mixing

As a first problem, let us consider the case where gravel, representing the sediment, slides on an inclined plane within a pool of water. In this scenario, we consider sediment as something that is homogeneously mixed with water, thus always following the laws of fluid. The behaviour of water is described by the Navier-Stokes equations.
The problem of interest is to determine the behaviour of the sediment as it slides along the inclined plane under the action of gravity. In particular, it is important to understand how the movement of the sediment affects the flow of water around it. Being considered a weakly coupled model, the concentration of the sediment does not influence the motion of the fluid.

5.1.1. Problem setup

The problem domain is shown in figure 5.1. A square with $c = 1$, slides inside the pool with $c = 0$. The two fluids with different concentration mix to form a homogeneous substance which tries to get to a static condition with a particular final fraction of sediment in water.

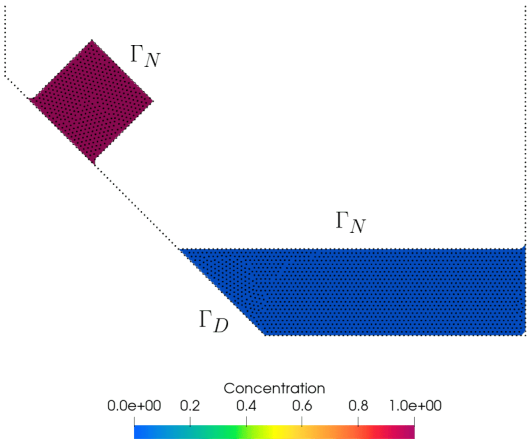

Figure 5.1: Initial domain

The equations to solve are: the Navier-Stokes (NS) ones and the advection diffusion equation (AD) for the sediment. For what concerns boundary conditions, they are defined in 5.1 and 5.2. The boundaries are divided in two: Γ_N is the free surface boundary; while Γ_D are all the other boundaries, which will have a type of condition of Dirichlet.

$$NS = \begin{cases} \boldsymbol{\sigma} \cdot \mathbf{n} = 0 & \text{on } \Gamma_N \\ \mathbf{u} = 0 & \text{on } \Gamma_D \end{cases} \tag{5.1}$$

$$AD = \begin{cases} \nabla c \cdot \mathbf{n} = 0 & \text{on } \Gamma_N \\ c = 0 & \text{on} \Gamma_D \end{cases} \tag{5.2}$$

5.1.2. Results and discussion

The result in figure 5.2 shows that the square with concentration equal to 1 slides correctly into the pool and the concentration is diffused inside it, giving rise to a mixture with varying concentration within. As soon as contact occurs, a ridge is formed that allows the first major mixing. Afterwards, all the momentum that the square had is slowly dissipated towards an equilibrium condition. Meanwhile, inside the tank there are internal

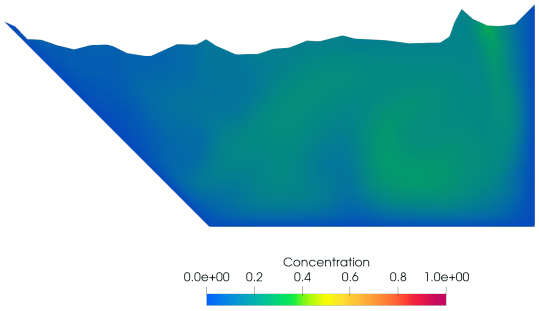

Figure 5.2: Concentration plot at $T = 20\ s$, $\nu_t = 0.01\ \frac{m^2}{s}$, $w_s = 0.05\ \frac{m}{s}$, $h = 0.05\ m$

movements in the form of eddies that allow the homogenisation of the sediment. The concentration inside slowly tends to reach a value between 0.2 and 0.25. The natural condition imposed on the free surface allows the nodes that come to the surface to maintain their concentration. To evaluate the sediment concentration at the equilibrium, consider the mass balance on the sediment in time:

$$M\left(t=0\right) = M\left(t=T_F\right) \tag{5.3}$$

Define ρ_s as the mass of the sediment, V_p the volume of the pool and V_s the volume of the water-sediment pile. Assume that T_F is the instant where the new equilibrium condition is reached. By the definition of volumetric concentration, the volume of sediment is computed by multiplying the volume in which the sediment is present with the concentration itself.

$$M\left(t=0\right) = \rho_s V_p c_p + \rho_s V_s c_s = \rho_s A_p dz c_p + \rho_s A_s dz c_s = \rho_s \left(A_p c_p + A_s c_s\right) dz \tag{5.4}$$

$$M\left(t=T_F\right) = \rho_s \left(V_p + V_s\right) c_{eq} = \rho_s \left(A_p + A_s\right) dz c_{eq} \tag{5.5}$$

Substituting in 5.3:

$$\rho_s \left(A_p c_p + A_s c_s\right) dz = \rho_s \left(A_p + A_s\right) c_{eq} dz \tag{5.6}$$

$$c_{eq} = \frac{A_p c_p + A_s c_s}{A_p + A_s} = \frac{2}{9} = 0.222 \tag{5.7}$$

This value is in line with what the result shows in figure 5.2.

5.2. Cavity flow problem

Cavity flow is a computational fluid dynamics problem that occurs when a fluid flows through a cavity or slot of complex shape. This type of flow is of particular interest in numerical mathematics because it presents certain difficulties that make it a challenging problem to solve using numerical methods. In particular, cavity flow is characterised by the presence of regions of high turbulence, vorticity and flow separation, which can cause numerical instability and non-convergent results.
In this thesis, having a Lagrangian model available, it is necessary not to fall into the non-laminar regime region. Therefore, a very simple case with not too complicated boundary conditions is considered here. The sediment is inserted inside the upper slot, and its diffusion-transport motion is studied inside the domain. The aim is to see how it behaves when coming into contact with a vortex.

5.2.1. Problem setup

The domain is a square of size $[0,1] \times [0,1]$ m, shown in figure 5.3. The boundary conditions are shown in 5.8 and 5.9.

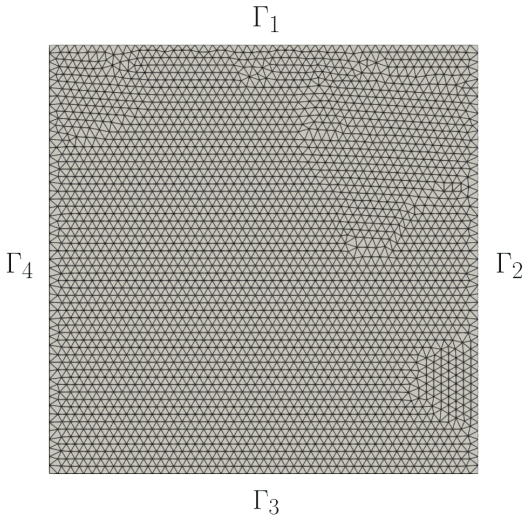

Figure 5.3: Starting domain for the cavity problem

$$NS = \begin{cases} \mathbf{u} = 2\mathbf{i} & \text{on } \Gamma_1 \\ \mathbf{u} = 0 & \text{on } \Gamma_2 \cup \Gamma_3 \cup \Gamma_4 \end{cases} \tag{5.8}$$

$$AD = \begin{cases} c = 0.1 & \text{on } \Gamma_1 \\ c = 0 & \text{on } \Gamma_2 \cup \Gamma_3 \cup \Gamma_4 \end{cases} \tag{5.9}$$

While the starting conditions are 5.10 and 5.11.

$$\overline{\mathbf{u}}\,(\mathbf{x}) = 0 \;\text{ in }\; [0,1] \times [0,1] \tag{5.10}$$

$$\overline{c}\,(\mathbf{x}) = \begin{cases} c = 0.1 & \text{if } \; y = 1 \\ c = 0 & \text{otherwise} \end{cases} \tag{5.11}$$

The problem is studied considering the totally coupled model seen in section 4.4. In order to fulfill the hypothesis of small concentration involved, the imposed concentration on the top side is 0.1.

5.2.2. Results and discussion

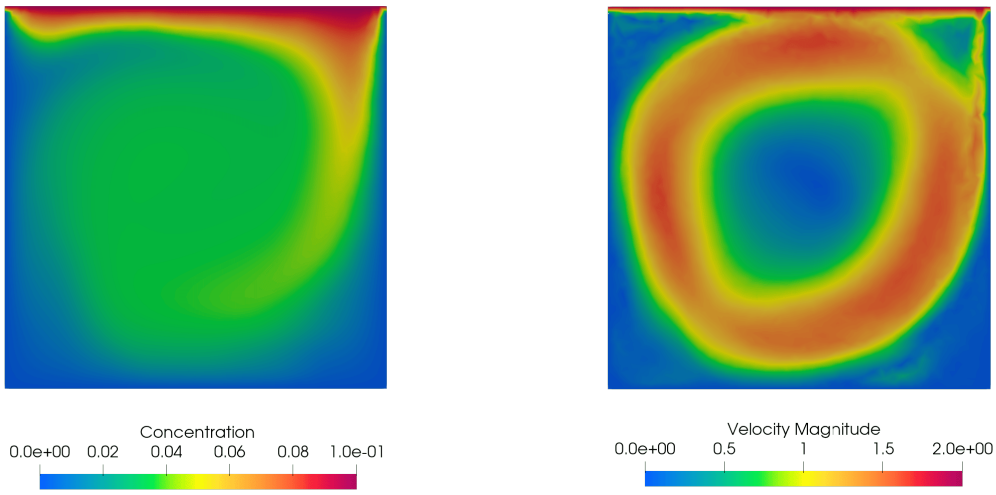

(a) Concentration plot (b) Velocity plot

Figure 5.4: $T = 60\ s$, $\nu_t = 0.01\ \frac{m^2}{s}$, $w_s = 0.05\ \frac{m}{s}$, $h = 0.02\ m$

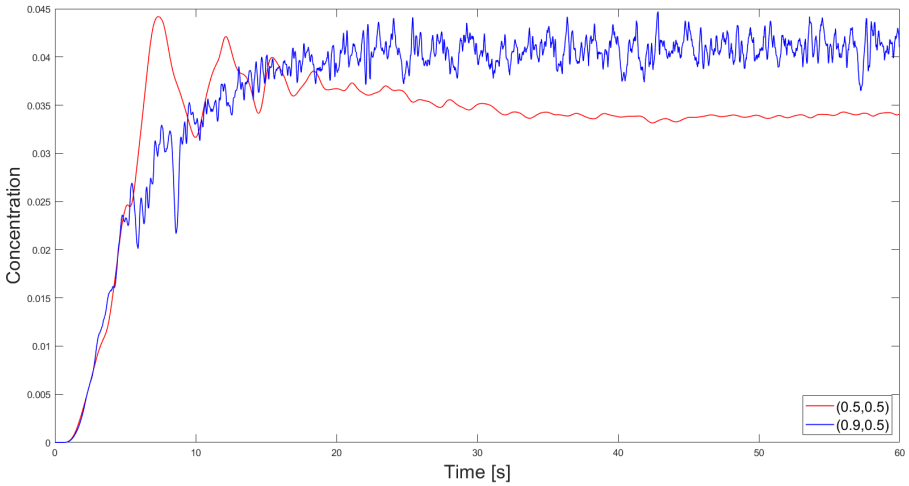

Figure 5.5: Time plot of the concentration in two points: one inside the vortex and the other on the vortex

The sediment is inserted from the upper slot and spreads downwards as in the case seen in chapter 2. Added to this effect is the transport due to the horizontal movement imposed on the fluid. The final plot is the superposition of the two phenomena: in the case shown in figure 5.4a and in 5.4b, it can be seen that the sediment mainly enters the domain from the right-hand edge. In the centre of the square, a vortex is formed in which the sediment gets stuck inside. The concentration of the sediment reaches a constant solution: in figure 5.5, one can see the reaching of the plateau with the following oscillation around a steady state value. The figure shows the concentration plots in $(0.5, 0.5)\, m$ and in $(0.9, 0.5)\, m$. The concentration value reached in the middle of the vortex is around 0.03.
Reaching an equilibrium point would seem to be meaningless, as the concentration at each instant is set at 0.1 on the upper edge. In reality, from a certain time instant, the sediment is not continually drawn in. From the flow lines it can be seen that the vortex forms a barrier and since the diffusion of the sediment is of an order of magnitude smaller than the transport of the fluid, the concentration does not have time to pass the barrier that has been made by the vortex. In this way the inserted sediment stays on the top without going down.

5.3. Fixed circular source in channel flow

In this problem, we are studying the diffusion and transport of a contaminant in a water channel with a circular source of contamination at its center. The equation that describes its movement inside the water channel is the same of the sediment one. The Lagrangian

mesh will be used to analyze the areas in the channel that are affected by the contaminant. The nodes move along with the fluid, allowing us to accurately simulate the transport of the contaminant as it moves downstream. By tracking the particles of the contaminant in the mesh, it is possible to see how the contaminant spreads and diffuses in the channel, and identify the areas that are most affected.

One of the main challenges in this problem is accurately modeling the interactions between the contaminant and the fluid in the channel. The contaminant can affect the flow of the water and vice versa, since a totally coupled model is considered. This requires a detailed understanding of the physics involved, as well as a robust numerical model that can accurately simulate the interactions between the fluid and the contaminant.

Overall, this problem is an important one in the field of environmental engineering, as it helps us understand how contaminants move and spread in water channels, and can inform strategies for mitigating the impact of pollution on natural ecosystems.

5.3.1. Problem setup

The domain is a channel of size $[0, 10] \times [0, 4]$ m, shown in figure 5.6. The boundary conditions are shown in 5.12 and 5.13. The source in the circle is imposed through all the time of the simulation, as if there is a constant injection of a contaminant.

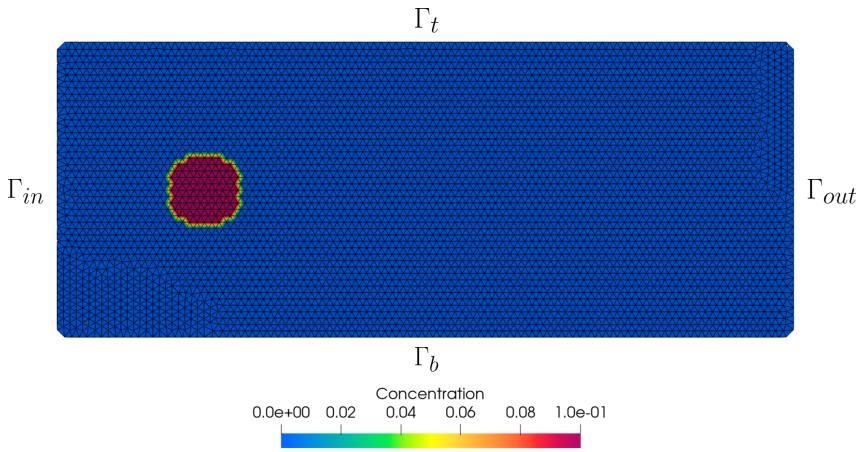

Figure 5.6: Starting domain of the problem

$$NS = \begin{cases} \mathbf{u} = 1\mathbf{i} & \text{on } \Gamma_{in} \\ \mathbf{u} = 0 & \text{on } \Gamma_t \cup \Gamma_b \\ \boldsymbol{\sigma} \cdot \mathbf{n} = 0 & \text{on } \Gamma_{out} \end{cases} \tag{5.12}$$

$$AD = \begin{cases} \nabla c \cdot \mathbf{n} = 0 & \text{on } \Gamma_t \cup \Gamma_b \cup \Gamma_{out} \\ c = 0 & \text{on } \Gamma_{in} \end{cases} \tag{5.13}$$

While the starting conditions are 5.14 and 5.15. This last condition is imposed as a source through all the time of the simulation.

$$\overline{\mathbf{u}}\,(\mathbf{x}) = 0 \;\text{ in }\; [0, 10] \times [0, 4] \tag{5.14}$$

$$\overline{c}\,(\mathbf{x}) = \begin{cases} 0.1 & \text{if } (x-2)^2 + (y-2)^2 \leq 0.6^2 \\ 0 & \text{otherwise} \end{cases} \tag{5.15}$$

5.3.2. Results and discussion

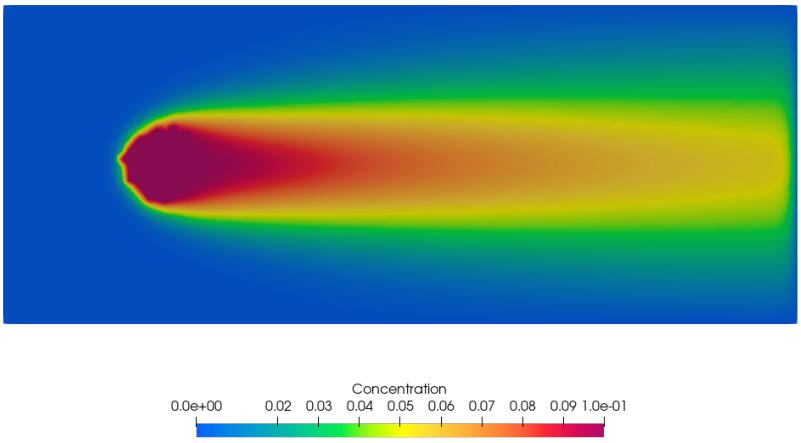

Figure 5.7: Concentration plot at $T = 5\ s$, $\nu_t = 0.1\ \frac{m^2}{s}$, $w_s = 0\ \frac{m}{s}$, $h = 0.1\ m$

The final instant $T = 5\ s$ of the simulation can be seen in 5.7. The falling velocity is null since the simulation is carried through by seeing the domain from the top. Diffusion and transport are active obviously. The result shows how and in which areas the contaminant emitted by the source fouls the water. This simulation can be useful in the context of groundwater protection, so that it can be known where water may or may not be withdrawn for service purposes. In fact, an area can be defined where a well should not be installed for collection, otherwise money would be spent on its installation in a contaminated and therefore unsuitable location.

5.4. Circular obstacle in channel flow

In this problem is studied the movement of a contaminant in a water channel with an obstacle at its center, onto which the contaminant is released. The focus in on how the contaminant moves within the channel under different flow regimes, by varying the geometry and velocity of the channel and changing the Reynolds number. The Reynolds number is a dimensionless parameter that characterizes the flow regime of the channel. At low Reynolds numbers, the flow is laminar and smooth, while at high Reynolds numbers, the flow becomes turbulent and chaotic. By changing the Reynolds number, it can be seen how the movement of the contaminant changes under different flow conditions.
The need of this problem is to accurately model the interactions between the contaminant and the fluid within the channel. This requires a in depth knowledge of the physics involved. The main application is in the environmental engineering, since the pollution problem of turbulent water channels is a fundamental open matter to address.

5.4.1. Problem setup

The domain is a channel with an obstacle inserted inside, which for the simulation purpose is modeled as a hole in the domain. The dimension of the channel, as it can be seen later, is variable. The overall shape of the domain Ω is shown in figure 5.8.

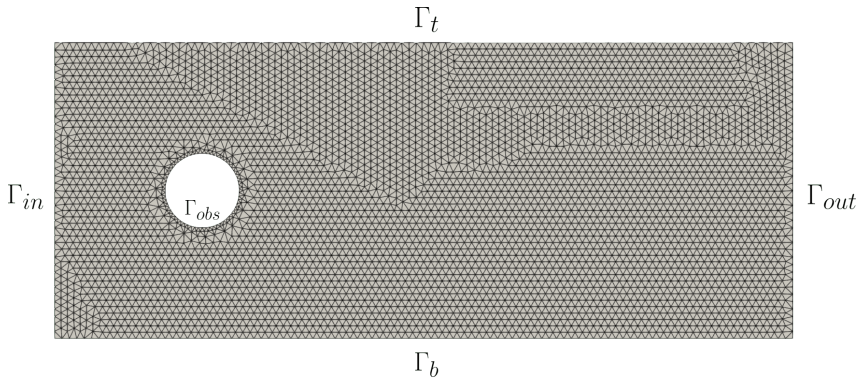

Figure 5.8: Starting domain

The boundary conditions are defined in 5.16 and 5.17. The velocity at the inlet U_{in} will be changed, since different regimes will be studied.

$$NS = \begin{cases} \mathbf{u} = U_{in}\mathbf{i} & \text{on } \Gamma_{in} \\ \mathbf{u} = 0 & \text{on } \Gamma_t \cup \Gamma_b \cup \Gamma_{obs} \\ \boldsymbol{\sigma} \cdot \mathbf{n} = 0 & \text{on } \Gamma_{out} \end{cases} \tag{5.16}$$

$$AD = \begin{cases} \nabla c \cdot \mathbf{n} = 0 & \text{on } \Gamma_{out} \\ c = 0 & \text{on } \Gamma_t \cup \Gamma_b \cup \Gamma_{in} \\ c = 1 & \text{on } \Gamma_{obs} \end{cases} \tag{5.17}$$

While the starting conditions are 5.18 and 5.19.

$$\overline{\mathbf{u}}\,(\mathbf{x}) = 0 \;\text{ in }\; \Omega \tag{5.18}$$

$$\overline{c}\,(\mathbf{x}) = \begin{cases} 1 & \text{if } (x-2)^2 + (y-2)^2 = 0.6^2 \\ 0 & \text{otherwise} \end{cases} \tag{5.19}$$

5.4.2. Results and discussion

The results part is divided in 6 different subsections, because the solution changes in function of the regime of the flow. Generally, far from the cylinder there is an inviscid flow, while near the obstacle a boundary layer is formed since the no slip condition must be fulfilled on the circle. With the boundary layers, there is also the presence of a separation point and the formation of a wake region. The separation point is the point on the obstacle where the flow detaches and it may change from each case. The regime of the flow is described by the Reynolds number, which is defined in this way:

$$Re = \frac{\rho D U_{in}}{\mu} \tag{5.20}$$

ρ is the fluid density, D is the diameter of the obstacle, U_{inlet} is the horizontal velocity imposed at the inlet and μ is the kinematic viscosity. All the values of the parameters of the problem are changed in order to have different Reynolds number. The six cases seen in this section are:

- $Re = 10$: Stokes flow
- $Re = 30$: Steady separation bubble
- $Re = 100$: Laminar von Karman street
- $Re = 10^4$: Laminar boundary layer with turbulent wake
- $Re = 10^6$: Laminar/turbolent boundary layer with turbulent wake

- $Re = 10^8$: Turbulent boundary layer with turbulent wake

In table 5.1 the parameters for each case are shown:

Parameters of each simulation						
Re	10	30	100	10^4	10^6	10^8
$T_f[s]$	10.0	5.0	10.0	10.0	10.0	10
$\mu[\frac{kg}{ms}]$	0.1	0.1	0.01	0.01	0.001	0.0002
$\rho[\frac{kg}{m^3}]$	100.0	100.0	100.0	100.0	1000.0	1000.0
$D[m]$	0.1	0.1	0.1	1.0	1.0	1.0
$U_{in}[\frac{m}{s}]$	0.1	0.3	0.1	1.0	1.0	5.0
$L[m]$	1.0	1.0	1.0	10.0	10.0	1.0

Table 5.1: Table of the parameters

Case 1: $Re = 10$

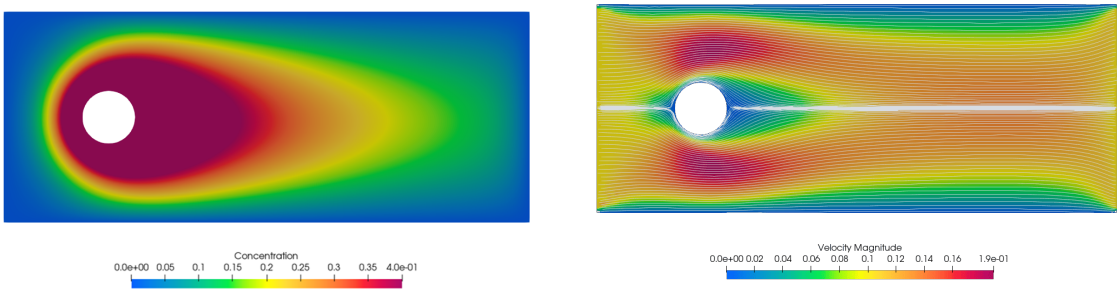

(a) Concentration plot (b) Velocity plot

Figure 5.9: $Re = 10$

The viscous component dominates, and so the velocity field is not affected by the presence of the obstacle. Everything is affected by the boundary layer, no separation and no wake are present. This case is actually considered when the fluid is very viscous and very slow with a very small diameter of the obstacle. The concentration field remains symmetrical to the centerline and there is no vortex formation. The contaminant is mainly diffused since the velocity of the fluid is small. Indeed, in figure 5.9a the concentration around the obstacle varies in a regular way, without any big variations.

Case 2: $Re = 30$

An initial formation of vortexes is created, which are enclosed within a stationary bubble. The two vortexes are counter-rotating and also stationary, maintaining the solution symmetry of velocity and concentration. The solution for concentration is very similar to

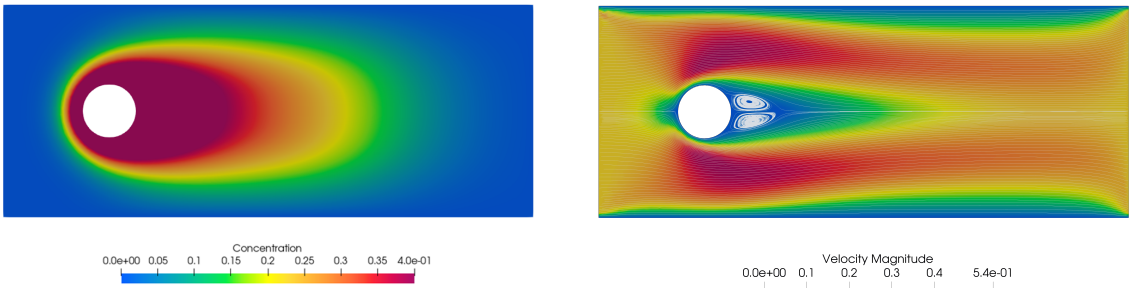

(a) Concentration plot

(b) Velocity plot

Figure 5.10: $Re = 30$

the case of $Re = 10$, but confronting figure 5.10a with the last case the concentration is a little pulled back by the bubble. A first case of laminar boundary layer can be seen with separation point at 108.8°. The result of the streamlines are shown in figure 5.10b.

Case 3: $Re = 100$

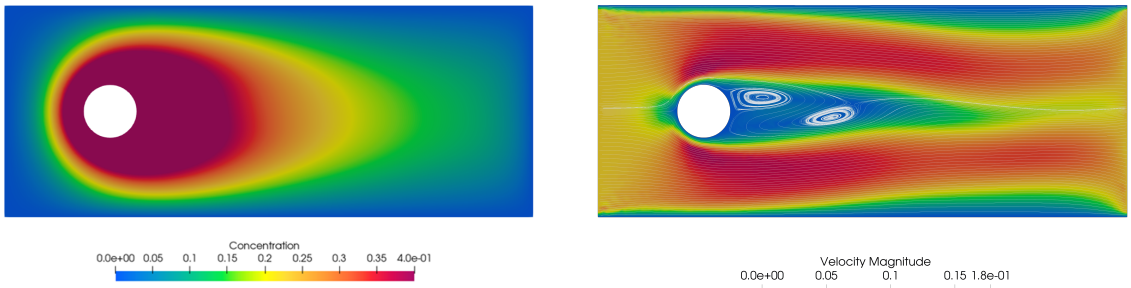

(a) Concentration plot

(b) Velocity plot

Figure 5.11: $Re = 100$

In the condition of motion shown in figure 5.11b, a laminar Von Karman wake is formed. Counter-rotating vortexes are created that recur with a constant frequency and so a periodic detachment of eddies is present in the wake through laminar rotating structures: the velocity and concentration solutions become unsteady. Diffusion overcomes the influence of the vortexes, so the solution for the contaminant remains similar to the previous cases, even if an initial asymmetry can be seen. Still, in figure 5.11a the concentration is more pushed back with respect to the first two cases.

Case 4: $Re = 10^4$

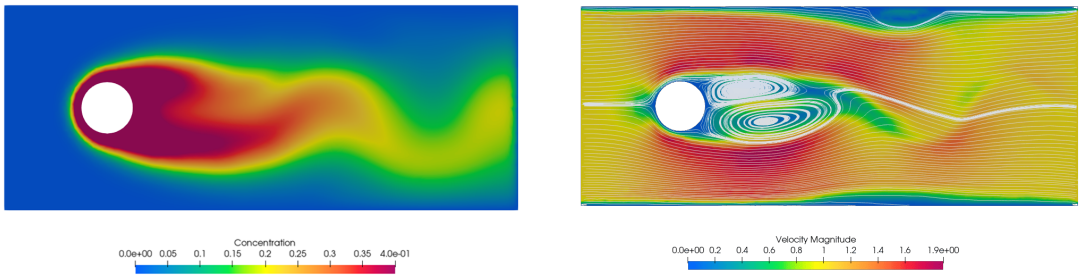

(a) Concentration plot (b) Velocity plot

Figure 5.12: $Re = 10^4$

After a transition phase, a turbulent wake is formed, making the behaviour of the fluid and also the contaminant highly unstable. Some periodicity in the flow is present: solving this problem together with some turbulence model, the vortex shedding should be seen. From experiments, the separation point is known to be situated at more or less 82° and this can be seen also in the results of 5.12b. The concentration field begins to be affected by the presence of turbulent eddies, as can be seen in figure 5.12a.

Case 5: $Re = 10^6$

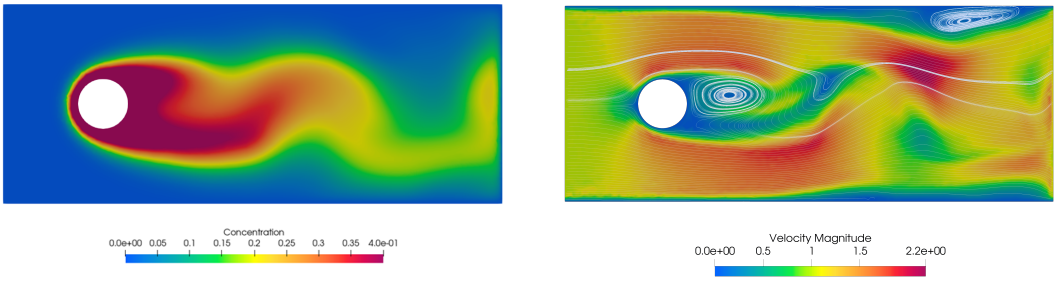

(a) Concentration plot (b) Velocity plot

Figure 5.13: $Re = 10^6$

Until now, only a laminar boundary layer has always been present downstream. When the $Re = 10^5$ limit is exceeded, a turbulent boundary layer is created between the laminar one and the wake. The wake as a result is narrower but inside the flow is more chaotic and eddies are more complex. The separation point is shifted once again towards the back end of the obstacle at 125°: this is due to the fact that the particles have more energy and can take an adverse pressure gradient for more space. The concentration shows more

complexity and in figure 5.13a the wake of the contaminant is underlined by changing colour scale.

Case 6: $Re = 10^8$

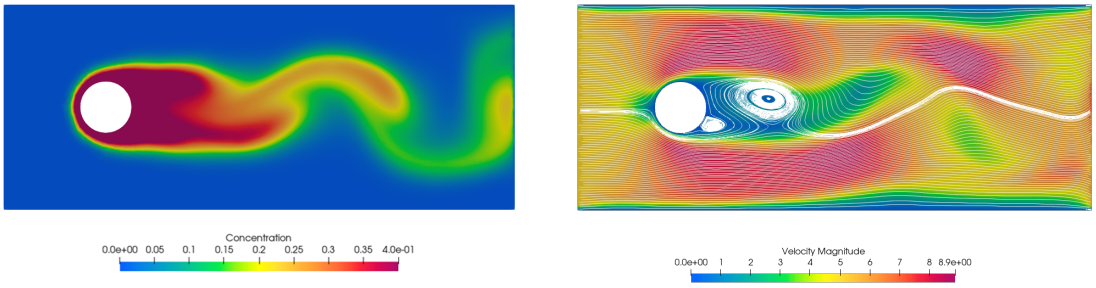

(a) Concentration plot

(b) Velocity plot

Figure 5.14: $Re = 10^8$

The extreme case is the fully turbulent flow and so only the turbulent boundary layer is present. The separation point is shifted towards the front and the flow behind the obstacle is totally chaotic. Eddies are extended in the whole vertical extension of the channel and the solutions are unsteady. The results for concentration and for the stramlines are shown in figure 5.14a and 5.13b.

6 | Bed erosion model

After having integrated the advection-diffusion equation in the code and checked that is working properly, the focus is shifted on the implementation of an erosion model for the movement of the bed due to the shearing action of the sediment-water flux. A model considering a shear stress (Shields) criterion is presented and used.

6.1. Scouring Shields criterion

As seen in 1.2.2, the Shields parameter is fundamental to evaluate if the particle of sediment on the bed is moving or not due to fluid transport. The critical condition where the resistance of the sediment is leveled by the force due to fluid motion is studied. This critical value is confronted to the Shields one evaluated on each particle (which in our model is each bed node) and if the critical value is exceeded the particle is freed.

6.1.1. Shear stress criterion

The basic idea of this criterion is to consider each node belonging to the interface and check if the shear stress applied is enough to snatch it away from the bed. In this case the node becomes a part of the fluid flow. Compute the Shields parameter, which is the adimensionalisation of the shear stress:

$$\theta = \frac{\tau}{(\rho_m - \rho)\, g D_m} = \frac{\rho \left\| \mathbf{u}^* \right\|^2}{(\rho_m - \rho)\, g D_m} \tag{6.1}$$

D_m is the mean dimension of the sediment, g is the acceleration of gravity, ρ_m is the sediment density and $\mathbf{u}^*$ is the friction velocity. If this value is bigger than the critical one, the node is freed. The critical value is computed using an empirical law shown in [15]:

$$\theta_c = 0.22 R_{ep}^{-0.6} + 0.06\ 10^{-7.7 R_{ep}^{-0.6}} \tag{6.2}$$

Where R_{ep} is particle Reynolds number and is defined as

$$R_{ep} = \frac{D_m \sqrt{D_m g \left(\frac{\rho_m}{\rho} - 1\right)}}{\mu} \tag{6.3}$$

To compute the friction velocity, its profile near the wall bed is supposed to be a logarithmic one. In this case its value can be approximated to:

$$\mathbf{u}^* = \kappa \frac{\mathbf{u} - (\mathbf{u} \cdot \mathbf{n})\,\mathbf{n}}{\ln\left(\frac{z_\Delta}{z_0}\right)} \tag{6.4}$$

$\kappa = 0.41$ is the Von-Karman constant while z_Δ is the distance between the wall and its nearest node. This log law supposition can be made if this distance is in a particular range:

$$30 \leq \frac{z_\Delta}{z_0} \leq 130 \tag{6.5}$$

$z_0 = \frac{D_m}{30}$ is the equivalent roughness length. From 6.4, it can be noted that the considered velocity is the tangential one, since the Shields parameter is the adimensionalisation of the shear stress (which is related to the tangential velocity).

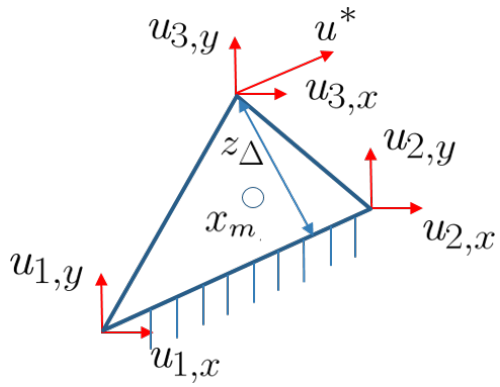

Figure 6.1: Boundary element: the friction velocity is computed using the velocities at the third node

6.1.2. Code implementation

To compute all the values of section 6.1 in the code, a loop has been made on all the scraping nodes. To each one, the nearest non bed node has been searched. Since there

is the need to compute the tangential velocity, an element has been chosen with the considered bed node and a side which is part of the bed surface. The tangential direction **t** is computed easily considering the direction of the bed side. While the velocity **u** in 6.4 has been chosen to be the one of the nearest non bed node.
The main problem with treating the soil as part of the domain is to differentiate it from the flow. To this matter, the input mesh domain is set by considering the soil domain and the fluid one as something unique, which is then differentiated in the code by imposing to the bed nodes a boolean label called "bed" with value equal to 1. In these nodes the solution is fixed as if they are part of the boundary: here $c = 1$ and $\mathbf{u} = 0\ \frac{m}{s}$. In fact, initially the bed nodes are labeled by fixing the "bound" boolean to 1: in this way it is easy to set the value of velocity to zero. When the node is freed due to violating the Shields criterion, the boolean is set to 0 so that the node becomes part of the fluid flow.

6.2. Bed erosion in a channel flow

In order to see the impact of these changes on the total model, some preliminary problems are treated. These are simple cases whose results should help in finding if the modifications are behaving good or not. The problem considered in this section is a channel flow where the bottom part is composed by an erodible soil. This problem is useful to see how the fluid-bed interface changes in time due to the movement of the flow.

6.2.1. Problem setup

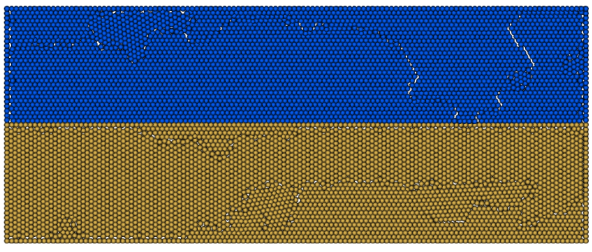

(a) Gaussian point of view

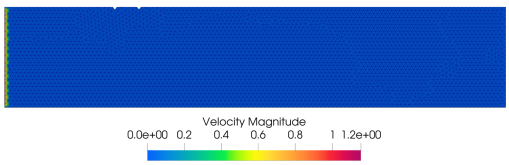

(b) Velocity at $t = 0\ s$

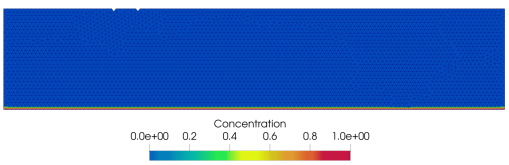

(c) Concentration at $t = 0\ s$

Figure 6.2: Initial domain

The system setup is shown in figure 6.2. The elements which are composed by only bed

nodes are automatically eliminated by the alpha shape method (figures 6.2c and 6.2b). The layer dividing the two subdomains can change in time since by erosion a node of the bed layer in contact with the fluid can be freed and become part of the fluid flow. The nodes belonging to the ground domain are considered as made by sediment and so a concentration equal to 1 is imposed to them (brown nodes in figure 6.2a). If the criterion is violated, the node is freed with concentration equal to 1, and from that moment it can change its concentration.

The boundary condition for the fluid flow are the same as the problems seen before regarding a channel in section 4.2: a inlet uniform velocity equal to 1 $\frac{m}{s}$ is imposed, while in the outflow boundary the Neumann condition is imposed. On the top boundary and on the interface the velocity is 0. As of the sediment nature, gravel has been considered and its parameters with the model ones are shown in table 6.1.

Model parameters			
Average sediment diameter	$D_m = 8.0\ 10^{-3}\ m$	Water density	$\rho = 1000\ \frac{kg}{m^3}$
Sediment porosity	$\phi = 0.25$	Sediment density	$\rho_m = 1680\ \frac{kg}{m^3}$
Equivalent roughness length	$z_0 = \frac{D_m}{30} = 2.66\ 10^{-4}\ m$	Explicit particle Reynolds number	$R_{ep} = 1.848$
Von karman constant	$\kappa = 0.41$	Critical Shields value	$\theta_{crit} = 0.1521$

Table 6.1: Value of the model parameters

6.2.2. Results and discussion

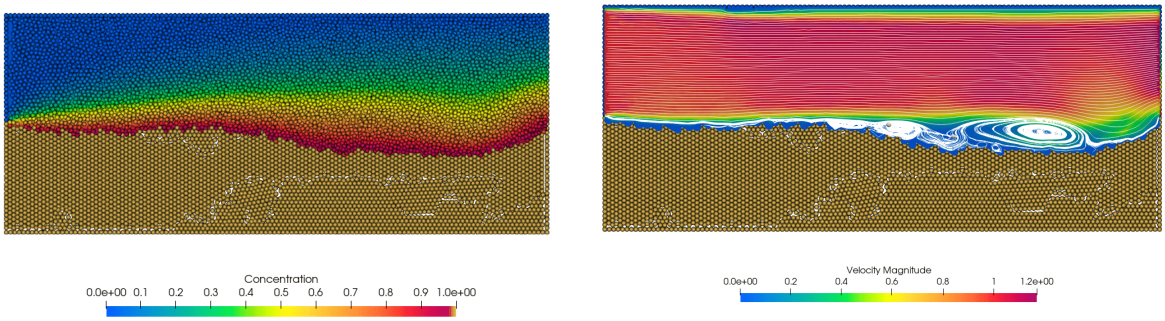

(a) Concentration plot

(b) Streamlines plot

Figure 6.3: $T = 20\ s$, $\nu_t = 0.1\ \frac{m^2}{s}$, $w_s = 0.05\ \frac{m}{s}$, $h = 0.1\ m$

The results in figure 6.3 show that the erosion process is preponderant towards the exit of the domain. This is due to the boundary conditions, indeed the outflow one allows

the particles to not have necessarily a horizontal velocity angle at the exit. When erosion starts to happen towards the end, the bed layer assumes a concave shape which allows the formation of swirls. These vortexes enhance the erosion process which accentuates the concave shape. In figure 6.3b, the streamlines at the end of the simulation are shown: many vortexes can be seen in the end part of the domain. At the front instead a horizontal velocity profile is imposed at the inflow boundary, so that the case happened at the back of the channel do not represent: the erosion stays controlled and is not enhanced since there are no vortexes here. For what concerns the concentration, the plot at the final time in 6.3a shows that the sediment made free by the erosion process gives rise to a diffusion of the concentration in the channel flow. The swirls do not affect so much the value of the concentration, since the diffusion process is much more faster than the velocity of the water inside the eddies. In this way the sediment does not have time to be trapped inside them because the diffusion acts in a more preponderant manner.

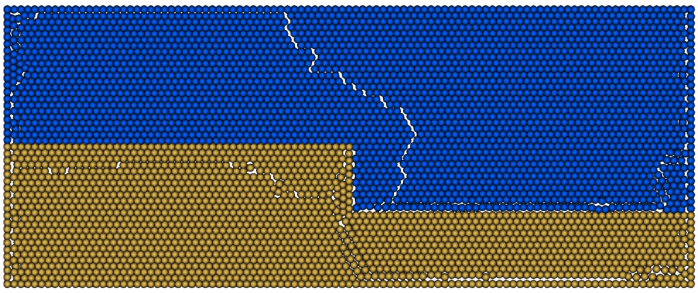

(a) Gaussian point of view

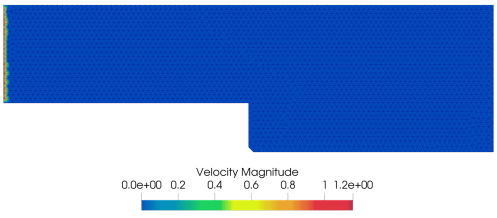

(b) Velocity at $t = 0\ s$

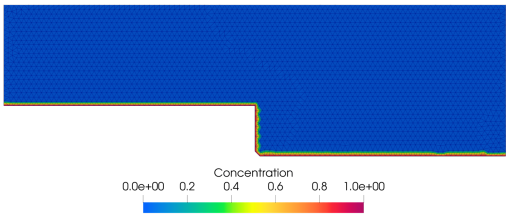

(c) Concentration at $t = 0\ s$

Figure 6.4: Initial domain

A little bit more complex problem is now treated, in order to see if the model behaves in a coherent and real way. Instead of having a plain starting bed level, a step is considered: this should be smoothed by the fluid flow in the best way possible. The starting domain is shown in figure 6.4. The bed level now can change only near the step. This is due to the fact that the behaviour at the outflow seen in the last case should not happen. In particular the bed can change between $x = 4\ m$ and $x = 6\ m$. The jump is correctly blunted by the fluid flow, although the soil height change is not so smooth. This is due to the fact that the step creates some eddies that erode bed level. To have better result,

maybe a mesh refinement should be introduced in the sand domain in order to have a more correct view of the shape of the gravel at the bottom of the channel. The concentration plot and the fluid streamlines are shown in figure 6.5a and 6.5b.

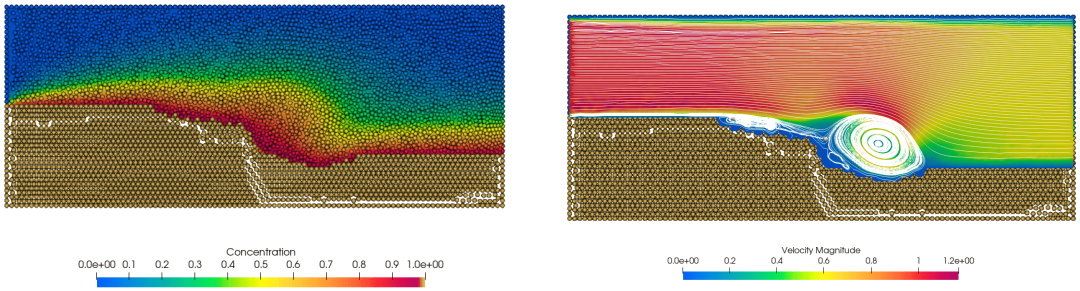

(a) Concentration plot (b) Streamlines plot

Figure 6.5: $T = 5\ s$, $\nu_t = 0.1\ \frac{m^2}{s}$, $w_s = 0.05\ \frac{m}{s}$, $h = 0.1\ m$

6.3. Sand dune erosion

The erosion of a sand dune in a channel through which water flows is a common problem in hydraulic and environmental engineering. When water flows through a channel, it can exert a force on the sand particles of the dune, causing some of them to detach.
From the results, it is possible to obtain information on water flow characteristics and sand particle behaviour in order to predict dune erosion over time. Understanding this phenomenon is important for land management and environmental protection, particularly in coastal areas prone to sand dune erosion.

6.3.1. Problem setup

The domain is a channel of size $[0, 3] \times [0, 1]\ m$, shown in figure 6.6. The boundary conditions are shown in 5.12 and 5.13. As long as the dune particles in $\Omega_d = [0.5, 1.5] \times (0, 0.5]\ m$ do not violate the shields condition, they have the imposed condition $c = 1$ and $u = 0\frac{m}{s}$. The boundary condition for the problem are described in 6.6 and 6.7.

$$NS = \begin{cases} \mathbf{u} = 1\mathbf{i} & \text{on } \Gamma_{in} \\ \mathbf{u} = 0 & \text{on } \Gamma_t \cup \Gamma_b \cup \partial\Omega_d \\ \boldsymbol{\sigma} \cdot \mathbf{n} = 0 & \text{on } \Gamma_{out} \end{cases} \tag{6.6}$$

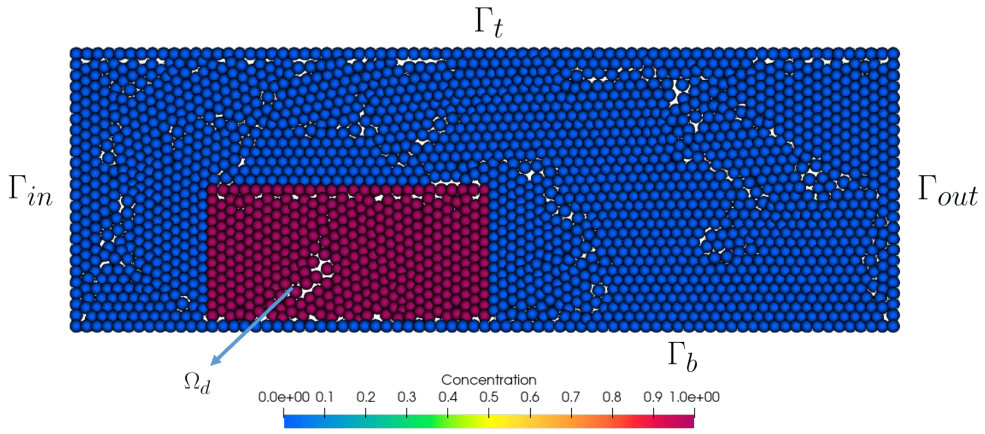

Figure 6.6: Starting domain of the problem

$$AD = \begin{cases} \nabla c \cdot \mathbf{n} = 0 & \text{on } \Gamma_{out} \\ c = 0 & \text{on } \Gamma_t \cup \Gamma_b \cup \Gamma_{in} \\ c = 1 & \text{on } \partial\Omega_d \end{cases} \tag{6.7}$$

While the starting conditions are 6.8 and 6.9.

$$\overline{\mathbf{u}}\,(\mathbf{x}) = 0 \;\text{ in }\; [0,3] \times [0,1] \tag{6.8}$$

$$\overline{c}\,(\mathbf{x}) = \begin{cases} 1 & \text{if } \mathbf{x} \in \Omega_d \\ 0 & \text{otherwise} \end{cases} \tag{6.9}$$

6.3.2. Results and discussion

The results show that the dune is quickly dismantled. At the start the erosion acts more aggressively since towards the center of the channel the velocity is higher. Then the erosion is limited but still acting, slowly eroding each sediment particle remaining in the dune. In figure 6.7 are shown 6 different times in which the erosion can be seen. At the final simulation time $T = 30s$, the dune has completely disappeared. From 6.8 the eroded area is plotted and all the comments made before find some evidence. The erosion is set to kick in after 0.5 s: this is a conscious choice because the aim is to wait until the flow reaches full capacity (since the simulation starts with null velocity).

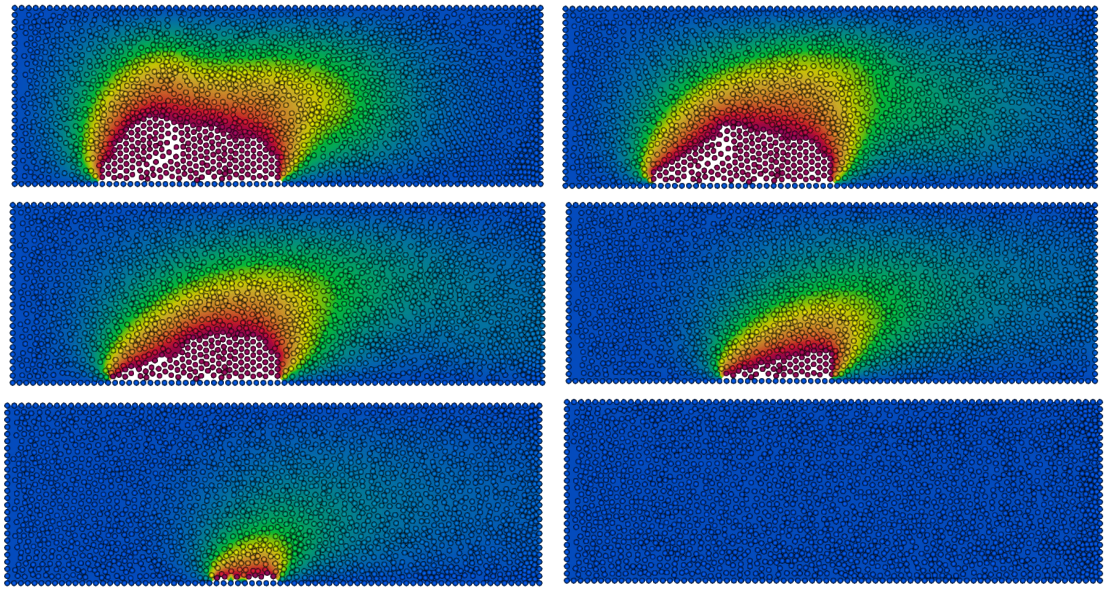

Figure 6.7: Concentration plot at: $t = 1s$, $t = 2s$, $t = 4s$, $t = 10s$, $t = 20s$ and $t = 30s$

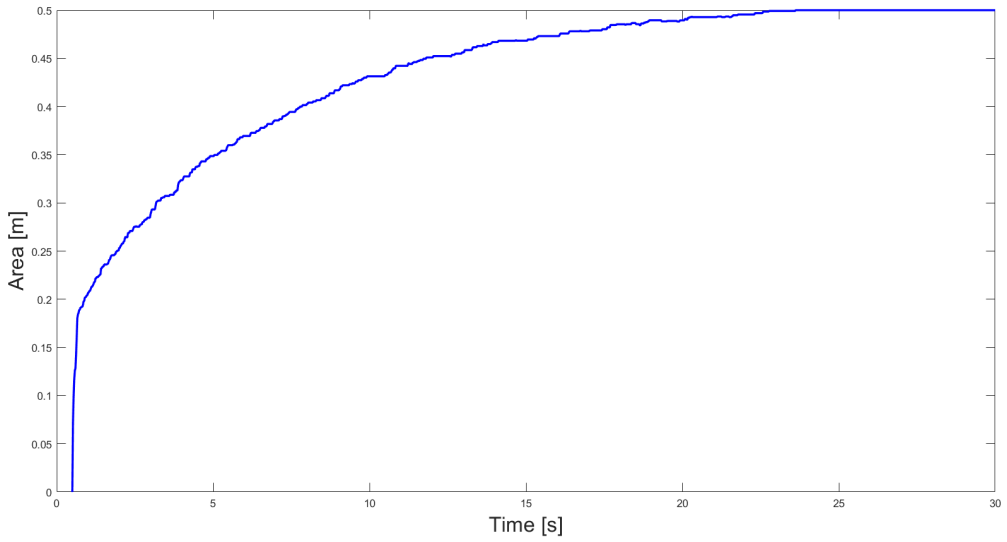

Figure 6.8: Plot of the eroded area

6.4. Beach erosion

When the sea is disturbed by waves with a certain average speed, the water begins to move and transport the sand particles on the beach. This process of eroding sand particles can be described using the Shields model, which takes into account the strength of the waves and the properties of the sediment. During erosion, sand particles are removed from the

beach surface and transported by the flow of water. These particles become part of the sea, contributing to its turbidity and making it dirty.
To ensure that the model is more accurate, a fully coupled approach is used between the sediment and the fluid. This means that the equations of motion of the fluid and sediment transport are solved simultaneously and interact with each other. This should fix the local energy balance at the beach interface due to the wave energy dissipation at the sediment surface. This means that the loss of energy due to the wave-beach interaction is considered and modelled to ensure that the energy balance is respected.

6.4.1. Problem setup

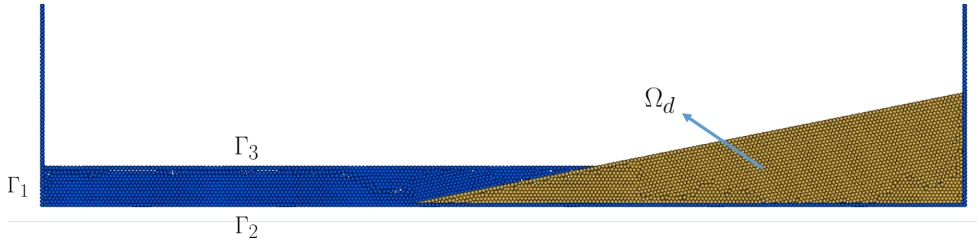

Figure 6.9: Starting domain of the problem

In figure 6.9, the initial domain is shown, composed by the sea and the beach. The sea is fluid without sediment inside at the start; while the beach is composed only by sediment, indeed here $c = 1$ and the nodes are still. The sea is perturbed by a set of waves which shatter on the beach causing its erosion. When the Shields condition is violated, the nodes are freed and become part of the sea. The parameters used are considered in table 6.2. The boundary conditions are shown in 6.10 and 6.11, while the starting conditions are 6.12 and 6.13.

Model parameters			
Average sediment diameter	$D_m = 2.0\ 10^{-3}\ m$	Water density	$\rho = 1000\ \frac{kg}{m^3}$
Sediment porosity	$\phi = 0.25$	Sediment density	$\rho_m = 1520\ \frac{kg}{m^3}$
Equivalent roughness length	$z_0 = \frac{D_m}{30} = 6.66\ 10^{-5}\ m$	Explicit particle Reynolds number	$R_{ep} = 0.2020$
Von karman constant	$\kappa = 0.41$	Critical Shields value	$\theta_{crit} = 0.5743$

Table 6.2: Value of the model parameters

$$NS = \begin{cases} \mathbf{u} = U_{in}\mathbf{i} & \text{on } \Gamma_1 \\ \mathbf{u} = 0 & \text{on } \Gamma_2 \cup \partial\Omega_d \\ \boldsymbol{\sigma} \cdot \mathbf{n} = 0 & \text{on } \Gamma_3 \end{cases} \tag{6.10}$$

$$AD = \begin{cases} \nabla c \cdot \mathbf{n} = 0 & \text{on } \Gamma_3 \\ c = 0 & \text{on } \Gamma_1 \cup \Gamma_2 \\ c = 1 & \text{on } \partial\Omega_d \end{cases} \tag{6.11}$$

$$\overline{\mathbf{u}}\,(\mathbf{x}) = 0 \quad \text{everywhere} \tag{6.12}$$

$$\overline{c}\,(\mathbf{x}) = \begin{cases} 1 & \text{if } \mathbf{x} \in \Omega_d \\ 0 & \text{otherwise} \end{cases} \tag{6.13}$$

The waves are created imposing a step boundary condition of Dirichlet type on Γ_1. Two different simulations are performed: one considering 4 singular waves with Dirichlet boundary condition defined as 6.15; the other one considers 6 waves that are imposed by pairs on the sea as 6.16. So the boundary condition for velocity on Γ_1 are:

$$U_{in} = \begin{cases} 2\ \frac{m}{s} & \text{if} \quad t \in \Theta_i \\ 0\ \frac{m}{s} & \text{otherwise} \end{cases} \tag{6.14}$$

where $i = 1, 2$ and:

$$\Theta_1 = [0, 2) \cup [23, 25) \cup [46, 48) \cup [69, 71) \tag{6.15}$$

$$\Theta_2 = [0, 2) \cup [4, 6) \cup [23, 25) \cup [27, 29) \cup [46, 48) \cup [50, 52) \tag{6.16}$$

In the previous test cases, there was a problem in the energy balance. In fact, to detach the nodes from the beach, the fluid must lose energy. This was not the case before since there was no influence of the concentration on the Navier-Stokes equations: no energy is released into the sea system. A way to address this problem is to consider a totally coupled problem since the change in the density or in the viscosity results in a change of

the orders of magnitude of the terms in the NS equation. The need is to search for a new model for viscosity since the limit of $c \leq 0.1$ is not good since on the soil the concentration must be equal to 1. Iverson [18] presents an extended model, which can work with higher concentrations in opposite to the model seen in 4.4. The main change is on the viscosity, whose formula is in 6.17.

$$\mu = \mu_w \left(1 + 2.5c + 10.05c^2 + 0.00273e^{16.6c}\right) \tag{6.17}$$

This model can be used considering some assumptions: spherical grains of sediment; drag and buoyancy forces on the grains more important than the interaction forces between sediment and fluid; $c \leq 0.4$. This last condition relaxes the limit of the last adopted model.

6.4.2. Results and discussion

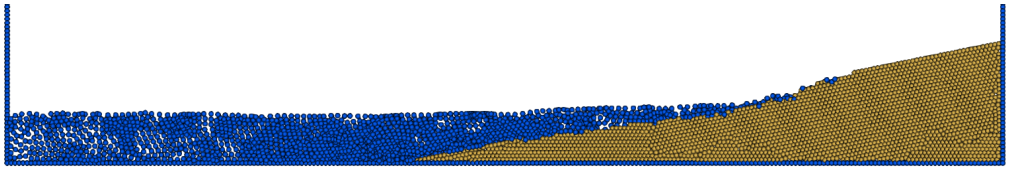

(a) Beach morphology

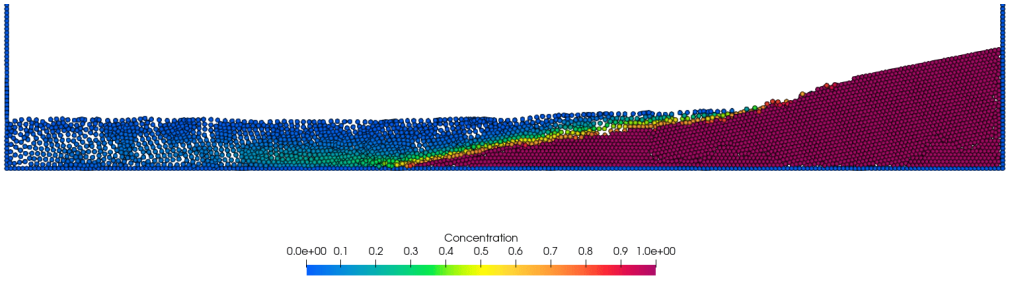

(b) Concentration plot

Figure 6.10: $\Theta_i = \Theta_1$, $T = 90\ s$, $\nu_t = 0.001\ \frac{m^2}{s}$, $w_s = 0.001\ \frac{m}{s}$, $h = 0.1\ m$

The results are shown in 6.10 and 6.11. The total simulation time is 90 seconds. The sediment considered is sand and from the screens of the images the sand is progressively eroded from the beach. This phenomena causes a change on the morphology of the beach and the consequent modification of the concentration in the fluid. The eroded sand carries its concentration into the fluid and it is diffused. At the end of the simulation, the sediment precipitates on the bottom of the sea while towards the surface the concentration is practically 0. This reflects that the density of the sediment is bigger than the water one.

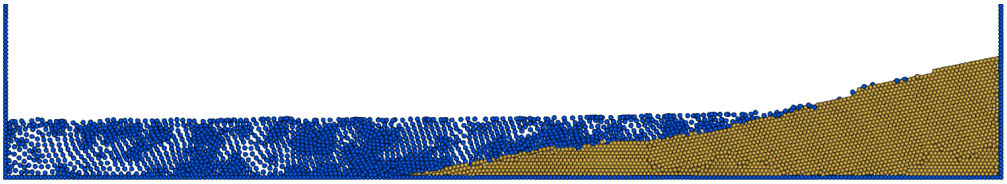

(a) Beach morphology

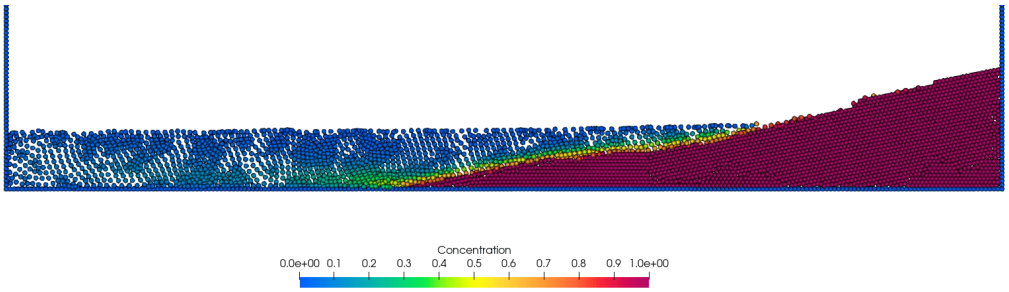

(b) Concentration plot

Figure 6.11: $\Theta_i = \Theta_2$, $T = 90\ s$, $\nu_t = 0.001\ \frac{m^2}{s}$, $w_s = 0.001\ \frac{m}{s}$, $h = 0.1\ m$

7 | Conclusions and future developments

This master thesis had the objective of finding a robust, fast and PFEM feasible model for the sediment propagation in a fluid. This aim has been achieved with many useful purposes and applications in environmental and civil engineering. Additionally, a way to describe the erosion process based on the Shields criterion has been introduced. Many tests have been performed in order to see the correct behaviour of the model. In particular, the main cases seen in this work are: diffusion-advection in channel flows, mixing phenomena, contamination of the groundwater environment and erosion of the territory. The mathematical robustness of the model is checked by considering convergence and stability analysis, transport dominated problems and totally coupled problems.

The main limit of this model consist in the error made by not considering a two-phase flow. This choice has been explained by the high computational cost of this type of approach and the difficult integration to the PFEM model from which the work has started. A totally coupled problem can in part solve this problem by adding some assumptions, but still the concentration of the sediment must remain somehow low.
Clearly, the next thing to do is to extend the code to cover 3D problems, which are the ones that actually matter. A future expansion of this model can cover the implementation of the Robin boundary condition, which can represent correctly the sedimentation of the particles on the bottom surface due to gravity. From Kumbhakar et al. [19], this condition is shown in 7.1.

$$\frac{\nu_t}{\sigma_c}\left(\nabla c \cdot \mathbf{n}\right) + w_s c = \gamma\left(c - c_*\right) \tag{7.1}$$

c_* is an equilibrium concentration defined on the bottom, while γ is a parameter which represents the behaviour of the bottom surface. This new condition gives some concerns on the implementation in the code that must be addressed. Practically in the code the nodes and the elements belonging to this surface must be searched, and then all the local

boundary integrals must be computed.
Regarding the erosion model, a more comprehensive description of the bed level can be represented by the Exner equation, described in section 1.3.1. In a more concrete context, sediment may not only be eroded, but also deposited and transported on the bed surface so that its morphology can change. This equation addresses also these other possible behaviours, making the model more complete. However, it does not consider adding the eroded particles to the main flow with their concentration, which can change the total presence of the sediment in the flow. This equation is added to the total solution system, which will now have 4. The finite element discretization must be implemented, which can require some computational effort. In fact also here like in the implementation of the Robin condition, the bed nodes and elements must be selected in order to build the matrices and vectors of the discretized solution system.

From this work, a way to represent fluid-structure interaction can be built, in order to see for example if the buildings can resist to flooding events. Another possible application that this model can represent is the riverbank collapse: an implementation that considers the infiltration of water in the riverside and the consequent collapse can be found in literature and applied in this environment.

Bibliography

[1] J. Allen. Simple models for the shape and symmetry of tidal sand waves: Statically stable equilibrium forms. *Mar. Geol., 48*, pages 31–49, 1982.

[2] D. Avijit and S. Natesan. Convergence analysis of a fully-discrete fem for singularly perturbed two-parameter parabolic pde. *Mathematics and Computers in Simulation 197*, pages 185–206, 2022.

[3] P. Bohorquez and C. Ancey. Particle diffusion in non-equilibrium b e dload transport simulations. *Applied Mathematical Modelling 40*, pages 7474–7492, 2016.

[4] R. Bravo, B. Becker, and P. Ortiz. Numerical simulation of evolutionary erodible bedforms using the particle finite element method. *Computational Particle Mechanics 4*, pages 295–305, 2017.

[5] Z. Cao, G. Pender, and S. Wallis. Computational dam-break hydraulics over erodible sediment bed. *J. Hydraul. Eng. 130*, pages 689–703, 2004.

[6] M. Claire, J. Percival, and A. Angeloudis. Hydro-morphodynamics 2d modelling using a discontinuous galerkin discretisation. *Computers and Geosciences 146*, page 1–13, 2021.

[7] M. Cremonesi and A. Franci. A state of the art review of the particle finite element method (pfem). *Archives of Computational Methods in Engineering*, pages 1709–1735, 2020.

[8] M. Cremonesi, A. Franci, and U. Perego. A lagrangian finite element approach for the simulation of water-waves induced by landslides. *Computers and Structures 89*, pages 1086–1093, 2011.

[9] M. Cremonesi, F. Ferri, and U. Perego. 3d simulation of vajont disaster. part 1: Numerical formulation and validation. *International Journal for Numerical and Analytical Methods in Geomechanics*, pages 30–53, 2017.

[10] M. Cremonesi, S. Maduri, and U. Perego. Lagrangian–eulerian enforcement of non-

homogeneous boundary conditions in the particle finite element method. *Computational Particle Mechanics 7*, pages 41–56, 2020.

[11] A. Einstein. A new determination of molecular dimensions. *Ann. Phys. 19*, pages 289–306, 1906.

[12] F. Engelund and J. Fredsøe. A sediment transport model for straight alluvial channels. *Hydrol. Res. 7*, pages 293–306, 1976.

[13] A. Franci and M. Cremonesi. On the effect of standard pfem remeshing on volume conservation in free-surface fluid flow problems. *Computational Particle Mechanics 4*, pages 331–343, 2017.

[14] A. Franci, M. Cremonesi, and U. Perego. 3d simulation of vajont disaster. part 1: Numerical formulation and validation. *Engineering Geology 279*, pages 1–15, 2020.

[15] N. Galano, P. Moreno-Casas, and J. Abell. Extending the particle finite element method for sediment transport simulation. *Comput. Methods Appl. Mech. Engrg. 380*, pages 1–16, 2021.

[16] J. Gonzàlez-Aguirre, J. Gonzàlez-Vàzquez, and J. Alvarez-Ramirez. Numerical simulation of bed load and suspended load sediment transport using well-balanced numerical schemes. *Communications on Applied Mathematics and Computation*, page 1–38, 2021.

[17] K. Hutter, I. P. Chubarenko, and Y. Wang. *Physics of Lakes*, volume 3. Springer Cham, 2014. ISBN 978-3-319-34505-5. Chapter 31.

[18] R. M. Iverson. The physics of debris flows. *Reviews of Geophysics*, pages 1–52, 1997.

[19] M. Kumbhakar, S. Mohan, and K. Ghoshal. Semianalytical solution for nonequilibrium suspended sediment transport in open channels with concentration-dependent settling velocity. *Journal of Hydrological Engineering 27*, pages 1–12, 2022.

[20] C. Liu, X. Liu, and C. Jiang. Numerical investigation of sediment transport of sandy beaches by a tsunami-like solitary wave based on navier– stokes equations. *Journal of Offshore Mechanics and Arctic Engineering 141*, pages 1086–1093, 2019.

[21] X. Liu and J. Zhang. Supercloseness of linear streamline diffusion finite element method on bakhvalov-type mesh for singularly perturbed convection-diffusion equation in 1d. *Applied Mathematics and Computation 430*, pages 1–9, 2022.

[22] B. McLaury and S. Shirazi. An alternative method to api for predicting solids erosion in multiphase flow. *ASME J. Energy Resour. Technol. 122*, pages 115–122, 2000.

[23] S. Meduri, M. Cremonesi, and U. Perego. A partitioned fully explicit lagrangian finite element method for highly nonlinear fluid-structure interaction problems. *Int J Numer Meth Engng 113*, pages 43–64, 2018.

[24] G. Messa and S. Malavasi. A cfd-based method for slurry erosion prediction. *Wear 398–399*, pages 127–145, 2018.

[25] G. Messa and V. Matousek. Analysis and discussion of two fluid modelling of pipe flow of fully suspended slurry. *Powder Technology 360*, pages 747–768, 2020.

[26] G. Messa, G. Ferrarese, and S. Malavasi. A mixed euler–euler/euler lagrange approach to erosion prediction. *Wear 342-343*, pages 138–153, 2015.

[27] G. Messa, Y. Wang, M. Negri, and M. S. An improved cfd/experimental combined methodology for the calibration of empirical erosion models. *Wear 476*, pages 1–17, 2021.

[28] G. V. Messa. Key parameters affecting solid particle erosion, 2020. URL `https://www.youtube.com/watch?v=JfUK4rTXEzY&list=PLmKUwJ0KJQnUnTzn9w7OfxyWg_2fz6wdI&index=22`.

[29] J. Richardson and W. Zaki. Sedimentation and fluidisation: Part i. *Chem. Eng. Res. Des. 75*, page 82–100, 1997.

[30] L. Rijn. Sediment transport, part ii: Suspended load transport. *J. Hydraul. Eng. 110*, pages 1613–1641, 1984.

[31] T. Rowan and M. Seaid. Two-dimensional numerical modelling of shallow water flows over multilayer movable beds. *Applied Mathematical Modelling 88*, pages 474–497, 2020.

[32] R. Soulsby and R. Whitehouse. Threshold of sediment motion in coastal environments. *Pacific Coasts and Ports 1997 Conference, Christchurch*, pages 149–154, 1997.

[33] P. D. Thorne, A. G. Davies, and P. S. Bell. Observations and analysis of sediment diffusivity profiles over sandy rippled beds under waves. Technical report, School of Ocean Sciences, College of Natural Science, Menai Bridge, Anglesey, LL59 5AB, UK, 2009.

[34] W. Wu and S. Wang. One-dimensional modeling of dam-break flow over movable beds. *J. Hydraul. Eng. 133*, pages 48–58, 2007.

[35] Y. Xu and H. Nepf. Suspended sediment concentration profile in a typha latifolia canopy. *Water Resources Research 57*, pages 1–13, 2021.

A | Model work flow

Below is represented the work flow of the code that is used to solve the whole problem of sediment transport and erosion.

Algorithm A.1 Pseudocode

Read input mesh file .dat and model parameters
Set the starting solution values and introduce a partition in time
while $t < T$ **do**
    Check the mesh distortion and do the remeshing if necessary
    Divide the elements into each core
    1: Momentum equation
    Each core assembles its part of the momentum solution system
    Compute the stable Δt^n using the CFL condition
    Compose the global solution system and find u^{n+1}
    2: Sediment equation
    Each core assembles its part of the sediment solution system
    if $\mathbb{P}e > 1$ **then**
        Apply SD stabilization
    end if
    Compose the global solution system and find c^{n+1}
    3: Continuity equation
    Each core assembles its part of the continuity solution system
    Compose the global solution system and find p^{n+1}
    4: Erosion model
    Select the erodible nodes and insert them in Ω_b
    for $\mathbf{x_i} \in \Omega_b$ **do**
        if $\theta > \theta_c$ **then**
            Free the node into the flow
        end if
    end for
end while

List of Figures

List of Tables

Acknowledgements

I want to thank the professors Alberto Corigliano and Massimiliano Cremonesi for helping me throughout this master thesis work. Thank for their patience in answering all my doubts and correcting me when I made mistakes.
I want also to thank my family and my friends for always supporting me. With their moral and concrete support, they allowed me to complete successfully my university studies.